2016

Evaluating Groundwater Recharge in the Saloum Region of Senegal

Alexander Wohlgemuth
Michigan Technological University, amwohlge@mtu.edu

EVALUATING GROUNDWATER RECHARGE IN THE SALOUM REGION OF SENEGAL

By

Alexander M. S. Wohlgemuth

A THESIS

Submitted in partial fulfillment of the requirements for the degree of

MASTER OF SCIENCE

In Environmental Engineering

MICHIGAN TECHNOLOGICAL UNIVERSITY

2016

This thesis has been approved in partial fulfillment of the requirements for the Degree of MASTER OF SCIENCE in Environmental Engineering.

Department of Civil and Environmental Engineering

Thesis Co-Advisor: *David W. Watkins*

Thesis Co-Advisor: *John S. Gierke*

Committee Member: *Ann Maclean*

Department Chair: *David S. Hand*

Contents

List of Figures

List of Tables

Acknowledgements

I would like to dedicate this thesis to everyone who has played even a small role in its completion. Over the course of more than two years, I have met and received assistance from many people, from different backgrounds and nationalities, viewpoints and perspectives, who have all made an important contribution to this work. I cannot possibly name everyone who offered an alternative perspective or encouraging word, but a sincere attempt follows. The staff at *L'Institut Nationale de Pedologie* (National Pedology Institute), both in Dakar and Ndiaffate, helped enormously, especially Mamo Gallo, Alioune Dieye, Alfred Tine and François Mendy. Staff at *Le Direction de la Gestion et de la Planification des Ressources en Eau* (the Directorate of Water Resources Planning and Management) were an incredibly valuable resource as well, especially Mukhtar Sall, Mamadou Sise and Serigne Faye in Dakar, and Suleyman Bojang and Idrisa Badji in Kaolack. Local rain-gauge operators and borehole operators also provided me with valuable data: Ibu Ndao, Mandaw Yama, Pa Ñing, Tamsir Diop, Arona Massaly, and Lammiñ Sumare. The priests and brothers at Keur Mariama provided a welcoming place to rest and recuperate.

My friends and hosts in the villages in the Keur Soce Department are too numerous to mention each by name, but my host father, Mbaye Ndiaye, and counterparts Dom Ndiaye, Pape Dia, Abdul-Salam and Mandaw Ba, Ousseynou Diane and Andre Diouf, and their families, provided amazing support and encouragement. To the people of Sama Ndiayenne, Fas Toucouleur, and all the other villages that welcomed me: Jerengeenjef – Yalla na leen Yalla fay.

I cannot forget or neglect the tremendous role others have played in keeping me motivated, listening to me explain my research for the umpteenth time, or helped me take a step back when I became too enmeshed in the work itself. Those who served with me as Peace Corps Volunteers in Senegal and the staff thus deserve much credit. My site mate, Adel Uhlarik, was a tireless and constant source of support. Austin Mueller and Ian Yau lent support as well as expertise to help me address my many questions.

My co-advisors, Dave Watkins and John Gierke, were incredibly patient and helpful in 'batting practice' as I struggled with attempting to solve all of the universe's mysteries in a couple semesters. Ann MacLean provided extremely valuable guidance for the remote sensing portion of this work, and Veronica Webster was always happy to discuss hydrology and statistics with me. My fellow PCMIs and graduate students, who made this experience unforgettable, and who spent long hours with me in the computer lab, provided priceless support and assistance, while helping me process the previous two years. Luke Moilanen, Ben Savonen, Erinn Kunik, Wade Aitken-Palmer, Jordan van Sickle, Allie Archer, Anika Kuczynski, Amanda O'Toole, Chris Walkons, Monica Harmon, Jordan Mayer, Ashley Miller and Rebecca Midkiff deserve special recognition.

The loving support of my parents and sister made all of this possible in more ways than I can mention. Calls, cookies, bike tires…the list is endless.

Finally, I would like to credit those who may someday benefit from the work presented herein. Though we may in all likelihood never meet, you provided much motivation for me to complete this work to the best of my ability.

To each of you, much thanks.

Abstract

Approximately 1.2 billion people in the world live in an area facing physical, or absolute, water scarcity (defined as access to less than 1,000 cubic meters of water). This number is projected to increase to 1.8 billion by the year 2025 [1]. Thirty-eight percent of the world's population lives in arid, semi-arid or dry subhumid regions [2], which translates to a high dependence on the 30% of the world's freshwater present in the ground [3]. Further, the rate of water use is increasing rapidly – between two and two and a half times that of population growth, over the last century [4].

In regions such as Kaolack, Senegal, known locally as the *Saloum* and located in the Sahel, the vulnerability of the local population to water scarcity is well known. Compounding this precariousness are precipitation irregularities introduced by a changing climate, making reliance on historical trends for prediction of future patterns increasingly difficult. In addition, deforestation and over-grazing are reinforcing the damage caused by climate change and threatening the integrity of the hydrologic cycle.

To ensure the continued access to safe and plentiful water to those who rely on groundwater for domestic use, an improved understanding of the factors controlling supply to aquifers in the form of recharge is paramount. An in-depth look at each of the mechanisms contributing to recharge (precipitation, evapotranspiration, and runoff) is essential. When the relative contributions of assorted processes and variables to groundwater recharge are better understood, efforts can be more successfully directed to counter the antagonizing mechanisms compromising the health of the hydrologic system.

In this study, three established methods for estimating groundwater recharge were explored, all of which approached this phenomenon with different assumptions and data requirements. These were compared against a hydrologic simulation model developed over the course of this study which offers the possibility of a more detailed estimate of recharge; this new model provides recharge estimates comparable with the established methods. It can also evaluate changes in the system, such as vegetation and soil type, while also having the potential to directly account for the effects of daily rainfall patterns. Despite challenges in calibration and verification with limited data, the simulation model has the advantage of indicating which features control recharge, as well as providing the opportunity to explore changes in land management and climate change into the future, and their attending effects on recharge.

1. Introduction

1.1. Site Background

Senegal is located in Francophone West Africa and is the most western country in Africa (Figure 1.1). The region of Kaolack is located in west-central Senegal, bordered to the south by the Gambia (Figure 1.2). The Sahel, a transition zone between the Sahara desert to the north and more tropical biomes to the south, cuts right across much of Senegal, including Kaolack. The region is considered Sudano-Sahelian, with annual potential evapotranspiration ranging from 1500-2500 mm/yr, and rainfall varying from 600-800 mm/yr, with greater rainfall in the south [5]. Like most of Senegal, the local population is highly dependent on groundwater. This is despite the fact that the regional capital of Kaolack is located on the banks of an estuary of notable size, known as the Saloum Estuary (*Saloum*, meaning 'south' in Wolof, was the name of the kingdom located in the present-day Kaolack region, and is still used to refer to the region in day-to-day life). However, this estuary is highly prone to saltwater intrusion from the ocean. Partially as a result of this intrusion, much of the groundwater surrounding the Saloum is contaminated with salt. For more information on the interaction of the aquifer with the hypersaline Saloum estuary, Pages and Citeau [6] and Faye, et al. [5] provide an excellent discussion on the topic.

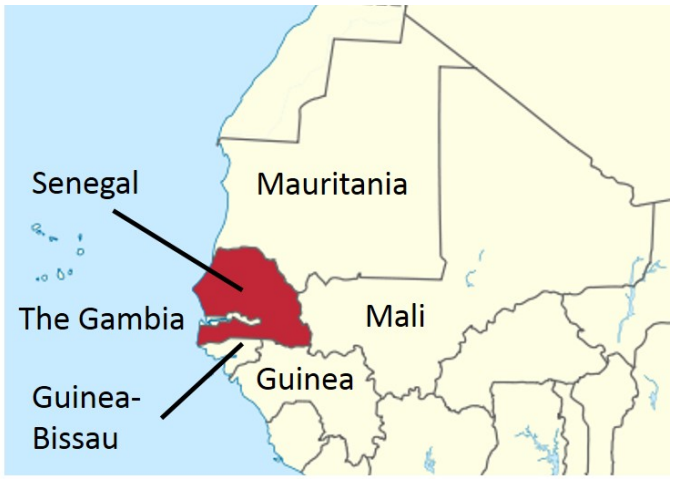

Figure 1.1 Senegal and Neighboring Countries in West Africa. Modified (country labels added) from [7]. Used under Creative Commons 3.0 (for permission, see Appendix 7.4.).

Figure 1.2 Administrative Regions of Senegal. Kaolack is highlighted in red [8]. Used under Creative Commons 3.0 (for permission, see Appendix 7.5).

The department, or sub-region, where the author served as a Peace Corps Volunteer is home to people of various ethnic groups and as such is an ethnic microcosm of Senegal as a whole. Wolof, Serere, Pulaar and Bambara communities dot the landscape. Each village has at least one hand-dug well, in addition to access to one of a handful of deeper boreholes, often dug with the assistance of foreign countries. There are three or four surface water bodies in the area, but these are only present during the rainy season and up to a couple months after its conclusion. While they are used occasionally for washing and watering livestock, they are not used for other purposes, so wells are the sole source of water for most people in the area.

The livelihood of the overwhelming majority of people in this region is agriculture. Millet and peanuts are the most common, with corn, sorghum, beans, rice, watermelon and cassava also playing an important role. Peanut cultivation was encouraged by the French colonizers who also brought with them modern agriculture [9]. This dynamic is responsible in many ways for deforestation of the area. With this reliance on agriculture comes an increased vulnerability to climate change. Efforts have been made at promoting dry-season gardening, but these rely on groundwater supplies for their feasibility, not to mention other substantial material inputs, such as pumps and fuel, seeds, tools and fertilizer.

1.2. Project Motivation

Climate change is a widely acknowledged feature of modern society, affecting basic needs, economic well-being, and even safety and security. However, the effects of climate change are not felt proportionately by those societies most responsible for it (on account of greenhouse gas emissions), nor are its effects even felt uniformly across the global community. In fact, those populations which are least developed economically face the harshest of ironies: they are both least to blame for the causes of climate change, and most vulnerable to its effects [10].

The people of the Sahel face another obstacle in addition to that of climate change. The Sahel itself is prone to erratic and highly variable rainfall patterns [11]. A drought lasting from 1972 to 1984 resulted in the deaths of over 100,000 people; in 1974, three-quarters of a million people were completely reliant on food aid [12]. The variability of Sahel rainfall patterns combined with the influence of climate change makes evaluating the availability of

groundwater resources especially difficult, and because of the reliance of the local population on such resources, all the more necessary.

Declining groundwater tables can have numerous effects. Lack of readily-available water carries with it the obvious risk posed to health and livelihoods, including farming which provides the vast majority of residents with income. Additionally, declining water tables can dramatically affect surface water features. These features which were previously fed by groundwater supplies, known as gaining reaches, may 'flip' and become losing reaches. This would be especially hazardous given the inflow of salt water intrusion from the Saloum estuary. Because of a hydraulic gradient between the Saloum and the aquifer to the south, salt water is able to migrate several kilometers inland and contaminate the groundwater there [5]. The farther water levels drop, the more susceptible those resources will be to saltwater intrusion. Thus, water quality and quantity are intimately connected.

In order to resolve these tensions, a method is needed that can estimate recharge with a reasonable level of confidence, and account explicitly for the myriad factors that affect it, such as soil characteristics and vegetation, and so make up for the limitations of established methods.

1.3. Objectives

The overarching goal of this project is to estimate recharge through a variety of approaches, as well as to provide a way to explore how soil and vegetation type affect groundwater recharge in the region of Kaolack, Senegal. The objectives supporting this goal are as follows:

1. Use three existing methods to estimate recharge in the study site:
   a. Water Table Fluctuation Method (WTF Method)
   b. Thornthwaite Mather Water Balance (TMWB)
   c. GMS MODFLOW Groundwater Model (GMS)
2. Develop an alternate model in a MATLAB environment to calculate components of the water budget at high resolution, both temporally and spatially, using the NRCS Curve Number Method [13], and the FAO-56 Penman Monteith method for calculating evapotranspiration and the water balance [14], as modified for remote sensing by González-Dugo and Mateos [15].

The rest of Section 1 will provide a brief review of climate change as it relates to West Africa, as well as groundwater recharge models, some of which are similar in many respects to the alternative hydrologic simulation model developed herein. Section 2 will review three established methods for estimating groundwater recharge, as well as present their estimates of recharge in the area. Section 3 will explore the development and application of a new recharge model in a MATLAB environment. Section 4 will compare these four models and their estimates. Section 5 will present opportunities for future work and discuss conclusions.

1.4. Background

1.4.1. Climate Change and Variability

There is substantial evidence in the field of climate science, as well as consensus among the scientific community, that the earth is experiencing dramatic changes in its climate [10]. Numerous factors have led to this paradigm shift, most of which are anthropogenically based. Increasing emissions, deforestation, expansion of livestock production and population growth,

among others, have contributed to rising CO_2 levels and the attending effects on the earth's climate system.

Climatic cycles relating to ocean temperatures and pressures, such as the El Niño-Southern Oscillation (ENSO), have wide-ranging impacts on the earth as a whole and are gradually becoming better understood. Their effects on climate around the world, or teleconnections, are an object of increasing scrutiny. Different cycles exhibit variations in magnitude, as well as in frequency, having periods on the order of years, decades or longer. Individual cycles can also manifest changes in frequency and magnitude (usually either normalized temperature or pressure differences) over time. Understanding the significance of each of these cycles and their variability over time, as well as any possible interaction effects, is crucial to interpreting changes in weather patterns.

The Intergovernmental Panel on Climate Change (IPCC) has explored possible radiative forcing scenarios based on greenhouse gas emissions, land use changes and population growth. From these simulation runs, they have established outcomes for various regions of the world with regard to changes in climate. For the Sahel, a decrease in annual precipitation, along with an increase in the number of extreme rainfall days, is predicted, coinciding with increasing temperatures. A decline in groundwater recharge for the Sahel (for those areas with 200-500 mm of annual rainfall) is predicted, whereas little change is anticipated for areas receiving greater than 500 mm annual rainfall. Greater sensitivity to this change is expected for areas reliant on shallow aquifers as opposed to deeper groundwater reserves. The Sahel and tropical West Africa are identified to be among the first regions to experience major climate changes in the late 2030s to early 2040s [10].

The Sahel is located at the northern extent of the tropical rain belt, known as the Inter-Tropical Convergence Zone (ITCZ) [16]. This explains its status as a transition zone and the associated steep decrease in rainfall from south to north, as well as its variable climate [11]. Variations in sea-surface temperatures (SST) have been noted as key factors in the movement of the ITCZ, with warmer temperatures in the southern oceans, relative to the northern oceans, shifting the ITCZ south and thereby restricting rainfall in the Sahel [16]. In the work of Held, et al. [16], the drying trend in the Sahel appeared to be the result of aerosols and greenhouse gas emissions, in combination with internal variability. Giannini, et al. [17] found that variations in SST control the sign of rainfall anomalies, while interaction between the land and atmosphere reinforces these anomalies, indicating land use changes are not as significant as SST in affecting rainfall in the Sahel.

1.4.2. Groundwater Recharge Estimation

Numerous methods have been developed for estimating groundwater recharge, ranging from physical methods to modelling approaches. A few approaches will be briefly examined here, and their merits and drawbacks discussed.

Lysimeters are tools that are able to represent the actual water drained from the soil column. This makes it possible to examine an explicit relationship between recharge and other components of the water balance. However, they are large and costly to install, and are not appropriate in many developing contexts. Furthermore, as an unsaturated-zone technique, recharge values obtained with lysimeters are better considered as point estimates [18], owing to the heterogeneity of soil and vegetation.

The water table fluctuation (WTF) method has been used in a number of studies to relate rises in well levels to recharge, via specific yield [19, 20]. Annual or seasonal estimates can be made based on periodic well-level measurements, but the approach is intended for evaluating

short-term fluctuations in the water table in response to precipitation events. Thus, frequent measurements of well levels, as well as specific yield estimates, are recommended. Estimates for the spatial validity of this approach vary, from a lower estimate of several square meters according to Healy and Cook [21], to an upper limit of one thousand square meters according to Scanlon, et al. [18]. Ideally, numerous wells should be surveyed in ordered to produce reliable areal estimates. Such monitoring may rarely be undertaken in developing contexts, however, again limiting the use of this method.

Groundwater modeling provides numerous advantages for the investigation of groundwater recharge. The ability to synthesize a wide variety of data into a coherent model is a tremendous advantage of programs such as GMS MODFLOW [22]. However, without flow values, multiple possible solutions can be produced without a sense of which is the best fit, owing to the non-uniqueness problem of modeling systems. In addition, head values must be continually measured in order to capture the variation in the system, which may be of concern in developing contexts where such information is limited. Where factors such as rainfall are not incorporated directly, it may be difficult to achieve an explicit relationship between rainfall and recharge. Once the relevant parameters (for instance, recharge and hydraulic conductivity) are established, exploration of alternative scenarios by altering parameter values is straightforward, allowing for consideration of multiple outcomes.

Soil water balance approaches are desirable for a number of reasons, but also have drawbacks. There are many terms in a typical water balance equation (evapotranspiration, runoff, groundwater flows in and out, withdrawals and storage), most of which are easier to calculate or estimate directly than recharge. Thus, recharge is calculated as the residual, and uncertainties associated with all other terms are lumped together with the recharge estimate [18]. The only way to reduce this uncertainty is to improve estimates of all other factors in the equation; one way of doing this is to increase temporal resolution of the accounting procedure [18].

One commonly used tool among water balance accounting procedures is the Thornthwaite-Mather Water Balance. Calculated on a monthly basis, it requires values of precipitation, temperature, field capacity and rooting depth. Without supplementary flow data, it is unable to separate recharge and runoff predictions. Despite its simplicity, it has been found to produce good estimates of monthly runoff, indicating that actual evapotranspiration is also estimated accurately [23].

Many studies have incorporated the FAO-56 Penman Monteith methodology in order to calculate actual evapotranspiration, generally for managing irrigated fields with substantial resources at their disposal [24, 25]. However, successful application of this method often requires extensive knowledge of the crops grown in a given area and their stage of development. González-Dugo, et al. [26] incorporated remote sensing into their work, allowing this methodology to be utilized over a larger area.

Eilers, et al. [27] applied the FAO-56 Penman Monteith methodology to agricultural land in Nigeria to estimate recharge on an annual basis. Results were lumped recharge estimates, assuming constant soil and crop type for two study sites, roughly 300 km apart. This is an indication of the difficulties of gathering suitable data in a developing context. One unique aspect of their study is the consideration of near-surface storage (NSS), which represents soil moisture near the surface for supporting germination and the growth of shallower roots.

Kendy, et al. [28] developed a multi-layer soil water balance model for estimating groundwater recharge in an agricultural area in northern China. The model operates on a daily

basis, and while data requirements are relatively high, there is potential to have a more accurate understanding of deep percolation processes in the subsurface. The subsurface is divided into layers corresponding to soil horizons, each with properties of field capacity, saturation and saturated hydraulic conductivity that govern flow from one layer to another. Once one layer is filled to saturation with infiltrating water, the excess is automatically transferred downward to the next layer. Water present below saturation flows down according to an exponential relationship between hydraulic conductivity and moisture content. The model was applied to the top two meters of the subsurface, but could in theory be extended for the entire vadose zone, to better capture dynamics of recharge and soil moisture storage. This method calculated recharge at several discrete locations in the study area. Runoff was neglected in this study, but the model could be easily modified to account for this.

High spatial variability often confounds the estimation of recharge [29]. Soil types, vegetation characteristics and, to a lesser extent, climate, can vary significantly over small areas. Thus, point-based or lumped models offer an important but incomplete look at recharge. The effect of temporal distribution on recharge is also becoming more widely appreciated. As Carter and Parker [30] have noted, rainfall depth affects its allocation into the various components of the water cycle. Low rainfall depths will contribute to evapotranspiration; rain falling at higher depths will be preferentially allotted as runoff. Studies in Uganda found that annual recharge correlated more strongly with the number of rainfall events exceeding 10 millimeters [31] or the total rainfall in these events [32], than annual rainfall. However, work remains to be done to evaluate the effects of other characteristics of rainy season patterns on recharge.

2. Established Recharge Estimation Methods

The three methods in this study used to determine recharge are the Water-Table Fluctuation (WTF) Method, the Thornthwaite-Mather Water Balance (TMWB), and GMS MODFLOW Groundwater Model. These methods were selected because they are practical given available data and resources. The WTF method relies on estimates of specific yield and water level data to relate changes in water table elevation with recharge. The TMWB uses soil and weather data to execute a monthly water balance. MODFLOW is a three-dimensional finite-difference groundwater model, developed by the USGS [22], for which GMS is an interface combining MODFLOW's functionality with data types and models. Various sources were explored in order to obtain the necessary data, either directly by the author or members of the community or from government offices.

2.1. Water-Table Fluctuation Method

The water-table fluctuation (WTF) method has been used in many studies [21, 33, 34] to estimate recharge to aquifers using well hydrographs. This technique is generally preferred for systems with shallower water tables (less than 10 meters according to Sophocleous [33]) and thus a quicker response to precipitation, as well as monitoring of changes over intervals of a few days or less. However, this method has also been applied in deeper groundwater tables with a longer monitoring interval [34]. While minor rises and falls are neglected in this latter approach, the method still gives a helpful estimate of recharge over a longer time span, on the order of months to a year. The two components required are a well hydrograph of the well, or wells, in question and an estimate of specific yield.

2.1.1. Well Data

Within the study area, numerous hand-dug wells are used for drinking, hygiene and dry-season gardening. Twenty-nine of these wells were surveyed regularly over the course of a year, from October 2013 to October 2014. The start and end dates coincide roughly with the end of the preceding rainy season. A handful of these wells were not used, either because of structural instability or contamination with salt or trash. All salty wells were described by community members to have always been salty. In order to construct a well hydrograph, periodic well level measurements were taken at each well. Well level measurements were critical to establishing the height of the water table, and to provide a reference against which changes in well levels, either due to extractions or recharge, could be determined. Prior to surveying, each well's position was recorded on a handheld GPS unit (eTrex® 20, Garmin, Olathe, KS). The height of the casing for each well was also measured. Whether the well water was salty or not, or in use or not, was determined in conversations with community members. Surveying took place early in the morning, before any community members began drawing water. It was assumed that the water levels were at static conditions at this time, having had enough time to recover fully from pumping the evening before (roughly 8 to 9 hours).

Surveying took place in the following manner. Approximately every three weeks, the depth in each of the readily accessible wells was measured with a measuring tape. Initially, the tape was simply lowered into the well, with perturbations of the water (seen by reflections from the author's headlamp) indicating at what depth the tape reached the water table. The depth and time of the reading was then recorded. The lack of tension in the flexible tape and the construction of some of the wells led to some erroneous readings, which were discarded. Because of this, and to increase confidence in measurements, a small wooden float was attached to the tape after the first two rounds of readings. The tape was lowered into the

wells until the float reached the water table. It was then moved up and down vertically in order to ascertain the moment when the surface tension of the water had the greatest pull on the float, indicating that the line was relatively taut. This depth was recorded, along with the date and time of measurement.

When determining true depth to water table, the casing height above the ground surface was subtracted from the value recorded. Any additional length from the float, or from the end of the measuring tape to 0 cm, was added, giving a true depth to water table. The elevation at each point was determined from Shuttle Radar Topography Mission (SRTM) Digital Elevation Model (DEM) data, available at 30-m spatial resolution. Finally, the actual height of the groundwater table was determined by subtracting depth from the elevation at each well.

Once hydrographs were constructed for each well, these were arranged according to relative geographic location and visually analyzed. Four general trends were classified for the wells in the study area:

Class A: Consistently increasing throughout the recording period

Class B: Slight rise in water table, followed by a steep decline and a second, steep rise at the end of the recording period

Class C: Generally flat at the beginning of the recording period, with a strong rise in the last couple months of recording

Class D: A modest rise, followed by a plateau, succeeded by a second rise

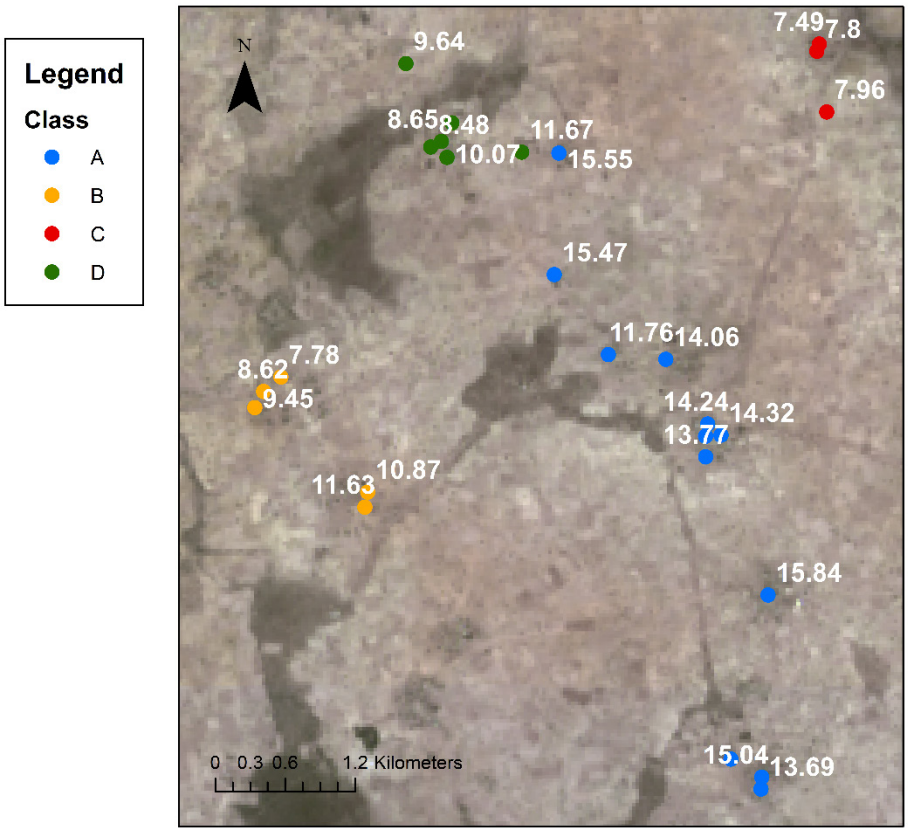

Figure 2.1 Areal distribution of classes of wells, based on hydrograph. Numbers next to markers are average depth to water table from ground surface in meters.

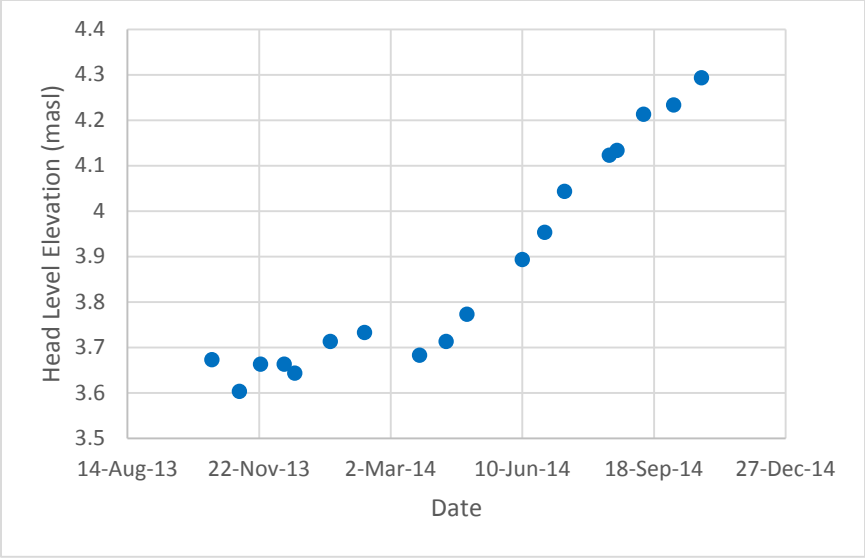

Figure 2.2 Sample Class A Well Hydrograph. masl = meters above sea level.

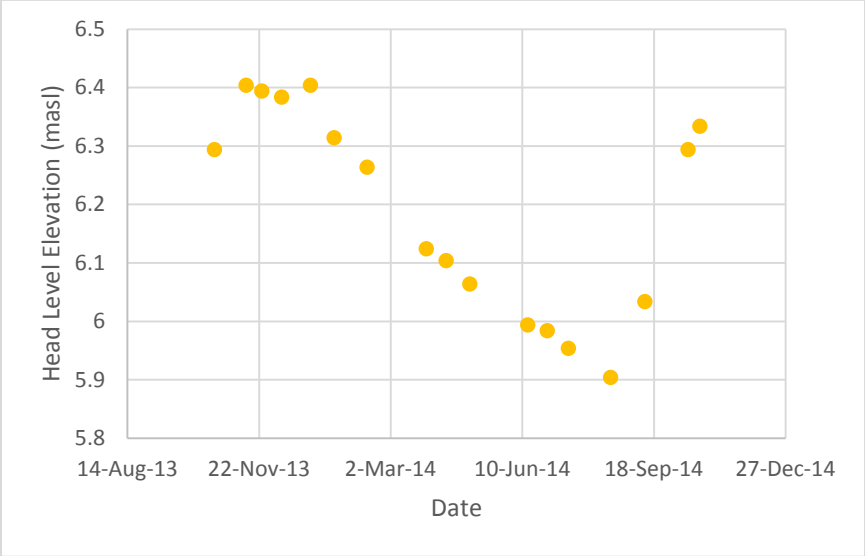

Figure 2.3 Sample Class B Well Hydrograph

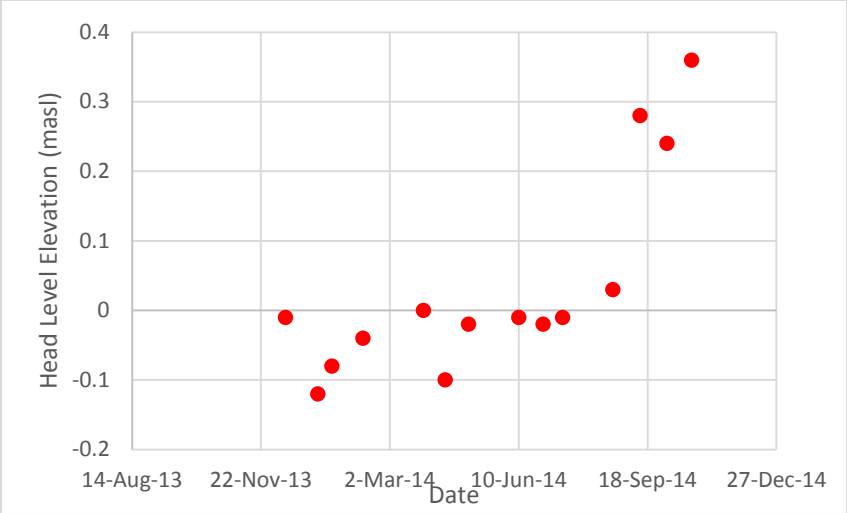

Figure 2.4 Sample Class C Well Hydrograph

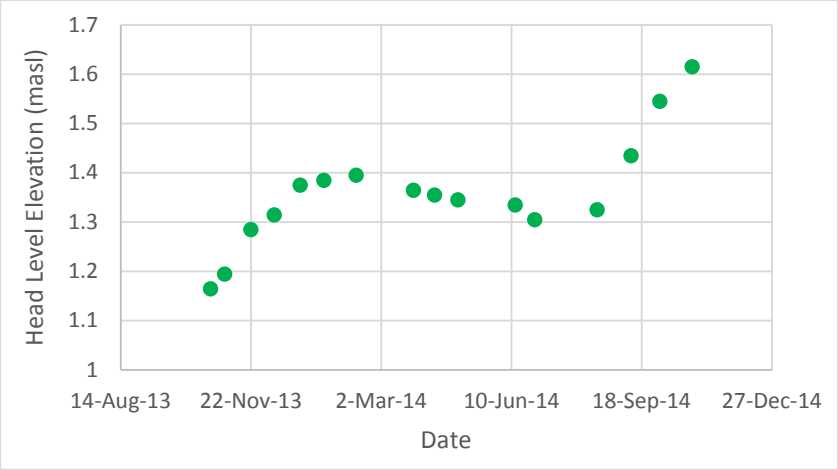

Figure 2.5 Sample Class D Well Hydrograph

Each well class corresponds to a water depth range and geographic location in the study area (Figure 2.1). Figure 2.2 through Figure 2.5 are actual well hydrographs from each class, selected because they tended to best represent the general behavior of each class. Class A was in the central and southern region of the wells studied, and tended to have the deepest water tables (ranging from 11 to 15 meters). The constant increase in water level could be due to the lag of transmitting water from the surface or root zone to the water table. For these, it was difficult to distinguish recharge from the previous rainy season from that of the more recent season.

Class B was in the west-central portion of the region, with mid-range water table depths, varying from 8 to 11 meters. It is hypothesized that this area has a higher hydraulic conductivity, which could explain why little recharge from the 2013 season appeared on the graph. It had likely already reached the aquifer and, as can be seen on the hydrograph, begun to rapidly discharge according to the hydraulic gradient.

Class C is characterized by a shallow water table (8 meters) and location in the northeast region of the study area. Class C is located near a fairly large seasonal water body which dries up around December (two months after completion of the rainy season). It may also have a

fairly high permeability, allowing for negligible recharge after the end of the rainy season. The water body may have been discharging into the aquifer, enabling its water level to remain fairly consistent, until recharge began again for the 2014 rainy season.

Class D is located in the northwest portion of the study area, and is characterized by moderate water table depths (8 to 11 meters). It is surmised, as for Class B and C, that this area had higher hydraulic conductivity, allowing for the rapid response of the water table.

The water table fluctuation method can be a powerful tool for estimating total recharge to aquifers by using specific yield values and water level information. However, there are important restrictions on its use. To better observe minor fluctuations in the groundwater table, water level data is preferably collected on a daily basis. The WTF method also assumes that all recharge is happening naturally, i.e., no water is being artificially recharged to or removed from the aquifers (by evapotranspiration, pumping, etc.) [21].

The above assumptions were addressed as follows. The wells were used for consumption and not artificial recharge; to approximate water usage by the community, the number of vessels carried away from the well were counted and multiplied by the approximate volume of the vessel (Table 2.1). For most wells surveyed, withdrawals took place both in the morning and afternoon. The results of the water abstraction observations are displayed below. The three seasons in Senegal comprise the rainy season (June to October), where nearly all rainfall takes place; the cool dry season which follows directly after (November to February), characterized by relatively cool temperatures; and the hot dry season (March to May).

Table 2.1 Summary of Well Usage for Surveyed Wells

	Total Withdrawal (m^3/day)			
Well	Hot Dry	Rainy	Cool Dry	Average
1	-	-	1.779	1.779
2	-	-	0.900	0.900
3	-	-	0.863	0.863
4	0.874	0.105	0.874	0.618
5	8.311	6.768	-	7.539
6	-	2.779	-	2.779
7	-	-	2.826	2.826
8	-	0.851	-	0.851
9	-	2.304	-	2.304
10	-	-	5.947	5.947
11	-	-	4.763	4.763
12	5.884	1.874	1.295	3.018
13	-	-	1.442	1.442
14	-	-	0.526	0.526
15	-	-	0.837	0.837
Grand Mean			2.466	
Standard Deviation			2.044	
Coefficient of Variation			0.829	

Seven wells were not used for water withdrawals, due to poor construction or contamination with salt or trash. The area encompassing the wells that were surveyed comprises roughly 30 square kilometers. Using an average water usage for each well of 2.47 m^3/day, an equivalent depth of water for the study area can be determined.

$$\frac{Daily\ consumption\ per\ well\left(\frac{m^3}{day \cdot well}\right) \times Number\ of\ Wells\ \times 365\ \frac{days}{year} \times 1000\ \frac{mm}{m}}{Area\ (m^2)}$$

$$= Annual\ Equivalent\ Depth\ \left(\frac{mm}{year}\right)$$

The calculations based upon field observations result in an equivalent depth of withdrawal of 0.66 mm per year across the study site. Thus, water abstraction from hand dug wells is an insignificant part of the water budget for the area (0.094% of the average annual rainfall, 704 mm), and can be reasonably neglected in calculations with the WTF method. However, it is possible that withdrawals from the night before may have affected morning readings at several wells; this is an effect that is neglected in the current study. Water was also supplied to villages via five freshwater boreholes (see Figure 2.6). The borehole logs for these were analyzed, and it was observed that most well screens were situated beneath a sandy clay layer. This is an indication that this layer is restricting flow to an appreciable extent, and can be considered a semi-confining layer. Figure 2.6 shows the average elevation of water in meters of the hand dug wells (blue circles) and the static water elevation in meters of boreholes (black squares). From the figure, it is clear there is a significant difference in elevation between the water abstracted via hand dug wells and boreholes. Elevation data was retrieved from the Shuttle Radar Topography Mission (SRTM), and was available at 30-m resolution from the US Geological Survey. Thus, the aquifers into which the hand dug wells and boreholes tapped are regarded as separate and not hydrologically connected for the purposes of this study.

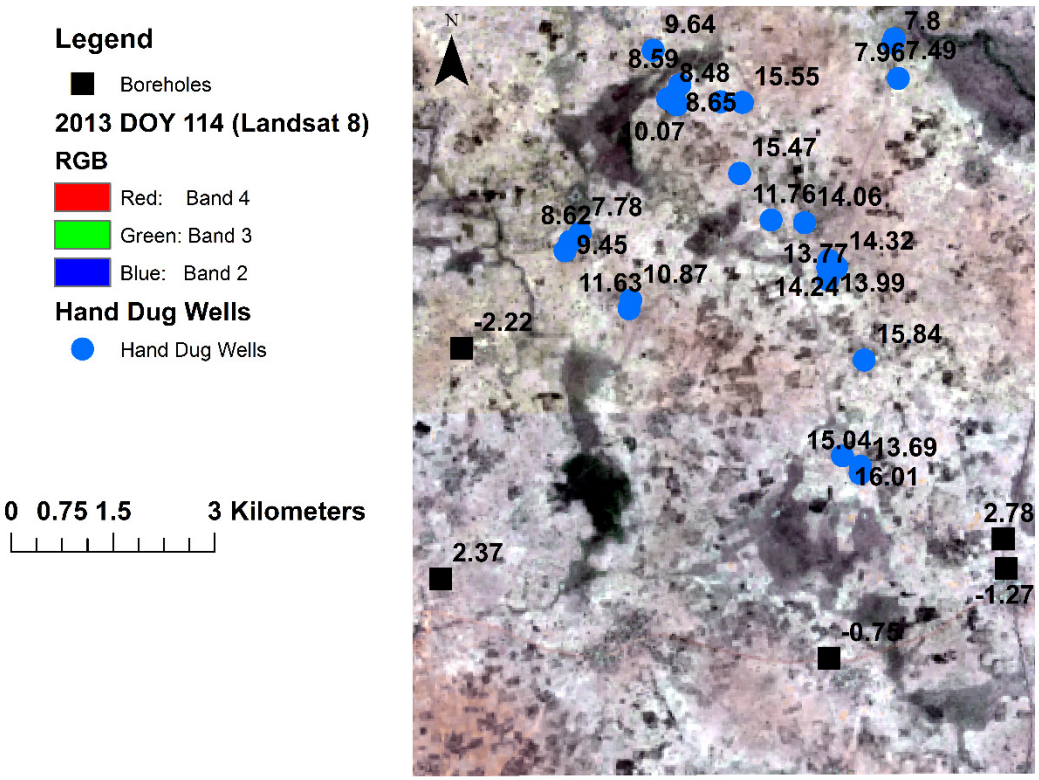

Figure 2.6 Hand dug wells and freshwater boreholes. Numbers next to hand dug wells indicate average elevation of water over surveying record, in meters above sea level. Numbers next to boreholes indicate static water level in meters above sea level.

Given that the water table was 8-16 meters below ground surface, it was assumed that no significant evapotranspiration (ET) occurred directly from the water table, which is consistent with other studies, such as Shah, et al. [35].

Because 22 of the 29 wells were used for consumption, level readings needed to be made before pumping began, typically soon after dawn. These wells were also spread out over a large area (30 square kilometers), and bicycle was the only available mode of transport. For this reason, level readings were made every 3 weeks on average, as opposed to daily. Well hydrograph information was collected beginning at the end of the 2013 rainy season (October) and concluding after the 2014 rainy season (October). Most well hydrographs did not exhibit a complete recharge/recession cycle in this time frame. Many deep wells displayed more drawn-out recharge patterns, owing to a thicker unsaturated zone, so recharge occurring after measurements stopped in 2014 is not accounted for. It is likely shallow wells would display significant recharge during the rainy season, which was not captured with respect to the 2013 season. For this reason, it was important to find a well hydrograph which seemed to have a complete recharge cycle contained within its hydrograph. Two wells, one each from Class A and Class B, exhibited these characteristics. For Well A, located in Class A, water levels began increasing several weeks after rains ended in 2013, and continued increasing throughout the recording period (see Figure 2.7). For Well B, located in group B, well levels increased slightly after the rainy season, then declined for the next several months, then increased again during the 2014 rainy season (see Figure 2.8). These are discussed in more detail in the following pages.

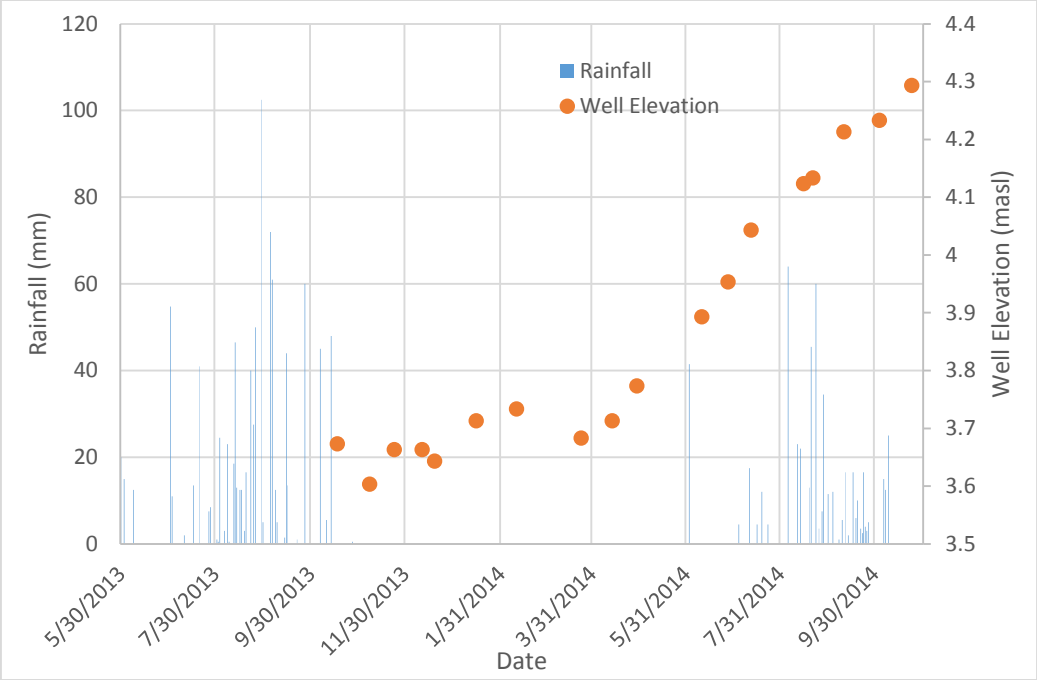

Figure 2.7 Well Hydrograph for Well A, Oct 2013 - Oct 2014

Figure 2.7 illustrates that that the period immediately following the rainy season saw small fluctuations in the water table, amounting to negligible recharge. Not until three or four months after the rainy season did the water table increase noticeably, and from this point it continued to increase through the surveying period. It is assumed that the water table would cease rising at about the same time every year, so the water table could be expected to cease rising shortly after surveying ended. Thus, all of the water table rise observed in this hydrograph is considered the result of the 2013 rainy season.

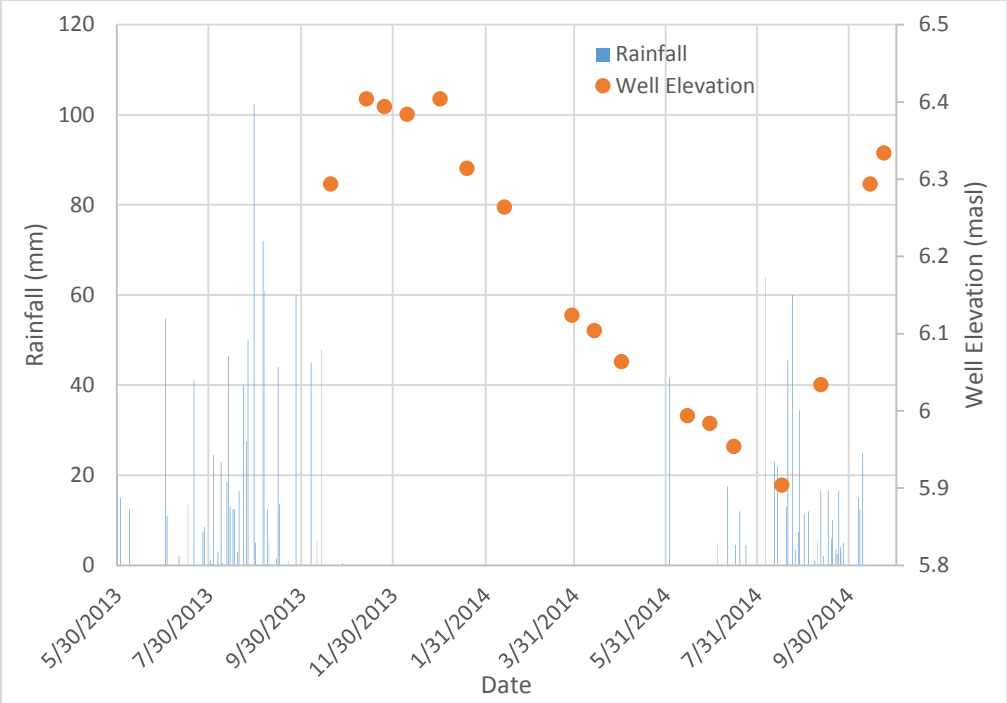

Figure 2.8 Well Hydrograph for Well B, Oct 2013 - Oct 2014

In Figure 2.8, a slight rise follows the end of the rainy season, with a subsequent and sustained decline, followed by a second, significant rise. Because the peak of the recharge owing to the 2013 rainy season occurred in mid-November, it is assumed the peak of the recharge owing to the 2014 rainy season would also occur in mid-November. Rainfall in 2013 and 2014 was 955 mm and 526 mm, respectively. Furthermore, rainfall in October 2013 was almost twice as much as in October 2014, and occurred later as well (see Table 2.2). This could explain the slight rise in the well hydrograph after the November 12th peak in 2013, as well as demonstrate that a similar such rise would be unlikely to occur in 2014 after surveying ceased.

Table 2.2 Daily Rainfall, October, 2013 and 2014.

Calendar Date	Rainfall (mm)	
	2013	2014
10/1	0	0
10/2	0	0
10/3	0	0
10/4	0	0
10/5	0	0
10/6	45	15
10/7	0	12.5
10/8	0	0
10/9	0	25
10/10	5.5	0
10/11	0	0
10/12	0	0
10/13	48	0
Total	98.5	52.5

Lastly, the rate of change for the well hydrograph dropped noticeably at the end of the surveying period (Figure 2.9). Rate of change is defined as the change in water table elevation from one survey date to the next, divided by the number of days in between surveying dates. Comparing the rate of change at the first and final survey dates further demonstrates that additional recharge was unlikely to occur.

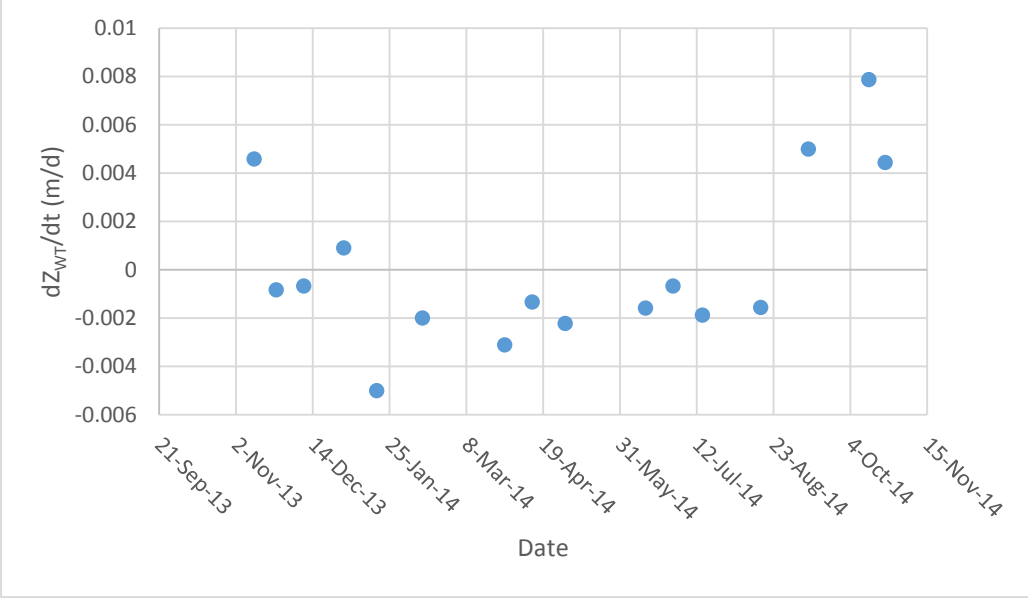

Figure 2.9 Rate of Water Table Change over surveying period, Well B. Note that the rate of change of the first point and the last are nearly equal.

2.1.2. Specific Yield Data

Soil samples were taken throughout the study area, and while these were primarily from shallow strata (40 cm or less), one such sample site was in close proximity to Well A. At one additional site, less than a mile from Well B, another well had been recently dug. Soil samples were secured for each layer or stratum from ground surface to the water table. The thickness of each strata and representative soil samples for each were identified by the well digger, soon after its completion. The National Pedology Institute in Dakar, Senegal, provided a texture analysis of both the surficial soil samples as well as those from the well. Surface-level soil samples were analyzed for Well A, and deep soil samples were analyzed for Well B, based on their relative locations. Results from this texture analysis are presented in Table 2.3.

Table 2.3 Soil Texture Characteristics

	Texture Class				
Location	Coarse Sand	Medium Sand	Fine Sand	Silt	Clay
Well A, % by weight	1.04	19.36	28.09	19.01	32.5
Well B, % by weight	0.63	13.63	9.655	51.835	24.25
Avg Specific Yield [36]	0.27	0.26	0.21	0.08	0.02

The samples near Well A and Well B are classified as a sandy clay loam and a silty loam, respectively, by the USDA soil classification system [37]. Using average specific yield values for coarse, medium and fine sand, silt and clay from Johnson [36] and finding the weighted average resulted in a specific yield of 13.38% and 5.74% for Well A and B (Table 2.3). Healy and Cook [21] reference a study by Duke [38] which found a specific yield of 34% for silt loam at 1.6 meters below the water table. Lastly, values of 30% are often assumed for unconfined aquifers, but this would apply to the entire aquifer, not just the layer closest to the water table, as it is applied here in the case of Well B. Clearly there is tremendous uncertainty in the value of specific yield; however, values of 13.5% and 6% will be used moving forward for Well A and B, respectively.

2.1.3. Master Recession Curve Approach

Once a well hydrograph has been constructed and specific yield estimated, it is important to estimate the recession curve that occurs before recharge takes place. Water table elevations will decrease according to the hydraulic gradient, and will theoretically decrease more rapidly for a steeper gradient, indicating a relationship between water table elevations and water table decline rates. Since recession is theoretically constantly occurring, any recharge observed is also making up for that water lost to recession. Thus, the water table rise must be calculated with reference to the level at which the water table would have been in the absence of recharge. A few methods exist for calculating the recession, including a graphical approach, and a Master Recession Curve (MRC). A MRC takes into account the fact that the rate of water table decline will change according to water table elevation, owing to the difference in hydraulic gradient that causes the recession. Heppner and Nimmo [39] developed a MATLAB code, known as MRCR, in order to determine the MRC, as well as total recharge.

Well hydrograph data for each of the two wells selected for further analysis, including day and water table elevation, were read into the MATLAB program. The MRCR program offers four options for calculating recharge using water table information: linear, power, bin-averaged,

and user-defined tabulated. Only the linear and bin-averaged options were explored. The linear approach relies on a linear fit to water-table decline rate vs water-table elevation data. The bin-averaged option breaks the water-table elevation data into a user-specified number of bins, into which elevation data is evenly separated. Water-level decline information is assigned to the corresponding bin. The user selects whether to use the mean or median decline rates from the binned data. The program then interpolates between these average points to calculate the decline rate.

The linear approach relies on selecting coefficients that give a best fit to the data according to the equation:

$$Decline\ rate = \frac{dZ_{WT}}{dt} = aZ_{WT} + b$$

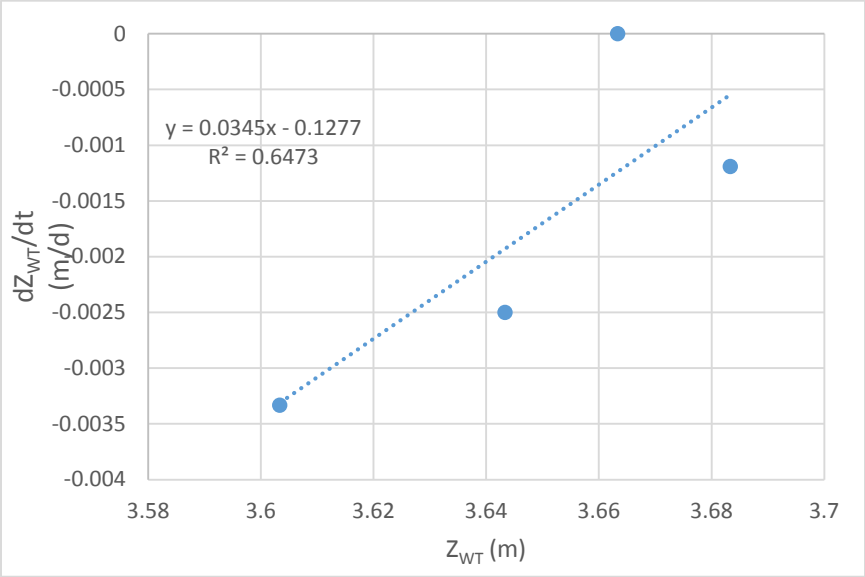

Figure 2.10 Water Table decline rate vs WTE with trendline for Well A

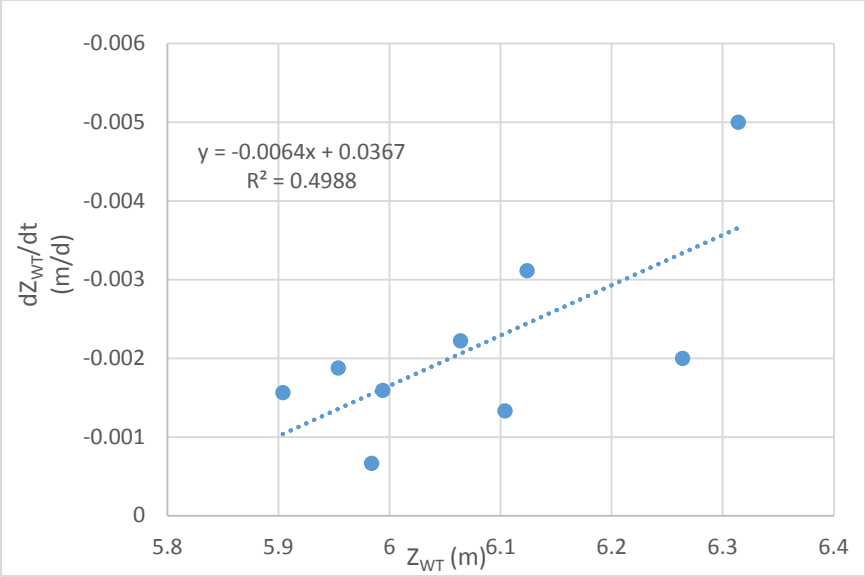

Figure 2.11 Water Table decline rate vs WTE with trendline for Well B

Figure 2.10 and Figure 2.11 were used to calculate the slope and intercept using a best-fit linear regression for each well. The MRCR program also requires information regarding the minimum and maximum rate of water table decline. These were found from the 2013-2014 hydrograph data, and were -0.00119 m/d and -0.003333 m/d for Well A, and -0.00067 m/d and -0.005 m/d for Well B. Negatively valued recharge estimates can be included, but as they are primarily used when working with high frequency hydrographs, they were not used in this approach. The relationships presented here were used to determine a decline rate at each data point on the corresponding well hydrograph. This resulted in a recession curve, indicating the decline of the water table according to the hydraulic gradient, presented in Figure 2.12 for Well B. If subsequent data points had higher well levels, then the change in water level was calculated as the difference between the observed water level, and the projected water level according to the recession curve. Thus, individual recharge events were determined on a point-by-point basis, and summed to find total recharge.

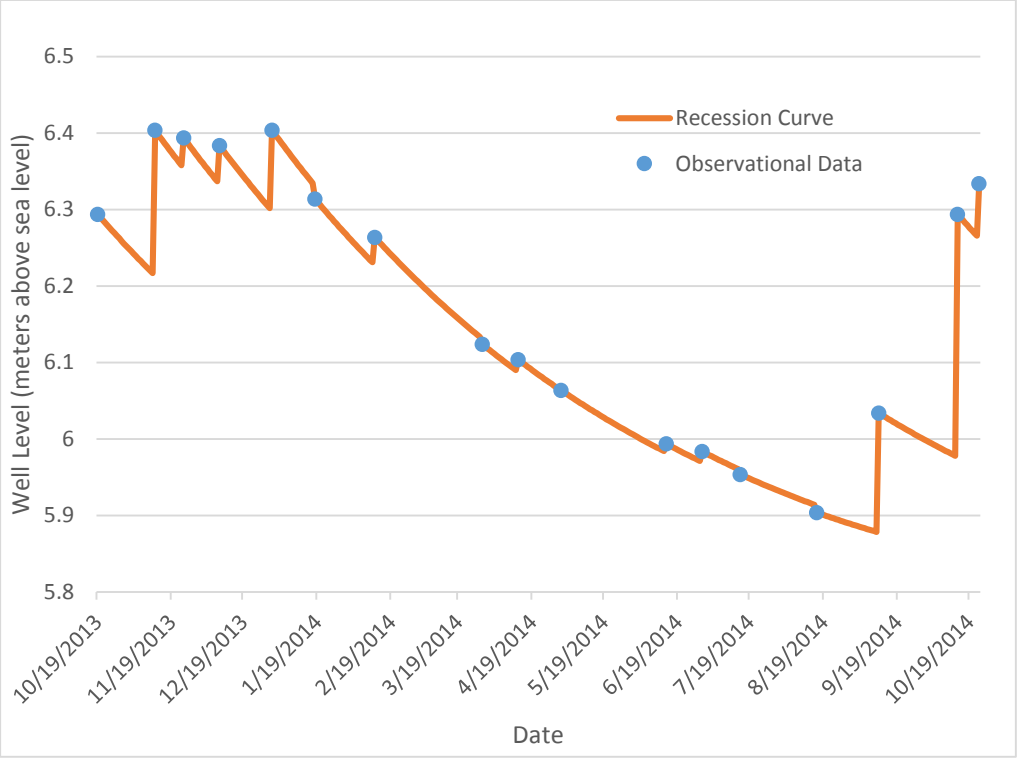

Figure 2.12 Recession Curve for Well B, demonstrating decline of water table due to the hydraulic gradient.

The bin-averaged approach was also explored. The elevation information of the well, including rate of decline of the water table at a given depth, was divided into 4, 5 and 6 bins to evaluate the sensitivity of this to the number of bins used.

Results from these runs are summarized in Table 2.4. Recharge for Well B was considered only after June 2014, to reflect only recharge corresponding to the 2014 rainy season.

Table 2.4 Recharge estimates

	Recharge Estimate by Method (mm)			
	Linear	Bin		
		Number of Bins		
Well		4	5	6
Well A	158	150	150	150
Well B	33	33.7	32.2	33.6

For the sake of comparison, simply taking the difference between low and high water table elevations over the period studied (ignoring the recession curve) gives results of 93.2 and 20.4 mm for Well A and Well B, respectively. Heppner and Nimmo [39] note that linear or power methods may be more suitable when less data is available and the data have a clear trend. Additionally, there is good agreement between linear and bin estimations. Thus, the estimates of 158 mm for 2013 and 33 mm for 2014 will be used hereafter in this work to compare with

other model estimates. Again, the spatial applicability of this method is highly variable as noted in Section 1, but these estimates will be considered applicable to the entire study area.

2.2. Thornthwaite-Mather Water Balance

The Thornthwaite-Mather Water Balance (TMWB) is an accounting procedure used for determining climatic trends in the water budget on a monthly basis. Its data requirements are fairly modest, and thus lends itself to easy application to many locations around the world.

2.2.1. Weather Data Sources

The TMWB can be conducted with just temperature and precipitation data (using the Hamon method of calculating ET, for instance [40]); however, for consistency with the MATLAB model in calculating ET, the FAO 56 Penman-Monteith method was used, which requires humidity, wind speed and solar radiation data as well. Daily data compiled from the National Oceanic and Atmospheric Administration, the Norwegian Meteorological Institute, and World Weather Online was utilized. Weather data was available for the Kaolack weather station, located roughly 15 km northeast of the study site, and was utilized for subsequent calculations. Weather parameters collected are summarized in Table 2.5.

Table 2.5 Weather Parameters and Units used in determination of evapotranspiration

Weather Parameter	Units
Cloud cover fraction	-
Minimum and maximum dew point	Degrees Celsius
Minimum, maximum and average relative humidity	Percent
Minimum and maximum temperature	Degrees Celsius
Average wind speed	m/s

Additional parameters were available (pressure, minimum and maximum wind speed, wind direction) but these were not used in the following calculations. Additionally, rainfall data at the same site as that where climate data were gathered for 2013 and 2014 were not available, and were drawn from that gathered by local rain gauges close to the study area.

2.2.2. FAO 56 Penman-Monteith Method

The Penman-Monteith method is the most extensively used methodology for assessing ET from terrestrial surfaces, and is preferred when the requisite data are available [23]. The Food and Agriculture Organization of the United Nations, in the 56th Crop and Irrigation paper, developed a modified form of this equation that can be modified for use with most vegetation [14]. The base form of the Penman-Monteith equation is:

$$\lambda ET = \frac{\Delta(R_n - G) + \rho_a c_p \frac{(e_s - e_a)}{r_a}}{\Delta + \gamma\left(1 + \frac{r_s}{r_a}\right)}$$

where

λET = Latent heat flux

R_n = net radiation

G = soil heat flux

(e_s – e_a) = vapor pressure deficit of the air

ρ_a = Mean air density at constant pressure

c_p = specific heat of the air

Δ = slope of the saturation vapor pressure temperature relationship

γ = the psychrometric constant

r_s = bulk surface resistance

r_a = bulk aerodynamic resistance

This equation was then simplified assuming a reference grass crop that is 0.12 m in height, with a surface resistance of 70 s m^{-1} and an albedo of 0.23. These assumptions result in reference ET (RET or ET_0), which describes the depth of water that would be transpired by this reference grass crop, assuming it is actively growing, covers the ground, and has plentiful water. It is calculated in the following equation:

$$ET_0 = \frac{.408\Delta(R_n - G) + \gamma \frac{900}{T + 273} u_2(e_s - e_a)}{\Delta + \gamma(1 + 0.34u_2)}$$

where:

ET_0 = reference evapotranspiration (mm day^{-1})

R_n = net radiation at the crop surface (MJ m^{-2} day^{-1})

G = soil heat flux density (MJ m^{-2} day^{-1})

T = mean daily air temperature at 2 m height (°C)

u_2 = wind speed at 2 m height (m s^{-1})

e_s = Saturation vapor pressure (kPa)

e_a = Actual vapor pressure (kPa)

e_s – e_a = saturation vapor pressure deficit (kPa)

Δ = slope of the vapor pressure curve (kPa $°C^{-1}$)

γ = psychrometric constant (kPa $°C^{-1}$)

Calculation of net radiation at the crop surface, R_n, begins with calculating extraterrestrial radiation, R_a:

$$R_a = \frac{24(60)}{\pi} G_{SC} d_r [\omega_s \sin(\varphi) \sin(\delta) + \cos(\varphi) \cos(\delta) \sin(\omega_s)]$$

where

R_a is extraterrestrial radiation (MJ/m^2 d)

G_{SC} is the solar constant = 0.082 MJ/m^2 min

d_r is the inverse relative distance from Earth to the Sun

ω_S is the sunset hour angle (rad)

φ is latitude (rad)

δ is solar declination (rad)

The inverse relative distance Earth-Sun is:

$$d_r = 1 + 0.033 \cos\left(\frac{2\pi}{365} J\right)$$

where

J is the Julian day.

Solar declination is given by:

$$\delta = 0.409 \sin\left(\frac{2\pi}{365} J - 1.39\right)$$

The sunset hour angle is calculated as:

$$\omega_S = \cos^{-1}[-\tan(\varphi)\tan(\delta)]$$

Daylight hours are calculated by:

$$N = \frac{24}{\pi}\omega_S$$

Solar radiation can be calculated with the Angstrom formula:

$$R_S = \left(a_s + b_s \frac{n}{N}\right) R_a$$

where

R_s is solar or shortwave radiation (MJ/m^2 d)

n is the actual duration of sunshine (hr)

N is the maximum possible duration of sunshine or daylight hours (hr)

n/N is relative sunshine duration

R_a is extraterrestrial radiation (MJ/m^2 d)

a_s is a regression constant, expressing the fraction of extraterrestrial radiation reaching the earth on overcast days (n=0)

a_s+b_s is the fraction of extraterrestrial radiation reaching the earth on clear days (n = N)

Recommended values for a_s and b_s where no calibration has been carried out, and no actual solar radiation data are available, are 0.25 and 0.5, respectively.

Clear-sky solar radiation is calculated as:

$$R_{so} = (0.75 + 2 \times 10^{-5} z) R_a$$

where

z is station elevation above sea level (m)

The station elevation is 14 m.

Net shortwave radiation is given by:

$$R_{ns} = (1 - \alpha) R_s$$

where

R_{ns} is the net solar or shortwave radiation (MJ/m^2 d)

α is albedo or the canopy reflection coefficient. This is .23 for the hypothetical grass reference crop (dimensionless).

Net longwave radiation is

$$R_{nl} = \sigma \left[\frac{T_{max,K}^4 + T_{min,K}^4}{2}\right] (0.34 - 0.14\sqrt{e_a}) \left(1.35 \frac{R_s}{R_{so}} - 0.35\right)$$

where

R_{nl} is net outgoing longwave radiation (MJ/m^2 d)

σ is the Stefan-Boltzmann constant (4.903x10-9 MJ/K^4 m^2 d)

$T_{max,K}$ is the maximum absolute temperature during the 24-hour period (K)

$T_{min,K}$ is the minimum absolute temperature during the 24-hour period (K)

e_a is the actual vapor pressure (kPa)

Net radiation, finally, is

$$R_n = R_{ns} - R_{nl}$$

The calculation for wind speed at 2 m above ground is as follows:

$$u_2 = u_z \frac{4.87}{\ln(67.8z - 5.42)}$$

where

u_2 is the wind speed at 2 m above ground surface (m/s)

u_z is the measured wind speed at z m above ground surface (m/s)

z is the height of measurement above ground surface (m)

The height of measurements at the Kaolack weather station was estimated to be 10 m, in line with standard practice for recording wind speed.

Atmospheric pressure is calculated according to:

$$P = 101.3 \left(\frac{293 - 0.0065z}{293}\right)^{5.26}$$

where

P is atmospheric pressure (kPa)

z is elevation above sea level (m)

Pressure was also provided, but since it varied minimally over the course of measurement, a constant pressure value, calculated here, was used instead.

The psychrometric constant is given by:

$$\gamma = \frac{c_p P}{\varepsilon \lambda} = 0.665 \times 10^{-3} P$$

where

γ is the psychrometric constant (kPa/ºC)

c_p is the specific heat of air at constant pressure, 1.013x10-3 (MJ/kg ºC)

ε is the ratio of molecular weight of water vapor to dry air = 0.622

The latent heat of vaporization, λ, is assumed constant at 2.45 MJ/kg due to the fact that it varies minimally over a normal range of temperatures.

The average temperature of a 24-hour period is

$$T_{mean} = \frac{T_{max} + T_{min}}{2}$$

The saturation vapor pressure is calculated as:

$$e^o(T) = 0.6108exp\left[\frac{17.27T}{T + 237.3}\right]$$

where

$e^o(T)$ is the saturation vapor pressure at the air temperature T (kPa)

T is the air temperature (°C)

exp[..] is 2.7183 (base of the natural logarithm) raised to the power [..]

The mean saturation vapor pressure is calculated as:

$$e_s = \frac{e^o(T_{max}) + e^o(T_{min})}{2}$$

The slope of the saturation vapor pressure curve is:

$$\Delta = \frac{4098\left[0.6108exp\left(\frac{17.27T}{T + 237.3}\right)\right]}{(T + 237.3)^2}$$

where

Δ is the slope of the saturation vapor pressure curve at air temperature T (kPa/°C)

In the FAO Penman-Monteith equation, the slope is calculated at mean temperature.

Actual vapor pressure can be calculated using psychrometric data, as follows:

$$e_a = e^o(T_{dew}) = 0.6108exp\left[\frac{17.27T_{dew}}{T_{dew} + 237.3}\right]$$

where

e_a is actual vapor pressure (kPa)

T_{dew} is dew point temperature

Actual vapor pressure can also be calculated using relative humidity data:

$$e_a = \frac{e^o(T_{min})\frac{RH_{max}}{100} + e^o(T_{max})\frac{RH_{min}}{100}}{2}$$

where

$e^o(T_{min})$ and $e^o(T_{max})$ are saturation vapor pressure daily minimum and maximum temperatures, respectively (kPa)

RH_{max} and RH_{min} are maximum and minimum relative humidity, respectively

e_a was calculated as the average of both of the preceding calculations, since both dew point temperature and relative humidity were available. Reference ET (RET) was calculated on a daily basis according to the above calculations, and summed on a monthly basis for the calculations in the TMWB.

2.2.3. Water Balance Methodology

The equations that provide the baseline for computing the water balance follow. These are adapted from Shonsey [40].

$$If\ P_m \geq PET_m, then\ ET_m = PET_m$$

$$If\ P_m < PET_m, then\ ET_m = P_m - \Delta Soil_m$$

$$\Delta Soil_m = Soil_m - Soil_{m-1}$$

$$Soil_m = Soil_{m-1}\left[exp\left(\frac{-PET_m - P_m}{Soil_{max}}\right)\right]$$

$$Soil_{max} = \theta_{fc} Z_{fc}$$

where:

P_m = Monthly Precipitation (mm)

PET_m = Monthly potential evapotranspiration (mm)

ET_m = Monthly actual evapotranspiration (mm)

ΔSoil = Monthly change in soil moisture (mm)

$Soil_m$ = Estimated soil moisture of current month (mm)

$Soil_{m-1}$ = Estimated soil moisture of previous month (mm)

$Soil_{max}$ = Maximum possible soil moisture (mm)

θ_{fc} = Field capacity of the soil (cm^3/cm^3)

Z_{fc} = Vertical extent of the root zone (mm)

When starting calculations, $Soil_{m-1}$ is equal to $Soil_{max}$.

Field capacity was estimated from soil samples retrieved from throughout the study area. Most of these samples were analyzed by the National Pedology Institute (INP) in Dakar. Using the texture analysis provided by the INP, the values for field capacity were calculated according to a program developed Saxton and Rawls [37]. The averaged results for varying locations throughout the study area are summarized below in Table 2.6, and displayed according to geographical location in Figure 2.13.

Table 2.6 Soil Sample Data

Location Number	Land Use	Soil Type	Total Depth (cm)	Average Field Capacity (cm^3/cm^3)
1	Field	Sandy loam	40	0.217
2	Forest	Sandy clay loam	40	0.249
3	Field	Sandy loam	40	0.162
4	Shrubland	Sandy loam	40	0.120
5	Forest	Loam	40	0.288
6	Field	Sandy clay Loam	40	0.287
7	Shrubland	Loam	40	0.231
8	Field	Silty loam	40	0.314
9	Field	Sandy loam	40	0.234
10	Farmstead	Sandy clay loam	227	0.276
			Mean	0.238

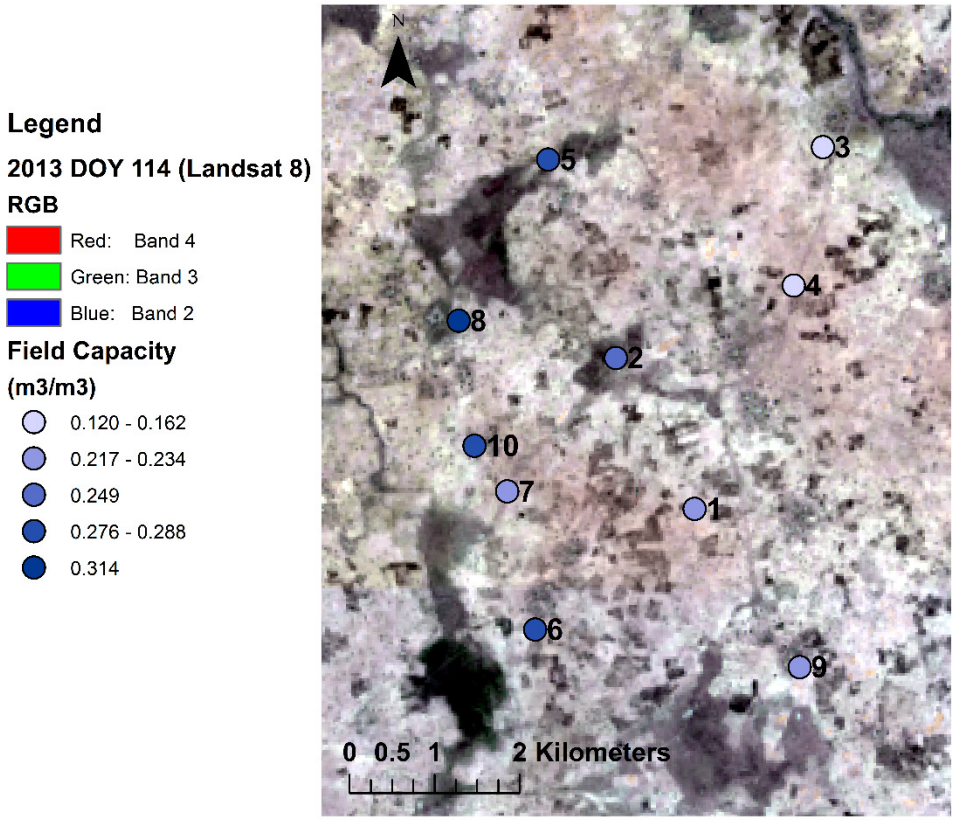

Figure 2.13 Relative location of soil samples within study area. Numbers correspond to location number, as in Table 2.6

The average for this set of soil samples is 0.238 cm^3/cm^3. The standard deviation was found to be about 0.057. Thus, three values were used for the Thornthwaite-Mather water balance incorporating this, to test the sensitivity of the model to field capacity: 0.18, 0.24, and 0.3 cm^3/cm^3.

Root depth was estimated to be an average of 1800 mm throughout the study area. This comes from values for tree and crop rooting depth in the literature, which provided values of 4 meters for Acacia seyal (representative of forested areas in the study site, [41]) and a maximum crop root depth of 1.05 m [14]. Based on analysis of the area after image classification, forested areas comprise approximately one-quarter of the area in question, and agriculture composes the remaining three quarters, resulting in an average root zone of 1800 mm for the whole study area. The effect of this parameter on the model was also tested by exploring a second depth of 1500 mm.

Using weather data from the nearby regional capital of Kaolack, RET was calculated on a daily basis and then aggregated on a monthly basis. A similar procedure was followed for precipitation data from the 2013 and 2014 rainy seasons, collected from a rain gauge in the nearby town of Keur Soce. The weather data used are summarized on a monthly basis in Table 2.7 and Table 2.8.

Table 2.7 2013 Monthly Rainfall and RET

2013	Jan	Feb	Mar	Apr	May	Jun	Jul	Aug	Sep	Oct	Nov	Dec	Sum
P (mm)	0	0	0	0	20	28	139	399	271	99	0	0	955
RET (mm)	193	229	278	257	251	197	156	118	121	144	168	176	2288

Table 2.8 2014 Monthly Rainfall and RET

2014	Jan	Feb	Mar	Apr	May	Jun	Jul	Aug	Sep	Oct	Nov	Dec	Sum
P (mm)	0	0	0	0	0	42	43	285	104	53	0	0	526
RET (mm)	196	206	243	250	235	198	173	139	121	155	161	165	2240

Compared with long term (91 years of record) rainfall data from the regional capital of Kaolack, rainfall in 2013 and 2014 was in the 87th and 21st percentile, respectively. Average rainfall for the entire period of record was 704 mm. Rainfall statistics and patterns are explored more in the appendix.

In TMWB calculations, the first month's soil moisture is typically assumed to be equivalent to maximum soil moisture. However, this was unlikely to occur in reality, given that January is three months after the end of the rainy season, and negligible precipitation occurs between the end of the rainy season and the beginning of the next. Thus, the calculated soil moisture from December was input as the soil moisture for January. The next calculation of December soil moisture was input as January soil moisture, until the difference was negligible. With the preceding inputs to the model, water balance information was obtained.

Table 2.9 2013 Annual Water Balance Summary

Root Zone (mm)	1500	1500	1500	1800	**1800**	1800	Average	Standard Deviation
Field Capacity (cm3/cm3)	0.18	0.24	0.3	0.18	**0.24**	0.3		
Soil Moisture max (mm)	270	360	450	324	432	540		
Avg Soil Moisture (mm)	89	126	169	112	163	189	141	35
Total AET (mm)	794	878	955	847	946	955	896	61
Total Runoff + Recharge (mm)	161	77	0	109	9	0	59	61

Table 2.10 2014 Annual Water Balance Summary

Root Zone (mm)	1500	1500	1500	1800	**1800**	1800	Average	Standard Deviation
Field Capacity (cm3/cm3)	0.18	0.24	0.3	0.18	**0.24**	0.3		
Soil Moisture max (mm)	270	360	450	324	432	540		
Avg Soil Moisture (mm)	42	49	56	47	55	63	52	7
Total AET (mm)	526	526	526	526	526	526	526	0
Total Runoff + Recharge (mm)	0	0	0	0	0	0	0	0

Results from these model runs are summarized in Table 2.9 and Table 2.10. The conditions in bold reflect the base case, or most likely combination of variables. The TMWB does not distinguish between recharge and runoff. Predictably, these charts demonstrate that the increase of maximum soil moisture (product of field capacity and root zone) lead to an increase in soil moisture and AET, and a corresponding decrease in water available for runoff and recharge. Figure 2.14 and Figure 2.15 demonstrate the variability in the above statistics. The lines plotted are actual data for P and RET (dotted), and average values for each year of the 6 scenarios tested for soil moisture, actual evapotranspiration (AET) and runoff plus recharge (RO+RCH, solid lines). Error bars represent the standard deviation of soil moisture, AET, and RO+RCH for each month.

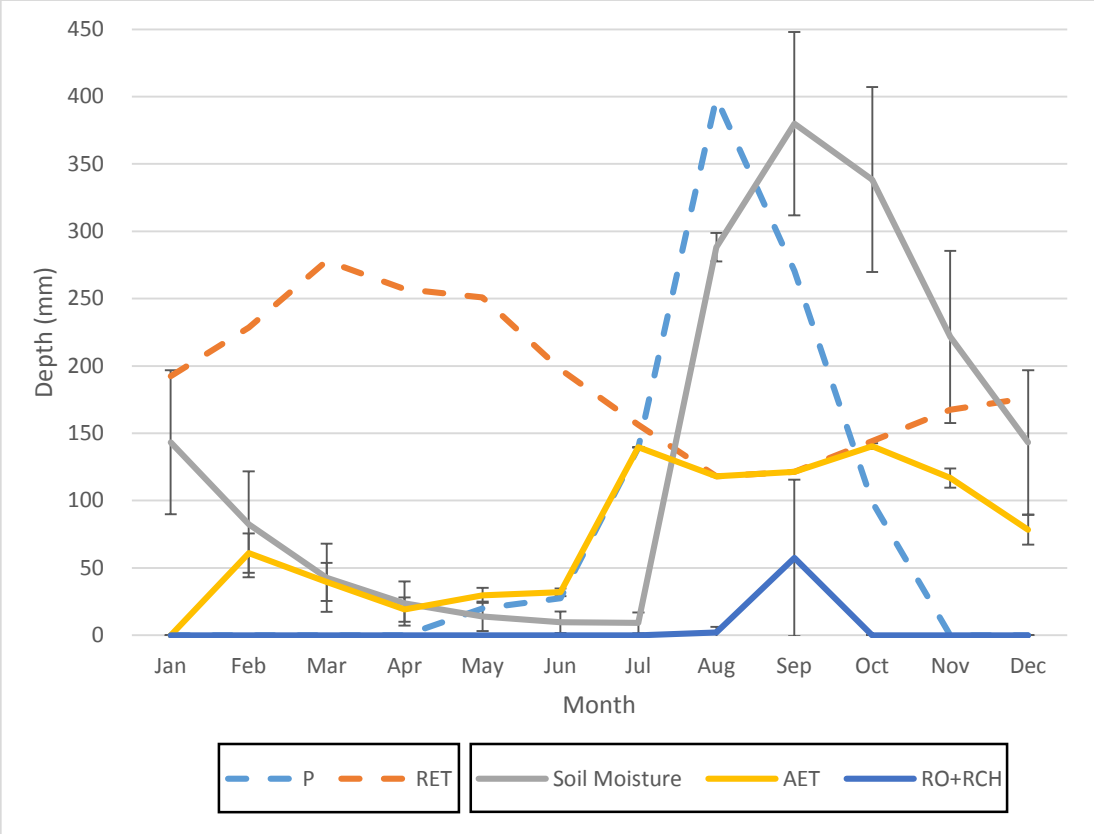

Figure 2.14 2013 Water Balance Summary

In 2013, recharge and runoff are mainly predicted to occur in September, with a negligible amount in August (Figure 2.14). Even so, there is high variability in this amount, owing to high dependence on the field capacity and rooting depth values. Recharge and runoff thus occurs only once the demands of RET and soil moisture have been met. Soil moisture is also highly variable, with most variability occurring in the first months of the balance, and the first couple of months after the peak amount of rain has fallen. AET shows very little variability between model runs.

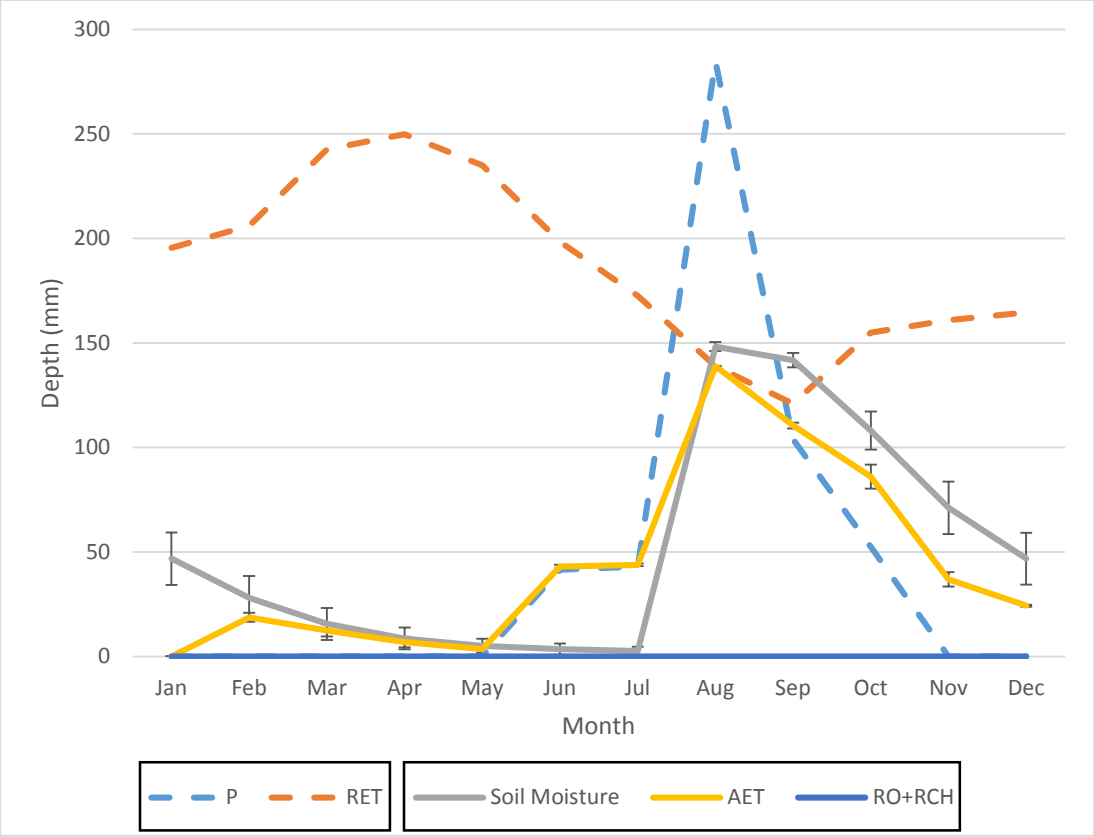

Figure 2.15 2014 Water Balance Summary

In 2014, all precipitation, after meeting the demands of RET, serves simply to replenish soil moisture (Figure 2.15). Soil moisture demonstrated moderate variability in the first two months of the model, but was consistent after that among model runs, owing in large part to the low rainfall input. AET was also consistent across model runs. 2014 had an unusually low amount of rainfall. In both cases, RET shows a trend of peaking during the hot dry season (March through May), and decreasing during the rainy season owing to an increase in humidity and cloud cover, and lower temperatures.

2.3. GMS MODFLOW Groundwater Model

GMS MODFLOW uses the finite difference method to evaluate groundwater flow in three dimensions, incorporating boundary conditions (such as head values), as well as properties of the subsurface (such as hydraulic conductivity) [22]. It is one of the most widely used groundwater modeling programs in the world, used by government agencies, researchers and companies.

2.3.1. Regional Model Setup and Calibration

In order to create a meaningful hydrologic model, boundary conditions must first be specified. However, the project site, outlined by the blue box shown in Figure 2.16, was not located near major topographic features that could be treated as boundary conditions, as the study area is predominantly flat. For this reason, a regional model was created that encompassed a much larger area, including several features that could be considered boundary

conditions. These are outlined in Figure 2.16. The map projection used was Universal Transverse Mercator 28-N.

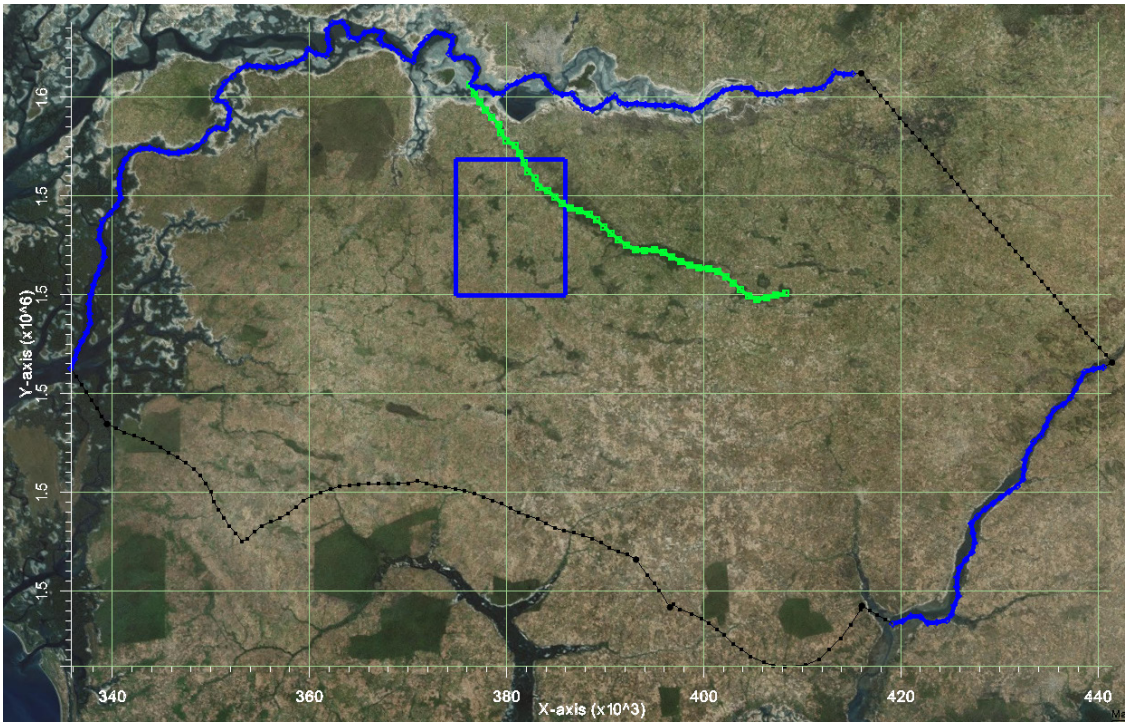

Figure 2.16 Outline of Regional Groundwater Model

The northern and western boundaries (blue) are concurrent with the Saloum Estuary and Diomboss River, respectively. The southern boundary was assigned a no-flow boundary (black), consistent with its demarcation as a groundwater divide, as in Faye, et al. [5]. The Bao Bolon River, a tributary of the Gambia River, formed the southeast boundary. The eastern boundary, finally, was modeled as a drain in initial models, but was later changed to a simple no-flow boundary (black). A chain of ephemeral ponds linked with the Saloum estuary extended far inland, and was modeled as a drain (green).

For each of the rivers and the chain of ponds, SRTM data was used to model the stage. A second elevation data set, offset below the SRTM data by 1.5 m, was used as the river bed. Head values were also needed to create a target for calibration. These were selected from Faye, et al. [5] and digitally imported into MODFLOW. A recharge value of 17.1 mm/yr, as determined by a British Geological Survey report [42], was used. This report included four estimates in the Kaolack region, located 60 km south of the study site: 11.7, 108, 18.1 and 21.6 mm/yr. Treating the 108 mm/yr estimate as an outlier, the average of the remaining results provides 17.1 mm/yr. It should be noted that the 108 mm/yr estimate was for an area of cleared vegetation. Further, these estimates were within a subset of the broader region of Kaolack, itself smaller than the extent of the regional model considered here. Therefore, additional variability beyond the values used for input to the model should be expected.

Borehole logs for each of the freshwater boreholes in the area were analyzed. Some provided values of transmissivity, according to the Cooper-Jacob and Jacob solutions. All logs were analyzed in AQTESOLV, using the Theis solution for a confined aquifer. These are summarized in Table 2.11.

Table 2.11 Summary of Hydraulic Conductivity Estimates

	Hydraulic Conductivity (m/d)	
Borehole	AQTESOLV	Borehole Log
Darou Mbiteyen	19.093	-
Keur Soce (New)	10.017	43.531
Lamaram Badiane	18.015	-
Ndiedieng	7.828	47.697
Taiba Niangene	9.403	-

No attempt was made to conduct a formal pumping test in the hand dug wells in the area, as relatively few wells in each community were available for pumping. A pumping test would require closing off access to a well, which would increase wait times at other wells, potentially severely affecting the ability of community members to draw the water needed for their daily tasks.

With these conditions set up, the conductance of each river and the ponds were varied manually, as well as hydraulic conductivity and horizontal anisotropy. Conductance is a measure of how quickly water flows through rivers or drains. As a finite-difference approximation method, GMS MODFLOW requires the area under study to be subdivided into three dimensional cells, the size of which are determined by the user. Within a MODFLOW model, cells are assigned values for head, conductance, hydraulic conductivity and other properties, based on available data and associated boundary conditions. Hydraulic conductivity was initially assumed constant for the whole region. Varying the conductance parameters for the rivers and drains had little effect on the agreement with observed head values, given that they predominantly controlled head values close to the boundary of the model. A series of forward runs were conducted with various values for each of the following parameters. The final modeled values for each boundary condition are presented in Table 2.12.

Table 2.12 Summary of GMS Boundary Conditions

Boundary	Location	Boundary Condition	Conductance ($m^2/d/m$)
Saloum River	North	River	200
Bao Bolon River	Southeast	River	25
Diomboss River	West	River	25
Ephemeral Ponds	Central	Drain	500

These runs gave poor agreement with the data set forth by Faye, et al. [5], given that one value for each hydraulic conductivity, horizontal anisotropy and recharge was chosen for the whole region. A value of 200 m/d for hydraulic conductivity and 10 for horizontal anisotropy returned a root-mean square error (RMSE) of 7.54 m.

The RMSE was calculated according to the following equation:

$$RMSE = \sqrt{\frac{1}{N}\sum_{i=1}^{N}\left(Y_i - \hat{Y}_i\right)^2}$$

where

N is the number of measurements

Y_i is the ith observed value

$\hat{Y}_i$ is the ith calculated value

Next, the entire region was broken up into 11 separate sub-regions to be calibrated by Automated Parameter Estimation (PEST) (see Figure 2.17). To use PEST, the user first specifies starting values, as well as maximum and minimum values for each parameter to be estimated. PEST then automatically varies the parameters specified by the user in order to best match observations. After 3 iterations with no reduction in error, calibration stops. Sub-region boundaries were chosen according to proximity to regional features, such as rivers. Remaining sub-regions which were not close to major features were divided arbitrarily to keep sub-regions of relatively uniform size. Each sub-region was independently calibrated by varying hydraulic conductivity; while hydraulic conductivity was constant within each sub-region, recharge and horizontal anisotropy were held constant throughout the study area.

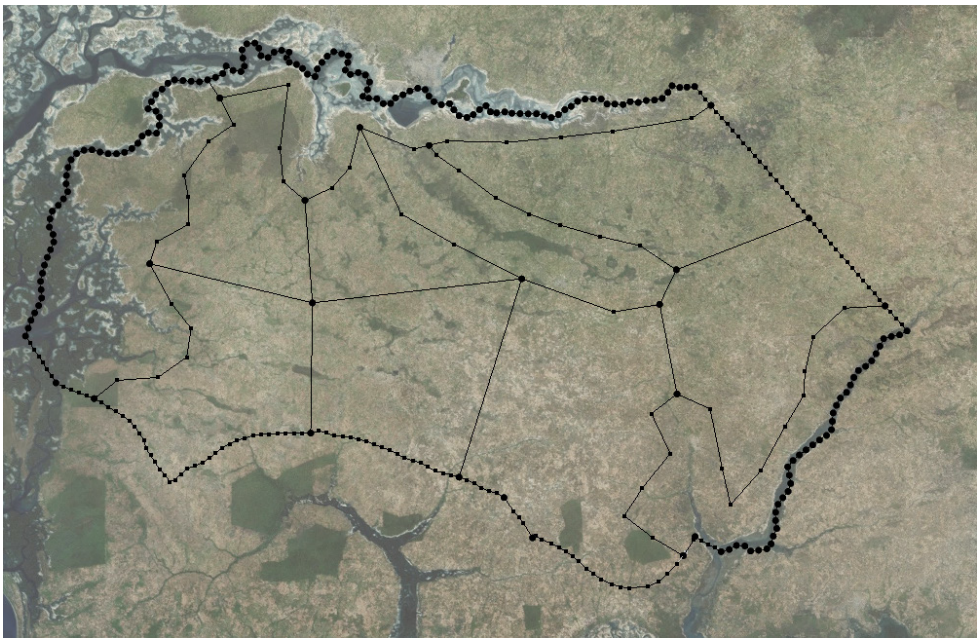

Figure 2.17 Regional Study Site, with 11 sub-regional partitions

For each sub-region, the starting value, minimum and maximum were the same: 50, 0.01, and 10,000 m/d. Recharge was set at a constant value of 0.00004685 m/d, or 17.1 mm/yr, as before. Horizontal anisotropy was set to 5. However, the calibration results were still poor. The RMSE was 6.12 m.

Finally, a method called pilot points was explored. Pilot points are used in conjunction with PEST. Pilot points are placed by the user throughout the region of interest. Each pilot point is then varied independently of other pilot points, and a surface is fit to the set of pilot points by interpolation. The calibration targets can then be compared with interpolated values at the same geographical location. Kriging was the method chosen for interpolation of the pilot point results. In contrast with previous runs, both hydraulic conductivity and recharge were varied by calibration throughout the area to best match the data.

In order to assist and improve the effectiveness of calibration, the author's own collected data regarding well levels in the study area were incorporated, along with well level information from Faye, et al. [5]. The average well level for each well surveyed was used. In addition, well data from Faye, et al. [5] sometimes produced water level elevations below sea level, which is unlikely. While this is likely attributable to the coarseness of SRTM data, in pilot point runs, these were eliminated to assist in convergence.

According to GMS guidelines [43], the following should be considered when placing pilot points:

1. Place points between observations, as opposed to collocated with observations
2. More observations should have more pilot points associated with them
3. Steep head gradients should be accompanied by more pilot points
4. Separate head-dependent boundaries and observation wells by a row of pilot points
5. Fill in the gaps

These points were placed according to the above suggestions (Figure 2.18). Furthermore, Tikhonov regularization was explored to relax the homogeneity constraint on the pilot points. The first option within Tikhonov regularization in MODFLOW is preferred homogeneous regularization. This in effect constrains pilot points to be similar to each other, in absence of other information. A prior information power factor controls this homogeneity constraint. Increasing this factor from its base value of 1 relaxes the homogeneity constraint; the reverse strengthens it [44]. In this case, the prior information power factor was set to 1.5.

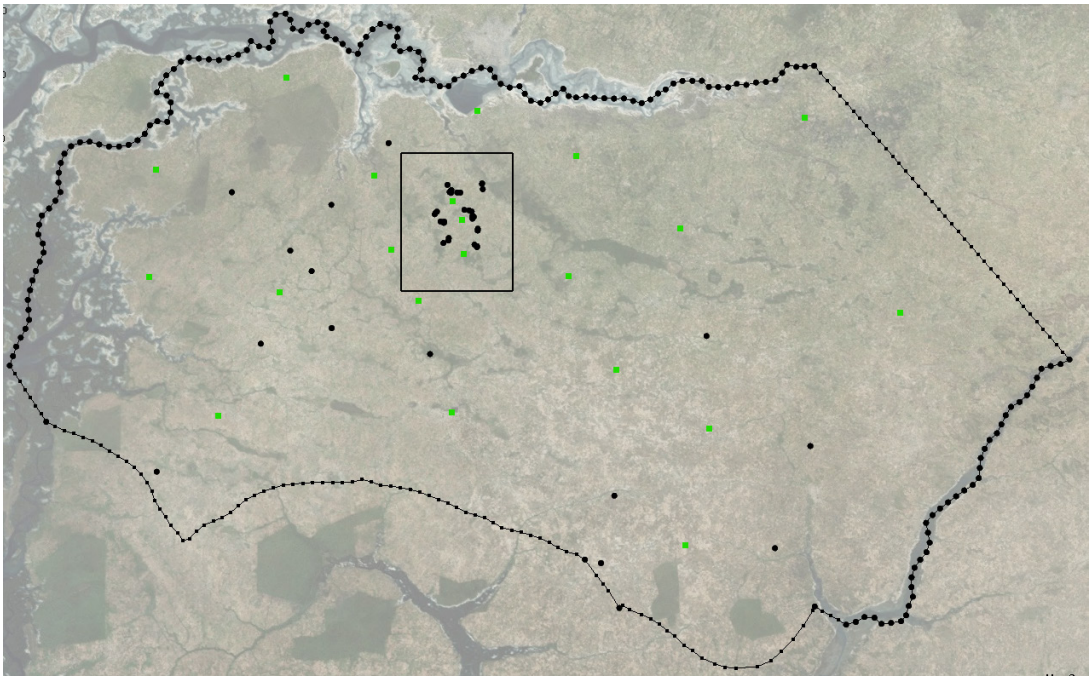

Figure 2.18 Location of observation points (black circles) and pilot points (green squares). The black box outlines the study area; note the concentration of observations within the study area compared to the rest of the model.

Kriging was chosen as the interpolation method for creating a surface from the pilot points. Ordinary kriging was used. Since all pilot point values were equal initially, an experimental variogram could not be computed. The range of values for hydraulic conductivity were 0.01 to

2000 m/d with a starting value of 200 m/d, and 1e-8 to 0.0002 m/d for recharge (0.00365 mm/yr to 73 mm/yr). The starting values for recharge varied among the pilot points.

Following this run, the results gave a good fit to the calibration targets. The Root Mean Square Error (RMSE) was calculated within GMS for the entire region, producing a RMSE of 2.315 m. Considering only the study site observations, the RMSE was 1.71 m. At this point, the model was considered sufficiently calibrated. Results for recharge and hydraulic conductivity are presented below.

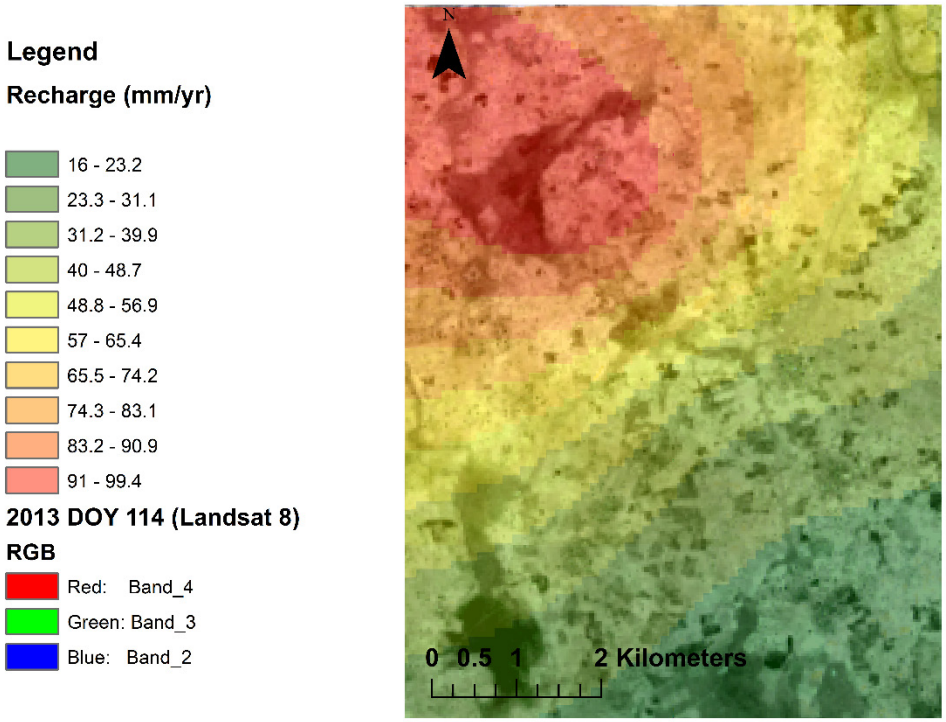

Figure 2.19 Distribution of Recharge (mm/yr) in Study Site, overlain on top of Landsat 8 scene

Values for recharge are quite variable, ranging from 16.22 to 102.06 mm/yr, with a standard deviation of 27.18 mm/yr (Figure 2.19). The mean value of 53.64 mm/yr is significantly higher than the mean value predicted by the British Geological Survey (BGS) report. However, this report also included an estimate of 108 mm/yr, as noted above, which would be characteristic of cleared vegetation, and consistent with the maximum value calibrated in GMS. A further note is that the BGS report was published in 1990. Since clearing of forested areas can result in increased recharge, owing to a shallower average root zone, the historic trend of deforestation may explain some of this difference. Furthermore, the values presented in the report are for a governmental department located some 60 kilometers southeast of the study site, which tends to have somewhat higher rainfall, but also more vegetation.

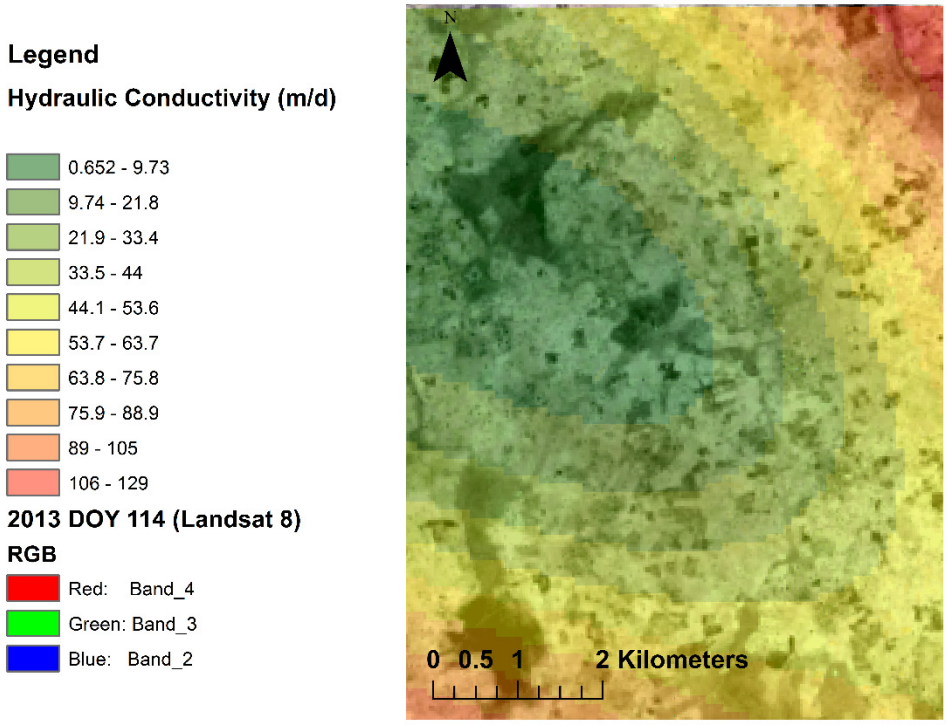

Figure 2.20 Distribution of Hydraulic Conductivity (m/d) in Study Area, overlain on Landsat 8 composite image of area

Values for hydraulic conductivity showed a much higher variability in the study site. Conductivity ranged from .691 m/d to 121.34 m/d, with a mean and standard deviation of 39.89 and 28.44 m/d (Figure 2.20). Faye, et al. [45] reported values of hydraulic conductivity ranging from 1.47 m/d to 197 m/d from Diluca [46]. To evaluate these hydraulic conductivity values further, the well level data collected was used to create monthly contour maps. First, the well level time series was interpolated to return values at the end of each month. These concurrent monthly well levels were then used to create monthly contour maps through kriging (Figure 2.21). It was assumed that annual recharge, applied to the area covered by the contour maps, would be equivalent to flow predicted by Darcy's law, in the direction of the largest gradient:

$$Recharge \times W \times L = K \times W \times b \times i$$

where

Recharge is annual recharge (mm/yr)

W and L are the width of the study area (4.7 and 6.4 km, respectively)

K is hydraulic conductivity (m/d)

b is saturated thickness (10 m)

i is the gradient parallel to flow (dimensionless)

The saturated thickness of the aquifer was assumed to be constant at 10 m. Recharge was taken as the average of the two values returned by the WTF method (95.5 mm/yr). The gradient was calculated for each month by dividing the drop in head by the distance over which the drop occurred. The average gradient for the time series was taken, and considered applicable to the whole area. Solving the above equation for hydraulic conductivity returned a

value of 94.3 m/d, which gives good agreement with both the MODFLOW model and the estimates by Diluca [46].

It should also be noted that persistently salty wells were located in the northeastern region of the study area, and had been salty as far back as community members could remember. The reason the salt water has not intruded further south seems to be on account of a persistent hydraulic gradient, originating in the west-central region of the study area, and oriented in a northeasterly direction (Figure 2.21). This gradient was persistent both in geographical extent and magnitude over the time frame where water levels were monitored.

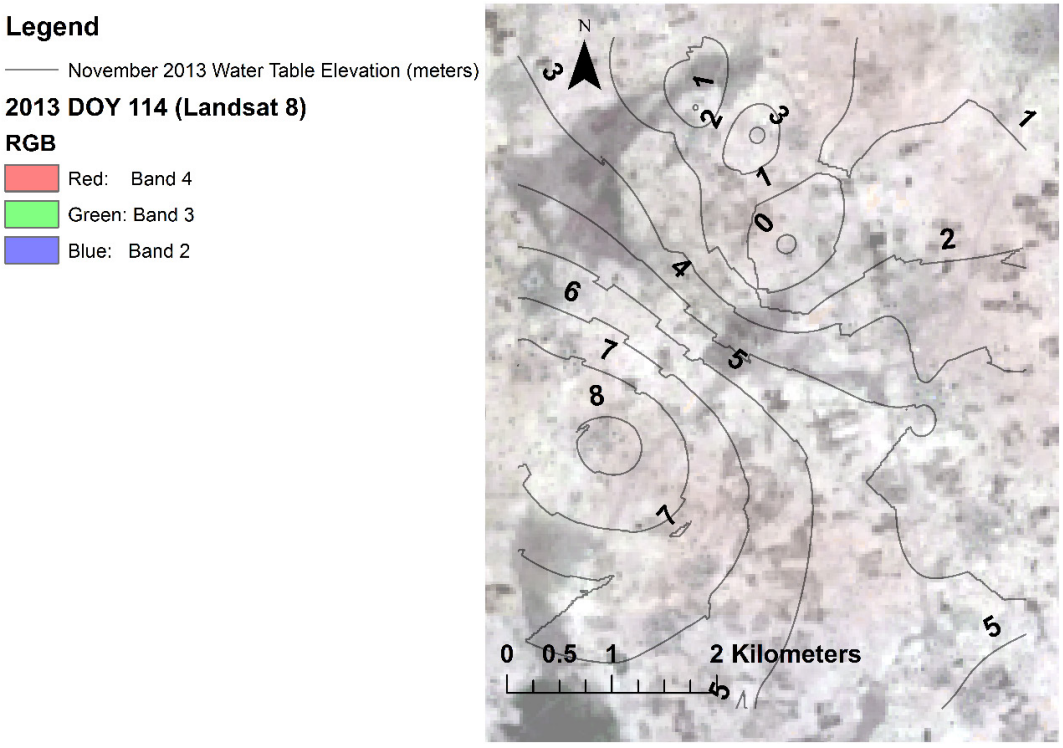

Figure 2.21 Contour map, November 2013 well levels, meters above sea level

The preceding models each have benefits and detriments, and have been utilized owing to their relative facility and compatibility with data requirements. A fourth model was developed in order to more explicitly account for various factors, and is discussed in the following section.

3. Distributed High-Resolution Recharge Estimation Model (DH-REM)

An important component that is not present in any of the preceding methods is an explicit relationship between recharge and rainfall that could be evaluated on short time scales (on the order of days). As noted in Section 1, Carter and Parker [30] have suggested that temporal distribution of rainfall is more important than annual rainfall with regards to quantifying recharge. Thus, a MATLAB model was developed that could explore this relationship further. This model uses the NRCS Curve Number Method to determine runoff [13], the FAO-56 Penman-Monteith equation to determine ET [14], and the water balance outlined in the FAO-56 document to determine recharge, including modifications for use with remote sensing by González-Dugo and Mateos [15]. The model was developed as an alternative to other methods that calculate point or lumped estimates of recharge, as well as those operating on a coarse resolution. This model will be referred to as the Distributed High-resolution Recharge Estimation Model, or DH-REM for short.

One anticipated advantage of this model, which can incorporate the effects of vegetation and soil type, is the ability to evaluate their impact on recharge. Contingent upon successful model calibration, possible changes in land use and land cover, such as deforestation or alternative farming practices, can also be explored. When using daily rainfall data, the relationship between short-term rainfall patterns and recharge can be explored. Once this relationship has been established, changes in rainfall patterns can be tested for their effect on recharge, enabling consideration of climate change.

3.1. Soil Data

The National Pedology Institute of Senegal, provided a soils type map of the area under study [47]. Soils were generally classified as either leached tropical ferruginous soils, or waterlogged and vertic soils. There were also two prevailing land cover types in the area – agricultural and forest or shrubland (villages made up a small part of the area under consideration, about 2%). In order to cover the range of soil combinations and land cover types, infiltration tests were conducted on each combination of soil type and land cover. Within the NRCS Curve Number Method, a key factor determining curve numbers is infiltration rate [13], which was analyzed using a constant head permeameter, or amoozemeter.

The general procedure was as follows [48]. A hole was dug to 40 cm, typically 10-12 cm in diameter. The permeameter was filled with water and quickly inverted into the hole. Time was kept, and volume of water in the permeameter and the height of the water in the hole were recorded every 5 minutes. The volume change from one reading to the next was divided by the time difference to calculate a flowrate, Q. Once three flowrate readings in a row returned the same value, the soil was assumed to be saturated, and the test was stopped. The height (H) of the water in the hole, the radius of the hole (r), and the flowrate (Q) of the water are needed to calculate the saturated hydraulic conductivity of the site. The Glover solution [49] is applied in the following way:

$$K_{sat} = \frac{Q}{2\pi H^2}\left[sinh^{-1}\left(\frac{H}{r}\right) - \left\{\left(\frac{r}{H}\right)^2 + 1\right\}^{1/2} + \frac{r}{H}\right]$$

Equation 3.1

where K_{sat} is the saturated hydraulic conductivity (cm/d),

Q is the flowrate at steady state (cm^3/day),

H is the height of water in the hole (cm) and

r is the radius of the hole (cm).

For most cases, three tests were performed, and the average taken. Lack of readily accessible water made it difficult to transport sufficient water for some tests. For some tests, only one or two results are available. Eighteen tests converged and produced a valid result, out of a total of 34 trials. The remaining results provided no information and were neglected. Results from the 19 successful tests are summarized in Table 3.1. Seasonal water bodies, such as that evaluated at Site 1, were not extensive in the study area; therefore, all soil was assumed to fall under hydrologic soil group A.

Table 3.1 Amoozemeter Test Results. Hydrologic Soil Group from USDA [13]

			K_{sat} (cm/d)				
Site	Land Use/Land Type	Number of Trials	Min	Max	Avg	Soil Description	Hydrologic Soil Group
1	Seasonal Water Body	1	-	-	10.1	Leached soil	B
2	Farmstead	6	12.9	51.0	24.0	Leached soil	A
3	Row Crops, Straight Row	3	14.8	35.1	27.0	Vertic and waterlogged soil	A
4	Row Crops, Straight Row	3	30.7	36.9	34.5	Leached soil	A
5	Forest	3	30.3	41.9	37.1	Leached soil	A
6	Forest	2	41.6	45.4	43.5	Vertic and waterlogged soil	A
7	Forest	1	-	-	53.6	Leached soil	A

While digging holes for the permeameter, soil samples were collected for the following strata: 0-15 cm, 15-30 cm, and 30-40 cm. Soil samples were collected at other locations in the study area, in addition to those sites where infiltration tests were conducted. The same protocol was followed for these sites, regarding depth of hole and stratum thickness. Soils were taken to the National Institute of Pedology in Dakar for a texture analysis.

One additional site provided soil data. One well, dug to about 10 m, had soil layers relatively organized around the well. In conversations with the well-digger, the order and thickness of each soil type was established. As noted in Section 3, the average field capacity for each site (Table 2.6), as well as average wilting point were determined from [37]. The difference between these, or available water, was calculated. This information was interpolated for the study area using inverse distance weighting (Figure 3.1).

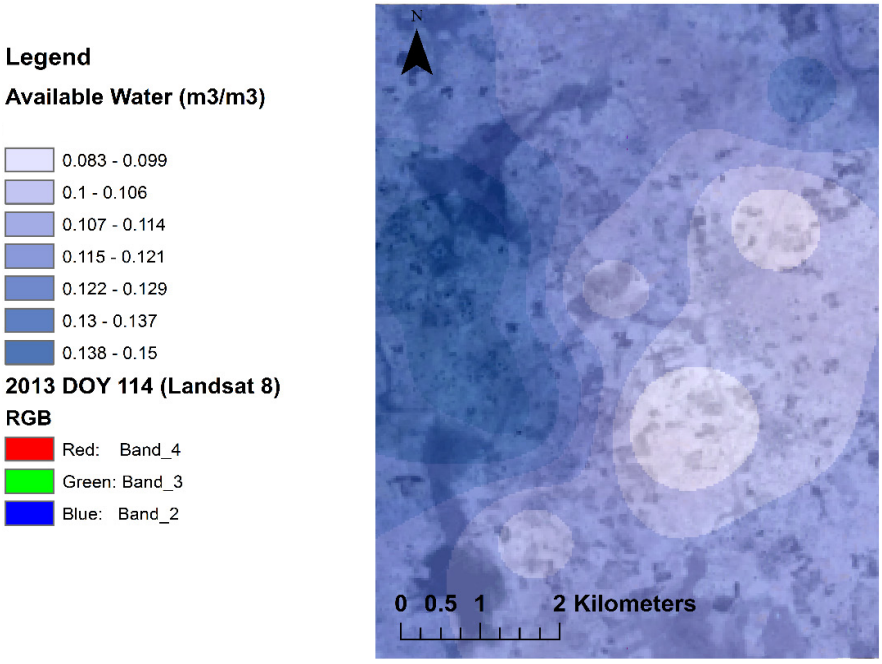

Figure 3.1 Available Water in study site, defined by inverse distance weighting in ArcGIS, and overlaid by Landsat 8 image

3.2. Remote Sensing Data

Remote sensing data were used to establish AET rates, according to crop type and vegetative cover, as well as land type for use in determining curve numbers for the NRCS method of runoff calculation [13].

3.2.1. Selection of Satellite Data

NASA's Landsat mission has been going on continuously since July 23rd, 1972, with the launch of the first Landsat satellite, Landsat 1. Landsat 7 and 8 are currently in orbit. Landsat 7 has been in orbit since April 15th, 1999, but in 2003 experienced a malfunction in the scan line corrector that led to severe striping on the left and right thirds of the image [50]. The study area falls directly in the region affected by striping, so Landsat 7 was not usable for the purposes of this study.

Landsat 8 was launched on February 11th, 2013, and has 30 m spatial resolution for most of its color bands, which is appropriate given the relatively large size of the study area (roughly 50 km^2). It also circles the earth every 16 days, which was considered sufficient to capture changes in land cover and crop growth to accurately portray evapotranspiration rates throughout the year. The study site is covered fully by scenes in Path 205 and partially by scenes in Path 204. These scenes were collected roughly eight days apart over the time period Landsat 8 has been in orbit until the present, and are available from the US Geological Survey. Furthermore, while the spatial resolution of Landsat 7 and Landsat 8 are the same, Landsat 8 has improved radiometric resolution over Landsat 7 (12-bit resolution vs 8-bit). It also features a 15-m panchromatic band which can be used to improve the resolution of color images. Band properties are given in Table 3.2.

Table 3.2 Band Properties for Landsat 8 [51]

Bands	Wavelength (micrometers)	Resolution (meters)
Band 1 - Coastal aerosol	0.43 - 0.45	30
Band 2 - Blue	0.45 - 0.51	30
Band 3 - Green	0.53 - 0.59	30
Band 4 - Red	0.64 - 0.67	30
Band 5 - Near Infrared (NIR)	0.85 - 0.88	30
Band 6 - SWIR 1	1.57 - 1.65	30
Band 7 - SWIR 2	2.11 - 2.29	30
Band 8 - Panchromatic	0.50 - 0.68	15
Band 9 - Cirrus	1.36 - 1.38	30
Band 10 - Thermal Infrared (TIRS) 1	10.60 - 11.19	100 * (30)
Band 11 - Thermal Infrared (TIRS) 2	11.50 - 12.51	100 * (30)

3.2.2. Classification of Imagery

In remote sensing studies, image classification is an important step in identifying different vegetation types, land use/land cover types, or other terrestrial phenomena. For this study, classification was essential for two reasons. First, since evapotranspiration rates vary according to the type and relative health of vegetation, accurately understanding the range of vegetative types and their geographical extent in the study area was critical. Second, the use of the NRCS Curve Number Method necessitates determination of land cover types in order to assign a curve number for runoff estimation.

The area was assumed to be made up of three separate land use classes – forest, agriculture and village. Villages were marked out manually in Google Earth, given the difficulty of distinguishing villages from forest and agriculture in remote sensing imagery. One Landsat scene from April 24th, 2013 (DOY 114), during the height of the dry season, was analyzed to delineate forested and agricultural land for 2013. For 2014, this date was February 22, 2014 (DOY 53). During the dry season, agricultural land was typically brown and barren with only scattered trees. However, shrub land and forested areas tended to be relatively green, though in a state of dormancy. For this reason, it was more straightforward to distinguish these areas using satellite imagery at this time.

An unsupervised image classification was run in ERDAS IMAGINE digital image processing software, creating 36 classes with a standard deviation of 3 in 12 iterations. During the classification, means were initialized along the diagonal axis. The classified image was overlaid on a false color Landsat image to better aid in distinction of the two classes. Once this was completed, this information was merged with village extent (delineated in Google Earth) to create a land use-land cover map.

Additional imagery was needed to depict the changing land conditions during the rainy season. Imagery was selected for the months of May through November. Excessively cloudy images were excluded from the study. The remaining images, if clouds were present, were subject to an unsupervised classification to distinguish between cloud, cloud shadow, agricultural land and forest. In reality, the separation between agricultural land and forest in these images was not of great importance, given that these had already been delineated using an image that more clearly showed the dividing lines between these areas. Furthermore, it

was assumed that no land changed classes during the time of study, i.e., forested land was not converted to agriculture, and vice versa. Once the images were classified, they were recoded, using a value of 0 to assign to those areas affected by cloud or cloud shadow, 1 for forest, and 2 for agriculture. Once all the images were classified and recoded, they were imported into MATLAB.

3.2.3. The Modified Soil-Adjusted Vegetation Index (MSAVI)

Vegetation indices are used in the field of remote sensing to gain information about vegetated surfaces, relating remote sensing information (namely, surface reflectance) to vegetation parameters such as leaf area index (LAI), fractional cover, and biomass. Hundreds of vegetation indices (VIs) exist, each with its own benefits and drawbacks [50]. One of the first to be developed was the Normalized Difference Vegetation Index, or NDVI [52]. This VI relies on the principle that healthy vegetation absorbs red light due to chlorophyll in its leaves, and it reflects energy in the near-infrared (NIR) wavelengths due to the high energy those wavelengths contain. If leaves absorbed energy in the NIR wavelengths, they would overheat and become damaged [50]. The equation for calculating NDVI is

$$NDVI = \frac{\rho_{NIR} - \rho_{RED}}{\rho_{NIR} + \rho_{RED}}$$

Equation 3.2

where ρ_{NIR} is the reflectance of light in the near-infrared band and

ρ_{RED} is the reflectance of light in the red band.

The NDVI has some shortcomings, including susceptibility to saturation at high vegetation content (i.e., change in leaf density or canopy cover is not well detected past a certain threshold). Additionally, the signal is also affected by soil background (i.e., light or dry soil can alter the signal, as well as dark or wet soil) [53].

An improved form of the NDVI was developed by Huete [54], called the Soil Adjusted Vegetation Index (SAVI). The SAVI attempts to minimize the soil background effect by incorporating an L factor that was originally intended to scale according to vegetation density, but was initially set equal to 0.5 to cover a range of vegetation types. The formula for SAVI is

$$SAVI = (1 + L)\frac{\rho_{NIR} - \rho_{RED}}{\rho_{NIR} + \rho_{RED} + L}$$

Equation 3.3

where L is a correction factor for the vegetation density. Note that when L = 0, SAVI = NDVI.

Finally, the Modified Soil Adjusted Vegetation Index (MSAVI) was developed by Qi, et al. [55]. The MSAVI incorporates the L factor from the SAVI, but adjusts it automatically based on vegetation density. This VI formula is arrived at by induction, with the result that the L factor does not appear explicitly in the equation. That is, the L factor is calculated as the residual of unity minus the original MSAVI (1-$MSAVI_1$). This L factor is then incorporated into a second MSAVI function, and the process is repeated until no improvement is attained ($MSAVI_N = MSAVI_{N-1}$). The final equation is

$$MSAVI_N = \frac{\rho_{NIR} - \rho_{RED}}{\rho_{NIR} + \rho_{RED} + 1 - MSAVI_N}(2 - MSAVI_N)$$

Equation 3.4

This is then solved for $MSAVI_N$, which results in the inductive form of the MSAVI:

$$MSAVI = \frac{\left(2 \times \rho_{NIR} + 1 - \sqrt{(2 \times \rho_{NIR} + 1)^2 - 8 \times (\rho_{NIR} - \rho_{RED})}\right)}{2}$$

Equation 3.5

In MATLAB, the MSAVI was calculated for each pixel that was not subject to cloud cover or cloud shadow. In order to fill in the gaps resulting from cloud cover and cloud shadow, another routine was run in which the average MSAVI value for all agricultural land that was not obstructed by cloud cover or cloud shadow was applied to agricultural land which had been obstructed. The same process was applied to forested land and villages.

Lastly, composite images were made, for each month. This was done by averaging the MSAVI values at each pixel, using scenes from the same month. For example, for the month of May, a given pixel in the final composite image was the result of averaging the corresponding pixel value in all scenes that were collected during May. It was assumed that little benefit would be gained by creating a new land cover map for each day, or even each week, of the study period, since relative change from day to day or week to week would be small. Using a monthly composite image, on the other hand, would be suitable for the purpose of the study.

This process produced a series of monthly images with MSAVI values for both 2013 and 2014, as well as a land use-land cover (LULC) map for each year that would be critical in determining ET and runoff, as outlined below.

3.3. Evapotranspiration and Runoff Methods

Semi-arid areas are commonly described in terms of an aridity index, which compares annual PET with annual rainfall [23]. In these areas, PET exceeds rainfall: for the study site in 2013 and 2014, this was by a factor of two and four, respectively. Thus PET is often the second-largest component of the hydrologic cycle in arid and semi-arid areas, after precipitation. It is also prone to high levels of uncertainty, owing to the wide array of factors that affect it. Due to its widespread acceptance as a standard method for calculating ET in cropland [15, 24, 25, 56, 57], the approach described in the Food and Agriculture Organization's 56th Irrigation and drainage paper is utilized in the present study. This approach is commonly known as the FAO-56 Penman-Monteith method, and is detailed in the appendix.

The Soil Conservation Service, now known as the National Resource Conservation Service, developed the Curve Number method as a way to estimate runoff from specific storm events in a watershed with known hydrologic properties [13]. As in the case of estimating evapotranspiration, alternate methods exist for calculating runoff. The NRCS method is one of the most well-known runoff estimation methods, owing to its widespread applicability and relative ease of use. This method is also detailed in the appendix.

3.4. Application to the Study Site and Site-Specific Conditions

The area as a whole, while predominantly agricultural, has a few large forested areas, most of which surround seasonal water bodies. The agricultural area has generally 8 different types of crops: millet, sorghum, corn, cassava, beans, rice, peanuts and watermelon. The forested areas have a wide range of shrubs and trees, predominantly acacia trees (*Acacia nilotica* (Egyptian thorn) and *A. seyal* (Red acacia) primarily) with *Piliostigma reticulatum* (Camel's foot), *Combretum glutinosum* and other species of shrub. There are also numerous small villages and a handful of larger towns. For simplicity, the study area was assumed to comprise three distinct LULC classes – forest, agriculture and village. Agricultural areas did have occasional interspersed trees, namely *Faidherbia albida* (Winter thorn), *Cordyla pinnata*

(Bush mango), and *Adansonia digitata* (Baobab), but in practice these were assumed to have minimal effect, and fields were assumed to be treeless.

Permeameter tests (see Section 3.1) were conducted at multiple points throughout the study area. With the exception of those conducted at the sites of seasonal water bodies (which covered a small portion of the total study area), tests showed that the hydrologic soil group was Group A, according to the NRCS methodology, having the following characteristics: "…low runoff potential and high infiltration rates even when thoroughly wetted. They consist chiefly of deep, well to excessively drained sand or gravel and have a high rate of water transmission (greater than 0.30 in/hr)." [13]. Villages were considered a farmstead and thus assigned a base curve number of 59. While farmers knew that planting on contour was beneficial, they planted taller crops (millet, corn, sorghum, cassava) in straight rows parallel to the direction of prevailing wind owing to the risk of wind damage to their crops if they planted in rows perpendicular to the wind. While shorter crops were planted on contour, the entire agricultural area was considered row crops planted in straight rows for simplicity. During the first part of the growing season, that is, until the fractional cover of the area exceeded roughly 50%, the hydrologic condition was considered poor and assigned a CN of 72; whereas upon exceedance of 50% ground cover, it was considered good and assigned a CN of 67. Wooded areas, including shrub land, were not regularly burned and had some leaf litter covering the soil, but were not protected from grazing. Thus, these areas were considered to have a fair hydrologic condition, and assigned a base curve number of 36.

The code for DH-REM can be found in the appendix. DH-REM runs in the following steps (Figure 3.2):

1. Read in composite MSAVI and land use-land cover maps
2. Read in daily rainfall data and calculate daily runoff
3. Read in reference evapotranspiration rates (calculated as in Section 3.2.2) and calculate daily actual evapotranspiration and deep percolation
4. Compile statistics on a monthly and annual basis for each component of the water budget (minimum, maximum and average)

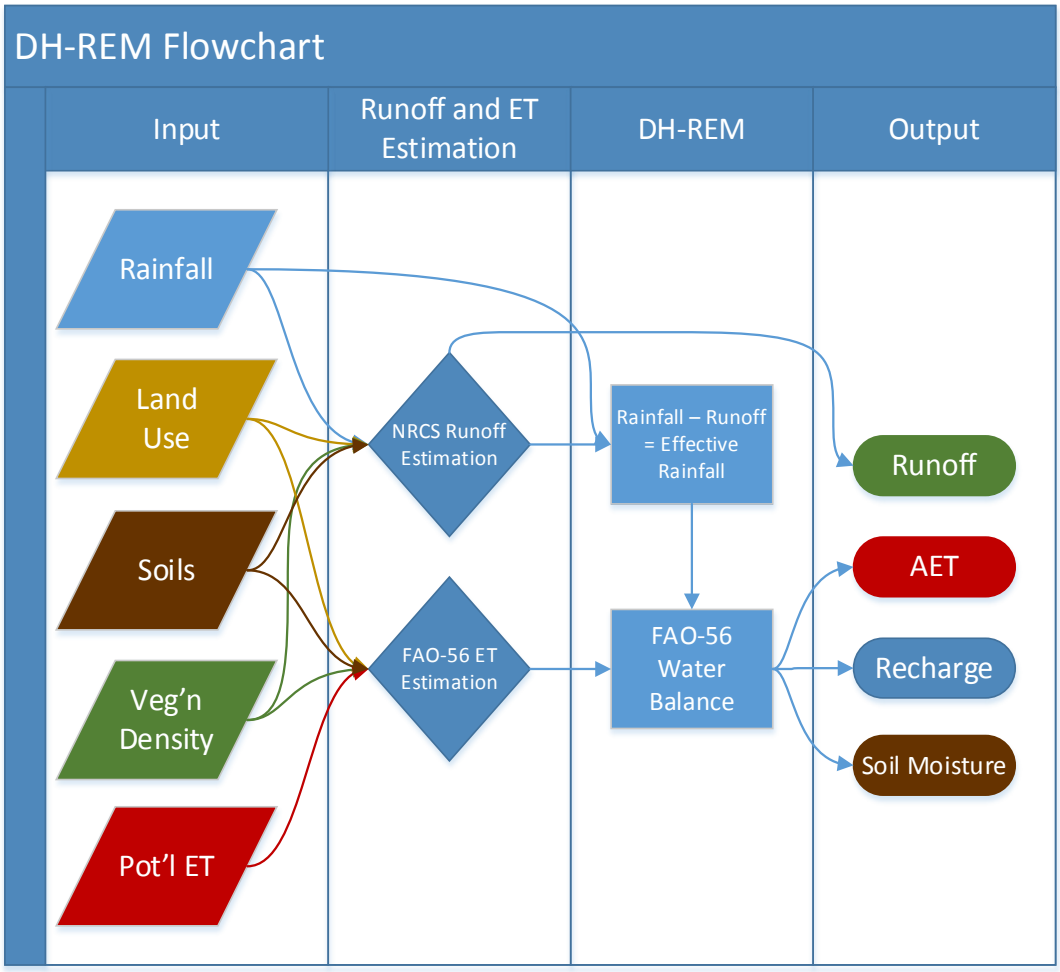

Figure 3.2 DH-REM Flowchart

Some parameters in DH-REM were not precisely known and needed to be estimated from the literature:

- Z_{forest} for forest rooting depth. This was assumed constant over time, and uniform over the study area. A higher value leads to more AET and less recharge. A value of 4 m was selected (characteristic of Acacia seyal, which was common in the area) and assumed representative of the site as a whole [41].
- Z_{crop} for agricultural rooting depth. This defined the maximum rooting depth of agricultural crops, corresponding with full cover. Rooting depth scaled linearly with fractional cover. Higher values lead to higher AET values and lower recharge values. 1.05 m was the average of rooting depth values from Allen, et al. [14] for the eight crops in the area.
- p, the fraction of TAW that can be transpired before water stress occurs. A higher value of p entailed a greater ability to transpire water before water stress occurred, which would in return lead to decreased rates of ET. Thus, higher p led to higher AET values, and lower recharge values. 0.8 was selected for forested areas, and 0.45 for crops. 0.45 was the average of values from Allen, et al. [14] for the eight crops in the area.
- $MSAVI_{min}$, the value of MSAVI corresponding to minimal fractional cover. This was important in calculating fractional cover, which in turn helped determine the crop coefficient (K_{cb}) and rooting depth ($Z_{r\ crop}$). This was selected as 0.2.

The model was run for both years with the above parameters. Results are presented and discussed below.

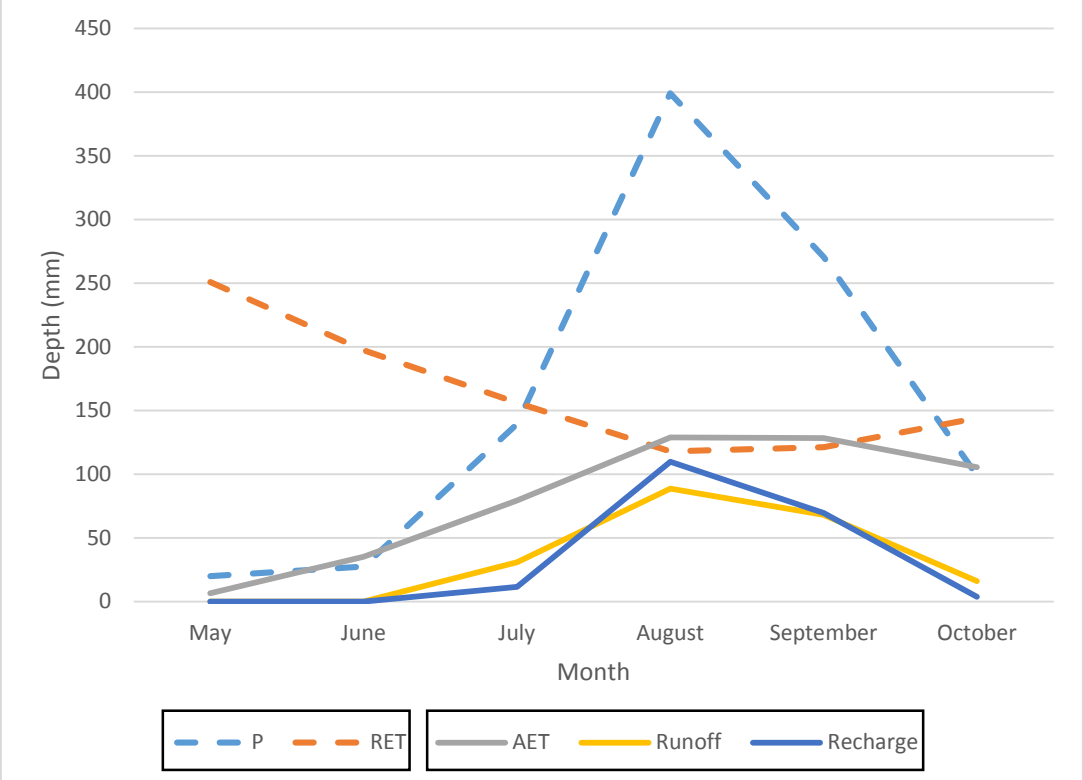

Figure 3.3 DH-REM Water Budget, May-October 2013

In 2013, AET is the dominant output in the water budget, followed by runoff and recharge (Figure 3.3). RET declines from May to August on account of decreasing temperatures and increasing cloud cover and humidity. AET increases monotonically through August, then levels off and begins to decrease. Water stored as soil moisture accumulates with the first rains and continues to increase, providing a reserve from which AET demand can be met. Recharge is focused in August and September. One aspect to note is that on a monthly basis AET sometimes exceeds RET slightly. This is due to the crop coefficient that scales the actual ET rate from that for grass to that for crops and trees, which has a maximum value of 1.15, coinciding with zero water stress. AET also exceeds P in June and October (Table 3.3), but this can be accounted for by soil storage. Average recharge for 2013 was calculated as 195.1 mm.

Table 3.3 DH-REM Water Budget, May-October 2013

Water Budget, May-Oct 2013					
Month	P (mm)	RET (mm)	AET (mm)	Runoff (mm)	Recharge (mm)
May	20	250.9	6.7	0.0	0.0
June	27.5	197.3	35.3	0.0	0.0
July	139.3	156.3	79.4	30.9	11.6
August	399	118.1	128.8	88.7	109.9
September	270.5	121.4	128.4	68.2	69.7
October	99	144.1	105.5	16.1	3.9

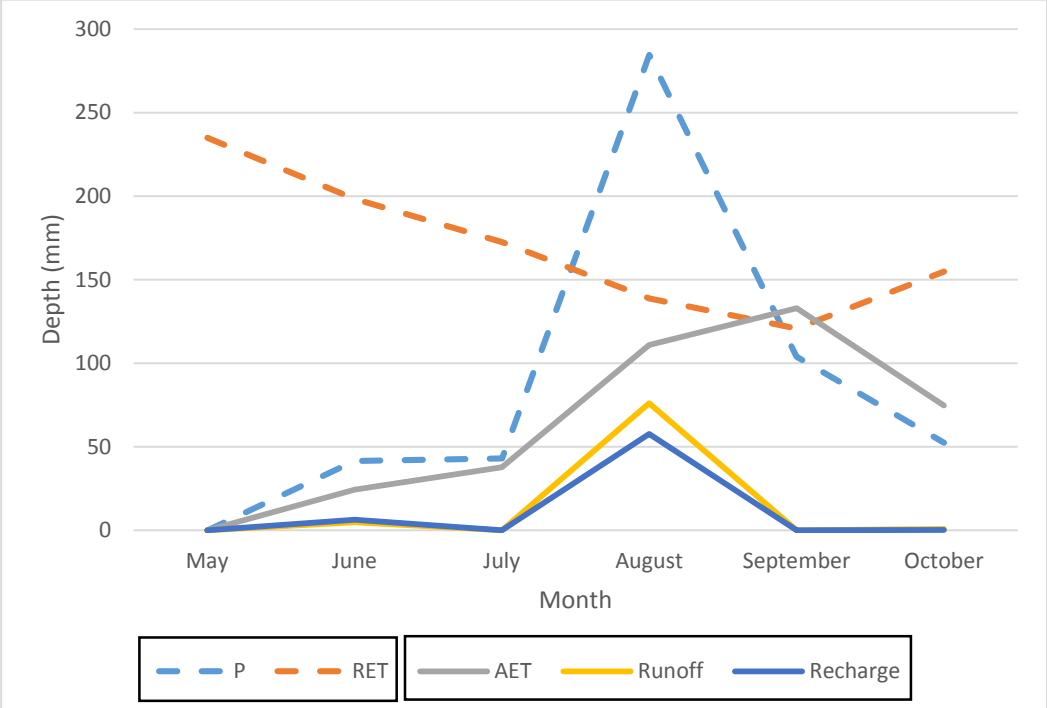

Figure 3.4 DH-REM Water Budget, May-October 2014

Runoff and recharge both occur almost entirely in August, instead of taking place over several months as in 2013 (Figure 3.4, Table 3.4). AET also increases monotonically through September, then decreases. AET in excess of RET only occurs in September, again on account of the crop coefficient which scales reference ET for grass to actual ET for crops and trees. Finally, AET exceeds P in September and October on account of soil water storage. Average recharge in 2014 was calculated as 64.4 mm.

Table 3.4 DH-REM Water Budget, May-October 2014

Water Budget, May-Oct 2014					
Month	P (mm)	RET (mm)	AET (mm)	Runoff (mm)	Recharge (mm)
May	0	235	0.0	0.0	0.0
June	41.5	198.4	24.4	4.8	6.5
July	43	172.6	37.7	0.0	0.0
August	284.5	138.9	110.9	76.1	57.7
September	104	120.9	133.0	0.1	0.0
October	52.5	154.9	74.7	0.8	0.2

The distributed nature of these results was explored. A map showing annual recharge values was constructed (Figure 3.5). Lowest values of recharge coincide with forested areas, owing to their deeper rooting depth. Highest values coincide with the 2% of the study area made up of villages. Of the remaining area, comprised of agricultural land, recharge varied strongly with available water, which was lower in the eastern side of the study area, and higher in the west. While these results indicate a good deal of spatial variability in recharge, it should be noted that as the water percolates through the subsurface, it will likely distribute itself more evenly by the time it reaches the water table. ET and runoff maps (not shown) also indicate a high degree of spatial variability. Runoff variability was dominated by land cover class, while both land cover type and soil type contributed to this variability for ET.

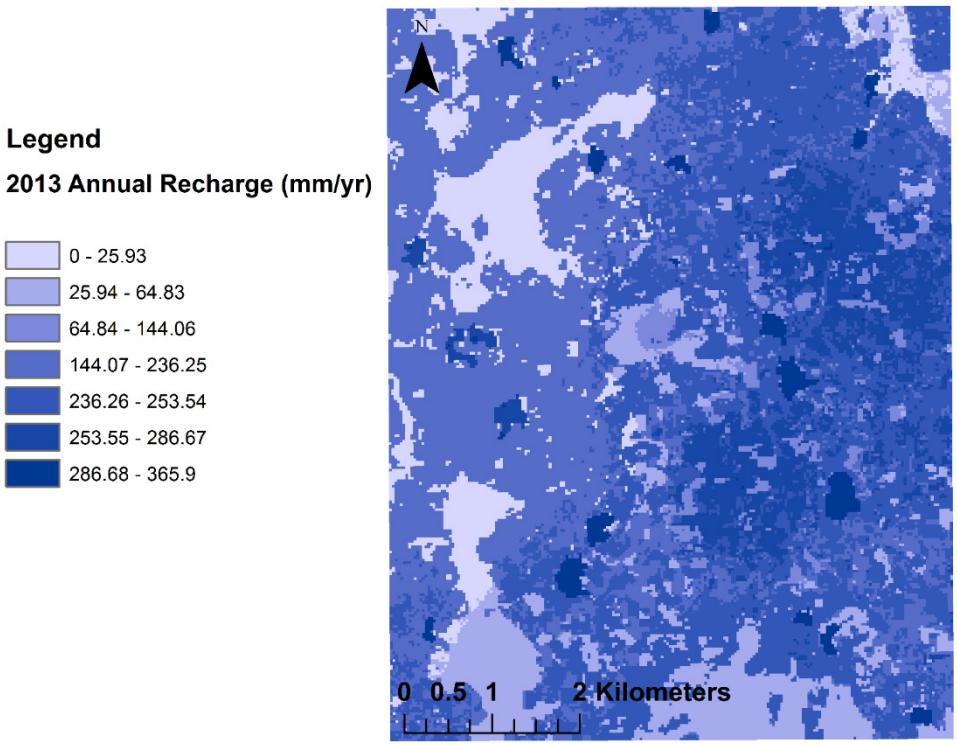

Figure 3.5 2013 Annual Recharge (mm)

Some parameters within DH-REM were adjusted to explore the sensitivity of the model. These are summarized below, and highlight a possible application of DH-REM.

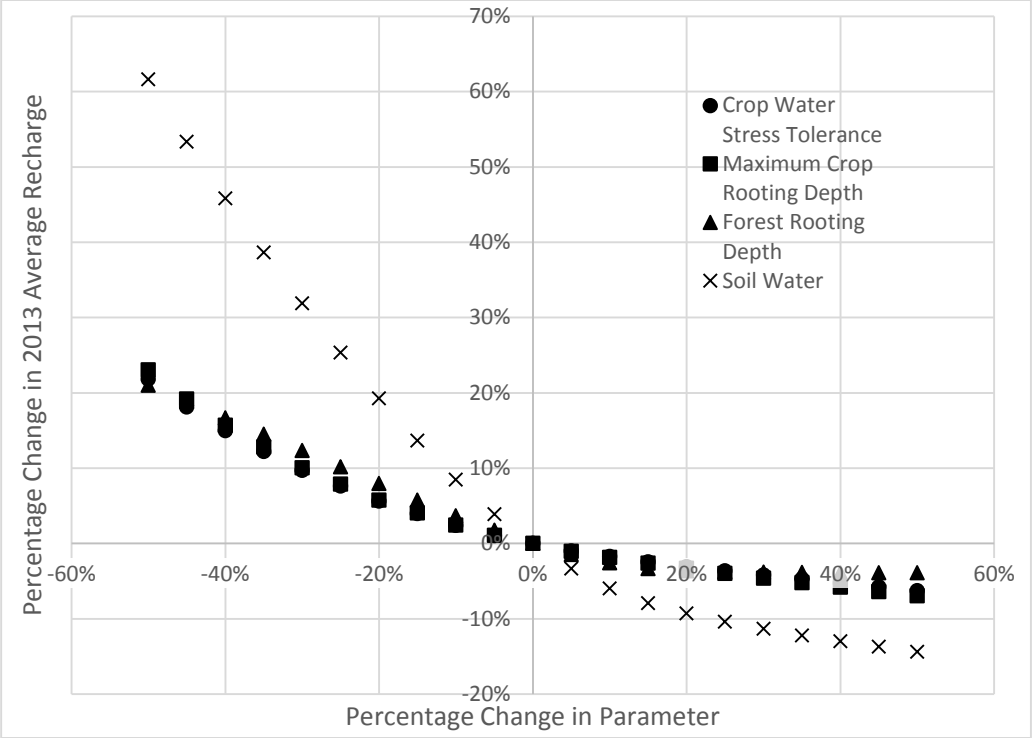

Figure 3.6 Sensitivity Analysis of 2013 Recharge to various parameters. Percent change in recharge measured relative to average recharge predicted by DH-REM.

Each of four parameters (crop water stress tolerance, maximum crop rooting depth, forest rooting depth, and soil water) were adjusted independently between -50% and +50% of their original values to evaluate the effects on 2013 simulated recharge (Figure 3.6). Soil water clearly has the greatest effect on recharge, whereas the sensitivity of recharge to the other three parameters is much more muted. It is interesting to note that decreasing a parameter by a given percentage has a larger effect on recharge than by increasing it the same percentage. For instance, the change in recharge as a function of increasing forest rooting depth levels out around 20% to 30% increase in rooting depth. This indicates diminishing returns, as there simply is not enough rainfall available to fill up the additional soil moisture reservoir provided by deeper rooting depth.

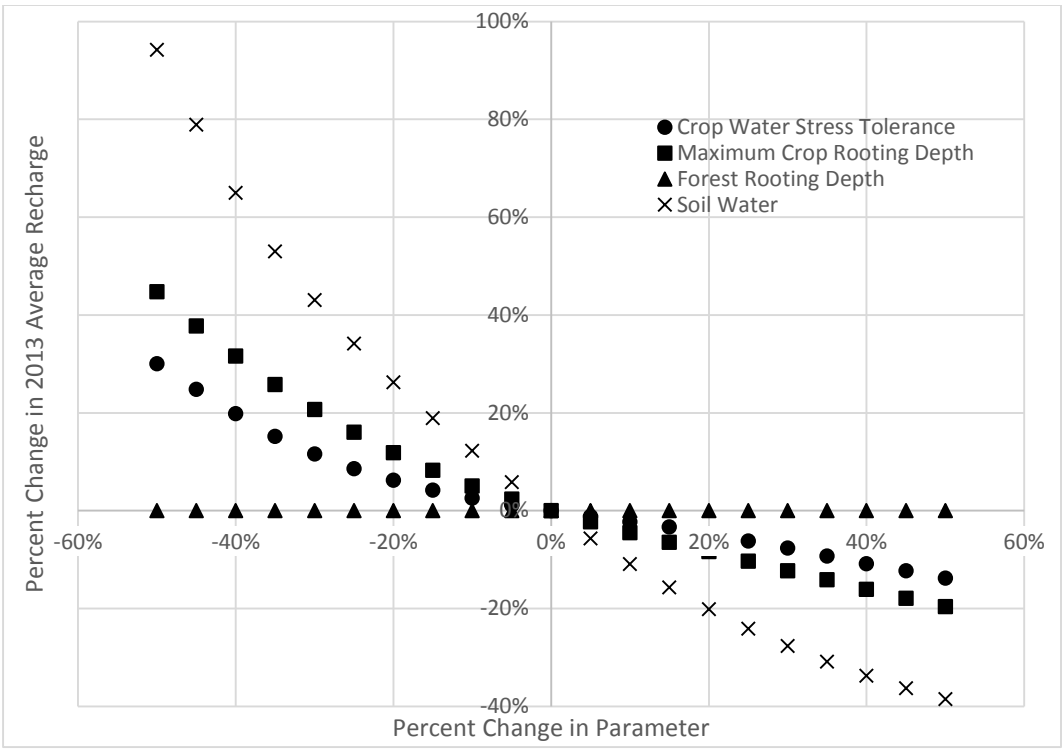

Figure 3.7 Sensitivity Analysis of 2014 Recharge to various parameters. Percent change in recharge measured relative to average recharge predicted by DH-REM.

Similar to 2013, simulated 2014 recharge sensitivity is greatest with regards to soil water (Figure 3.7). Effectively no change in recharge occurs as a result of changing forest rooting depth over the entire range of tested values; this again indicates, as in 2013, that insufficient rain was present to fill up the soil moisture reservoir calculated as a function of forest rooting depth. Maximum crop rooting depth and crop water stress tolerance have similar effects on simulated recharge in 2014.

The above figures indicate that the greatest improvement in model reliability would come from a greater confidence in soil water (available water, total evaporable water and readily evaporable water). Additional scenarios could be explored to simulate changes in land use and land cover, and their effect on recharge.

DH-REM, in its current iteration, has a number of limitations that should be considered thoroughly when assessing its results. It has intensive data requirements, as discussed below, which would make similar attempts in data-poor regions very difficult. DH-REM includes information about rooting depth, but neglects other subsurface conditions, such as the water table and hydraulic conductivity. Evapotranspiration, runoff and water balance methods were selected based on their widespread acceptance by the scientific community and relative ease of use; alternative methods may be more appropriate for this area. It also assumes that the top 40 cm of soil, corresponding to data collected, is representative of the following several meters of soil.

Required data include soil texture, surface permeability, general vegetation properties, surface reflectance and elevation, weather parameters (temperature, wind speed, humidity, solar radiation and cloud cover) and rainfall on a daily basis. Of these, soil and vegetation data are only available as a result of extensive field work in the study area.

Weather data were available from government offices in Senegal, and surface reflectance data and elevation were available freely from the USGS. Climate data was available for the regional capital of Kaolack, located about 20 kilometers from the study site. Rainfall for 2013 and 2014 were available from a rain gauge about 4 kilometers from the study site. Additionally, climate and rainfall data were assumed uniform over the study area. Re-creation of this model in other areas, even within Senegal, would be difficult without comparable field work and observational data.

These results indicate that DH-REM can provide a distributed estimate of recharge, on a daily basis, for pixels or cells corresponding to remote sensing data (in this case, 30 meters). It can also be utilized to explore the dependency of recharge on different soil, vegetation and land use/land cover parameters. Section 4 will compare results of this model with those of other existing methods. The appendix includes application of DH-REM to modeling the relationship between rainfall and recharge, as well as the relationship to climate cycles and change.

4. Comparison of Recharge Estimates

4.1. Review and Comparison of Methods

In any comparison of methods, it is important to consider the benefits and restrictions of each method. While natural systems are complex, models must balance complexity and simplicity to be reliable. Complexity comes at a cost: additional data requirements, computational time, and a deeper understanding of the relevant processes and variables. Models should be as simple as possible, provided they present a reasonably accurate view of reality relative to the question asked.

It is one of the key hypotheses of this thesis that the temporal distribution of rainfall has an important effect on recharge in the Saloum Region. Models without this sensitivity are insufficient to determine the relationship between rainfall and recharge accurately.

The Water Table Fluctuation method (WTF) relies on the principle that any rise in water table level can be related to recharge based on estimates of specific yield. As discussed in Section 3.1.2, this method makes several assumptions about the system, including the absence of injection into the wells, negligible effect of pumping and atmospheric conditions on recharge, and a constant specific yield. This method has often been suggested for shallow water tables experiencing dramatic rises in response to rainfall, but can be applied to deeper water tables with more gradual responses. Estimates of recharge can be made on a basis concordant with measurements. Such estimates should be considered representative of an area on the order of several square meters, up to one thousand square meters [18, 21]. Thus, while the WTF method has the benefit of fine temporal resolution (contingent on frequency of measurements), the extent of its spatial applicability is somewhat limited. As a recharge estimation method, it ignores any environmental or agronomic factors. While this dispenses with some data constraints often faced by other methods, obtaining reliable well level data can be difficult and time-consuming, and is not regularly recorded by government agencies, as compared to weather data. It also eliminates the possibility of developing an explicit relationship between environmental or agronomic factors and recharge.

The Thornthwaite-Mather Water Balance (TMWB) is a simple, accounting-style method for determining components of the hydrologic cycle on a monthly basis. One drawback of the monthly time step is that all precipitation that falls in a given month is subject to the total monthly demand of evapotranspiration and the root zone. Thus, total precipitation needs to exceed both of these in order for any recharge or runoff to be predicted. Evapotranspiration rates rarely if ever exceed about 10 mm/day, whereas rainfall events in excess of 10 mm are very likely. Monthly rainfall amounts are used to determine monthly ET depths. Therefore, the TMWB could be reasonably expected to overestimate evapotranspiration, at least in semi-arid sites like the one considered in this study, as it attenuates high rainfall events most likely to cause recharge [18]. The TMWB presents one estimate for an area, assuming the area is subject to the same precipitation and ET rates, and has homogeneous characteristics of field capacity and rooting depth. Finally, the TMWB does not distinguish between runoff and recharge; additional stream flow measurements are required to separate estimates of recharge and runoff.

GMS MODFLOW has numerous advantages, including its ability to model large areas on a steady-state or transient basis, as well as lumped or distributed approximations. It can incorporate subsurface geology and groundwater flow, factors that can significantly affect recharge. Ease of calibration within GMS means that improved estimates of various parameters can be made, remedying some of the uncertainty inherent in these approaches. However,

without flow values, results from the model are non-unique, so it is difficult to determine whether another set of results that also fits the data would be more appropriate, or if a different set of parameters would give the same result. Recharge is treated like another parameter that is adjusted to match calibration targets (head or flow values, or both), so any connection to climatic parameters is not considered. When recharge is unknown, or when estimates are subject to great uncertainty, initial estimates for calibration may have a wide range, and final results may be difficult to verify without additional estimates of recharge from other methods. In large models spanning tens or hundreds of kilometers, GMS may also be less capable of calibrating to very precise targets.

The MODFLOW model calibrates hydraulic conductivity and recharge by minimizing the error between computed and observed head values. These head values come from two different sources and were measured several years apart. Head values within the bounds of the study site were for a one year time period, so recharge values could be considered equivalent to an average value for 2013 and 2014.

DH-REM, described in Section 3, has the potential to overcome some of these shortcomings. It estimates recharge on a transient and distributed basis, and operates with very fine resolution both spatially and temporally (30 meters and daily). Recharge estimates are based on an explicit relationship between rainfall, ET rates, and soil and land cover/land use data. High resolution data and explicit incorporation of rainfall in the model permit exploration of the relationship between temporal distribution of rainfall and recharge, a prime driver for development of this model. Empirical data and remotely sensed land use/land cover information are required. Various parameters can be adjusted to permit exploration of their effect on recharge estimates.

A further point of difference between the TMWB and DH-REM is the order of calculation. In DH-REM, runoff is calculated first, followed by AET, deep percolation and soil moisture depletion. This “ensures” that water is available for runoff. In the TMWB, AET is calculated first, followed by soil moisture, and runoff and recharge are the residual.

It is also important to acknowledge the effect of results produced by one model with the development of another. Two of the parameters adjusted during calibration of DH-REM, crop rooting depth and forest rooting depth, were combined and applied to the TMWB as an overall average root depth. This was done to ensure consistency between the TMWB and DH-REM approaches.

The terms deep percolation and recharge are used interchangeably, though there are some important differences. The WTF and GMS models calculate recharge, i.e., the depth of water that reaches the water table. DH-REM estimates deep percolation – the residual of precipitation after the demands of evapotranspiration, runoff and soil moisture have all been accounted for. This is the water that will percolate past the root zone into the intermediate zone, and is assumed to eventually make its way to the water table, instead of replenishing soil moisture storage deficits in the intermediate zone. The TMWB model, as noted previously, combines estimates of runoff and recharge into one value. This recharge value is also the water that percolates past the root zone and is assumed to replenish the water table. Moving forward, however, deep percolation and recharge will be considered equivalent.

4.2. Comparison of Estimates

Model estimates will be compared in two ways: on a monthly basis and on an annual basis. The WTF estimates were only available from mid-October 2013 to late October 2014. Further, the GMS results were developed assuming a recharge “season” coinciding with the rainy season

(June through September) when most rainfall occurs. The GMS results were also calibrated based on an average of head levels collected from area wells in the study site – the same used for the WTF method – in addition to other well levels collected in November 2003 [5], spread throughout the larger region. Thus, the results from GMS should be considered as average recharge for both years. TMWB results are the average of the six parameter combinations explored in Section 2.2.3.

A summary of monthly average values predicted for recharge from each model is shown in Figure 4.1. Recharge predicted by the DH-REM and TMWB models is much more concentrated in time than the WTF and GMS recharge predictions, on account of the fact that these models predict the occurrence of deep percolation (i.e., excess water percolating past the root zone), as opposed to actual recharge (water reaching the water table). The GMS results reflect the assumption of a recharge season coinciding with a rainy season.

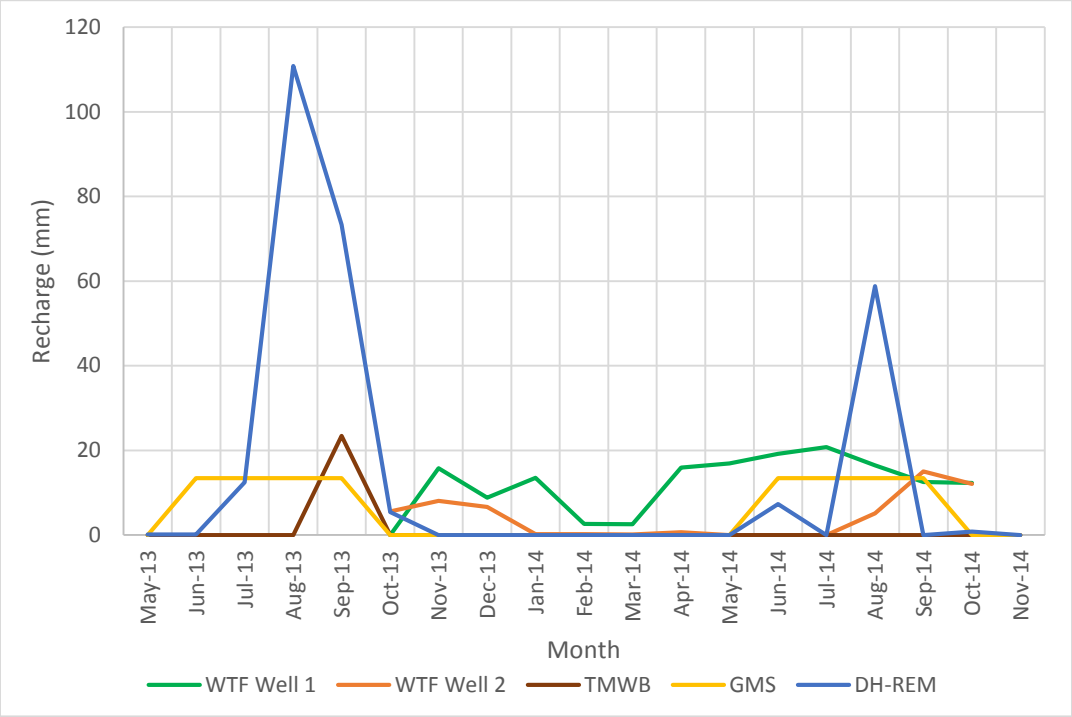

Figure 4.1 Monthly Comparison of Recharge Values from Different Methods

The WTF method could be considered the most accurate estimate of recharge timing, despite the limited range of applicability. Recharge times between the two WTF estimates vary: Well A has a prolonged recharge season, beginning after the end of the rainy season and extending for roughly a year. Well B, on the other hand, has pronounced and easily distinguishable recharge periods beginning with the latter half of the rainy season and ending a few weeks after its conclusion. These two wells are several kilometers away from each other, reinforcing that one well cannot be considered representative of other wells in the area.

Finally, areal and point estimates were compared for each model. DH-REM had the highest areal estimate for both years (Table 4.1). Point estimates for comparison were made by selecting the recharge value predicted by GMS and DH-REM that corresponded geographically with the wells used for the WTF method. DH-REM has an extremely high value for recharge in

2013, though this is the result of its location in a village which, because of minimal vegetation, has much higher recharge than other land use types. The GMS estimate for 2013 was on the opposite end of the spectrum, predicting much less recharge than the WTF method. In 2014, these trends are reversed, with DH-REM giving a more reasonable estimate of point recharge than GMS.

Table 4.1 Comparison of Areal and Point Estimates

	Areal Estimate			
Year	WTF	TMWB	GMS	DH-REM
2013	N/A	59	53.6	195
2014	N/A	0	53.6	66
Year	Point Estimate			
2013	158	N/A	37.2	346
2014	33	N/A	74.3	51.5

Since the TMWB calculates the water balance on a monthly basis, it may over-predict AET, as compared to DH-REM, which would explain the lower recharge values. To explore this aspect further, annual average estimates of AET for each method were compared (Table 4.2).

Table 4.2 Total AET Predicted by Each Model, in Each Year, May to October

Model	DH-REM		TMWB	
Year	2013	2014	2013	2014
AET (May - Oct, mm)	484.2	381.7	588.0	423.4

TMWB predicted more AET in both years (Table 4.2). This may be due to differences in soil moisture estimation in the two methods. The maximum soil moisture available in the TMWB model is the product of rooting depth and field capacity. In the FAO-56 method, upon which DH-REM is based, the equivalent soil water storage parameter, total available water (TAW), is the product of rooting depth and available water (the difference between field capacity and wilting point). Average available water was calculated according to Saxton and Rawls [37] as 0.117 cm^3/cm^3, whereas an average field capacity of 0.238 cm^3/cm^3 was used with TMWB. Assuming rooting depths are approximately equal, the soil water storage component is twice as large as in DH-REM. In addition, the TMWB model allows soil moisture to decrease below wilting point, which is unlikely to happen on account of transpiration alone. Wilting point defines the suction pressure with which soil particles hold water by capillary forces to the extent that plant roots cannot extract water for transpiration and wilt [23]. This decreases TMWB AET and recharge estimates compared with DH-REM, which does not incorporate stocks or flows of water present at or below the wilting point. Furthermore, there is an exponential relationship between ET and soil moisture in the TMWB model, whereas in DH-REM, a linear model approximates the decrease in ET with decreasing soil moisture. It is possible for crops to transpire more than the amount prescribed by RET, due to crop surface roughness and albedo values that differ from grass. The maximum crop coefficient (or ratio of maximum plant AET to RET) is 1.15, indicating that AET in DH-REM could exceed the reference ET by 15%. TMWB treats the reference ET as absolute maximum PET. The monthly time step in TMWB explains why TMWB ET is sometimes greater than DH-REM ET. Since TMWB simulates the soil moisture reservoir in this way (namely, including water present below wilting point in ET calculations), it is unlikely to provide reasonable estimates of recharge in semi-arid areas.

No observations can be made about a climatological average of recharge, given that only two years of data are available. However, the average recharge estimates presented here seem to exceed by a factor of at least 2 that estimated by the BGS report published in 1990. This could be due to deforestation, driven by expansion of agriculture and gathering of fuel wood. Deeper-rooted plants have a greater soil moisture storage capacity; thus, a reduction in the area of trees could increase recharge.

5. Future Work and Conclusions

5.1. Future Work

The model presented herein, DH-REM, offers some advantages over previously-developed approaches. It incorporates current, high-resolution data, both spatially and temporally, enabling consideration of the effects of short-term precipitation variability on recharge. While only briefly considered here, the results from such a model could be analyzed to better quantify the effect of soil and crop type on recharge, as well as the effects of precipitation patterns on runoff and AET.

Much more work could be undertaken to improve the accuracy of the model. Since DH-REM consistently provided the highest estimates of recharge, it should not be viewed as a reliable recharge estimation tool. Additional data sources should be explored to refine its approach and provide independent calibration targets. Directly measuring recharge, for instance with a lysimeter, would provide reliable values with which DH-REM could be calibrated. Monitoring of wells in rural areas should be continued and expanded to provide further information on recharge rates using the WTF method, which is a scientifically valid, inexpensive and straightforward (albeit labor-intensive), technique that could offer significant data on recharge in the area and possibly throughout Senegal.

Additional soils data should be gathered so that the subsurface can be better characterized, from the surface to the water table. Moisture measurements should also be taken at various near-surface depths to better understand the dynamics of soil moisture and its relationship to cropping patterns and climate. Supplementary work ought to be done to include the effects of evapotranspiration and land use-land cover aspects to estimate historical recharge rates with a greater degree of certainty. AET could be estimated either using temperature, or a suite of weather parameters as described by the Penman-Monteith equation. Efforts should also be directed towards consideration of how those factors are likely to change in the future, and their corresponding impacts on recharge. Kendy, et al. [28] developed a recharge model which described the subsurface as a series of discrete soil layers with different characteristics, which would provide more accurate estimates of total recharge, including its temporal distribution. Combining this with rooting depth information, including the portioning of water demand to different levels of the root zone, could lead to better estimates of evapotranspiration.

5.2. Conclusions

Each of the models discussed herein have their benefits and shortcomings. While the WTF method can provide accurate information about local recharge, including its temporal distribution, such estimates have limited spatial application and no connection to climatic factors. The TMWB, while easy to use, is better at providing long-term estimates of water budget interactions than precise, short-term estimates. In this study, it was shown to overestimate soil moisture and evapotranspiration and underestimate recharge and runoff, and thus may not be suitable for semi-arid environments. GMS is able to provide large-scale estimates of recharge, incorporating the flow of groundwater in the system, given observed head values and hydraulic conductivity estimates. By comparison, DH-REM has quite extensive data requirements, but it is able to form an explicit link between rainfall and recharge, and the dependence of the model on soil and vegetation characteristics.

It is also important to consider how these results may impact those living in Kaolack. Currently, it appears that there is sufficient recharge on an annual basis to provide for

drinking, hygiene and washing, assuming no dramatic changes in land use and land cover or population. Provided this influx of recharge is consistent, it should be sufficient to maintain the head gradient which appears to be slowing intrusion of saltwater into aquifers in the area (see Section 3.3.1). Further study should be directed towards the interaction between the various aquifers in the area, to understand how recharge to upper aquifers may interact with lower aquifers, if at all.

To encourage resiliency to climate change in dryland areas, a variety of rainwater harvesting methods have been developed, such as check dams and contour bunds. Garg and Wani [34] investigated possible effects on improving aquifer recharge using such methods in India. These technologies have the potential to provide threefold benefits: reducing the impacts of low-rainfall years, improving agricultural productivity in the area by harvesting runoff, and safeguarding groundwater reserves by avoiding the need for pumping for irrigation. Other adaptation strategies include drought-resistant crops, seasonal climate forecasts (which may be aided by investigating correlations between climatic cycles and weather patterns), and index insurance.

The preceding work has demonstrated that much can be gained by comparing different recharge models, by exploring their approaches, advantages, limitations and ultimate estimates. Incorporating additional data into more complex recharge models also has an advantage. The distribution of recharge in an area can be better elucidated, along with the impacts of vegetation, soil type, and management practices. Recharge can vary significantly over a small area, owing to variations in soil type and vegetation.

It is hoped that the foregoing analysis can offer an alternative viewpoint on the local hydrological system, one that will help ensure even a small improvement in the livelihoods of those influenced by climate change and dependent on groundwater in semi-arid regions.

6. References

[1] UN-Water, "Coping with water scarcity: challenge of the twenty-first century," United Nations Water and Food and Agricultural Organization2007.

[2] J. F. Reynolds, D. M. S. Smith, E. F. Lambin, B. Turner, M. Mortimore, S. P. Batterbury*, et al.*, "Global desertification: building a science for dryland development," *science,* vol. 316, pp. 847-851, 2007.

[3] P. H. Gleick, "Water resources," *Encyclopedia of climate and weather,* vol. 2, pp. 817-823, 1996.

[4] H. Tropp, "Water governance challenges: Managing competition and scarcity for hunger and poverty reduction and environmental sustainability," Human Development Report Office (HDRO), United Nations Development Programme (UNDP)2006.

[5] S. Faye, P. Maloszewski, W. Stichler, P. Trimborn, S. Cisse Faye, and C. Becaye Gaye, "Groundwater salinization in the Saloum (Senegal) delta aquifer: minor elements and isotopic indicators," *Sci Total Environ,* vol. 343, pp. 243-59, May 1 2005.

[6] J. Pages and J. Citeau, "Rainfall and salinity of a sahelian estuary between 1927 and 1987," *Journal of Hydrology,* vol. 113, pp. 325-341, 1990.

[7] User:TUBS. (28 January 2016). *Senegal in Africa*. Available: https://commons.wikimedia.org/wiki/File:Senegal_in_Africa_(-mini_map_-rivers).svg

[8] User:TUBS. (28 January 2016). *Kaolack in Senegal*. Available: https://commons.wikimedia.org/wiki/File:Kaolack_in_Senegal.svg

[9] P. Gill, "Working with local people to identify tree services, deforestation trends, and strategies to combat deforestation: A case study from Senegal's Peanut Basin," Master of Forest Resources, Environmental and Forest Sciences, University of Washington, 2013.

[10] C. B. Field and M. Van Aalst, *Climate change 2014: impacts, adaptation, and vulnerability* vol. 1: IPCC, 2014.

[11] I. Held. (2014, January 22, 2016). *Sahel Drought: Understanding the Past and Projecting into the Future*.

[12] UNEP. (January 14, 2016). *Western Africa: Climate Variability in Western Africa*. Available: http://www.unep.org/dewa/Africa/publications/AEO-1/056.htm

[13] S. USDA, "Urban hydrology for small watersheds," *Technical release,* vol. 55, pp. 2-6, 1986.

[14] R. Allen, L. S. Pereira, D. Raes, and M. Smith, "Crop evapotranspiration: Guidelines for computing crop requirements," 0254-5284, 1998.

[15] M. González-Dugo and L. Mateos, "Spectral vegetation indices for benchmarking water productivity of irrigated cotton and sugarbeet crops," *Agricultural water management,* vol. 95, pp. 48-58, 2008.

[16] I. Held, T. Delworth, J. Lu, K. u. Findell, and T. Knutson, "Simulation of Sahel drought in the 20th and 21st centuries," *Proceedings of the National Academy of Sciences of the United States of America,* vol. 102, pp. 17891-17896, 2005.

[17] A. Giannini, R. Saravanan, and P. Chang, "Oceanic forcing of Sahel rainfall on interannual to interdecadal time scales," *Science,* vol. 302, pp. 1027-1030, 2003.

[18] B. R. Scanlon, R. W. Healy, and P. G. Cook, "Choosing appropriate techniques for quantifying groundwater recharge," *Hydrogeology Journal,* vol. 10, pp. 18-39, 2002.

[19] W. C. Rasmussen and G. E. Andreasen, "Hydrologic budget of the Beaverdam Creek basin, Maryland," USGPO1959.

[20] O. E. Meinzer and N. D. Stearns, "A study of groundwater in the Pomperaug Basin, Connecticut," *US Geol. Surv. Water-Supply Pap,* vol. 2309, p. 23, 1927.
[21] R. W. Healy and P. G. Cook, "Using groundwater levels to estimate recharge," *Hydrogeology Journal,* vol. 10, pp. 91-109, 2002.
[22] M. G. McDonald and A. W. Harbaugh, "A modular three-dimensional finite-difference ground-water flow model," 1988.
[23] S. L. Dingman, *Physical hydrology*: Waveland press, 2015.
[24] B. Duchemin, R. Hadria, S. Erraki, G. Boulet, P. Maisongrande, a. Chehbouni*, et al.*, "Monitoring wheat phenology and irrigation in Central Morocco: On the use of relationships between evapotranspiration, crops coefficients, leaf area index and remotely-sensed vegetation indices," *Agricultural Water Management,* vol. 79, pp. 1-27, 2006.
[25] S. Er-Raki, A. Chehbouni, N. Guemouria, B. Duchemin, J. Ezzahar, and R. Hadria, "Combining FAO-56 model and ground-based remote sensing to estimate water consumptions of wheat crops in a semi-arid region," *Agricultural Water Management,* vol. 87, pp. 41-54, 2007.
[26] M. P. González-Dugo, S. Escuin, F. Cano, V. Cifuentes, F. L. M. Padilla, J. L. Tirado*, et al.*, "Monitoring evapotranspiration of irrigated crops using crop coefficients derived from time series of satellite images. II. Application on basin scale," *Agricultural Water Management,* vol. 125, pp. 92-104, 2013.
[27] V. H. M. Eilers, R. C. Carter, and K. R. Rushton, "A single layer soil water balance model for estimating deep drainage (potential recharge): An application to cropped land in semi-arid North-east Nigeria," *Geoderma,* vol. 140, pp. 119-131, 2007.
[28] E. Kendy, P. Gerard-Marchant, M. Todd Walter, Y. Zhang, C. Liu, and T. S. Steenhuis, "A soil-water-balance approach to quantify groundwater recharge from irrigated cropland in the North China Plain," *Hydrological Processes,* vol. 17, pp. 2011-2031, 2003.
[29] J. Houston, "Rainfall-runoff-recharge relationships in the basement rocks of Zimbabwe," *Estimation of natural groundwater recharge,* pp. 349-365, 1988.
[30] R. C. Carter and A. Parker, "Climate change, population trends and groundwater in Africa," *Hydrological Sciences Journal,* vol. 54, pp. 676-689, 2009.
[31] R. G. Taylor and K. W. Howard, "Groundwater recharge in the Victoria Nile basin of east Africa: support for the soil moisture balance approach using stable isotope tracers and flow modelling," *Journal of Hydrology,* vol. 180, pp. 31-53, 1996.
[32] M. Owor, R. Taylor, C. Tindimugaya, and D. Mwesigwa, "Rainfall intensity and groundwater recharge: empirical evidence from the Upper Nile Basin," *Environmental Research Letters,* vol. 4, p. 035009, 2009.
[33] M. A. Sophocleous, "Combining the soilwater balance and water-level fluctuation methods to estimate natural groundwater recharge: practical aspects," *Journal of hydrology,* vol. 124, pp. 229-241, 1991.
[34] K. K. Garg and S. P. Wani, "Opportunities to Build Groundwater Resilience in the Semi-Arid Tropics," *Groundwater,* vol. 51, pp. 679-691, 2013.
[35] N. Shah, M. Nachabe, and M. Ross, "Extinction depth and evapotranspiration from ground water under selected land covers," *Ground Water,* vol. 45, pp. 329-338, 2007.
[36] A. I. Johnson, *Specific yield: compilation of specific yields for various materials*: US Government Printing Office, 1967.

[37] K. Saxton and W. Rawls, "Soil water characteristic estimates by texture and organic matter for hydrologic solutions," *Soil Science Society of America Journal,* vol. 70, pp. 1569-1578, 2006.
[38] H. Duke, "Capillary properties of soils--influence upon specific yield," *Amer Soc Agr Eng Trans ASAE,* 1972.
[39] C. S. Heppner and J. R. Nimmo, *A computer program for predicting recharge with a master recession curve*: US Geological Survey, 2005.
[40] C. W. Shonsey, "Quantifying Available Water at the Village Level: A Case Study of Horongo, Mali, West Africa," Michigan Technological University, 2009.
[41] H. Breman and J. Kessler, *Woody plants in agro-ecosystems of semi-arid regions: with an emphasis on the Sahelian countries* vol. 23: Springer Science & Business Media, 2012.
[42] W. Edmunds, "Groundwater recharge in Senegal," British Geological Survey1990.
[43] Aquaveo. (2014). *Pilot Points*. Available: www.xmswiki.com/wiki/GMS:Pilot_Points
[44] Aquaveo. (2014). *Parameter Estimation Dialog*. Available: www.xmswiki.com/wiki/GMS:Parameter_Estimation_Dialog
[45] S. Faye, S. C. Faye, S. Ndoye, and A. Faye, "Hydrogeochemistry of the Saloum (Senegal) superficial coastal aquifer," *Environmental Geology,* 2003.
[46] C. Diluca, "Hydrogeology of the Continental terminal aquifer between the Sine and the Gambia," Technical report, BRGM DKR 76 DK (in French)1976.
[47] INP, "Soils Maps: Keur Soce, Ndiaffate and Ndiedieng Rural Communities," ed: National Pedology Institute, 2014.
[48] I. American Manufacturing Company, *Permeameter Manual*. Manassas, Virginia: American Manufacturing Company, Inc., 2011.
[49] C. N. Zangar, W. Moody, and H. B. Phillips, *Theory and problems of water percolation*: US Bureau of Reclamation, 1953.
[50] J. R. Jensen, *Introductory digital image processing: A remote sensing perspective*: Pearson College Division, 2005.
[51] P. Li, L. Jiang, and Z. Feng, "Cross-Comparison of vegetation indices derived from Landsat-7 enhanced thematic mapper plus (ETM+) and Landsat-8 operational land imager (OLI) sensors," *Remote Sensing,* vol. 6, pp. 310-329, 2013.
[52] J. W. Rouse Jr, R. Haas, J. Schell, and D. Deering, "Monitoring vegetation systems in the Great Plains with ERTS," *NASA special publication,* vol. 351, p. 309, 1974.
[53] T. N. Carlson and D. A. Ripley, "On the relation between NDVI, fractional vegetation cover, and leaf area index," *Remote sensing of Environment,* vol. 62, pp. 241-252, 1997.
[54] A. R. Huete, "A soil-adjusted vegetation index (SAVI)," *Remote sensing of environment,* vol. 25, pp. 295-309, 1988.
[55] J. Qi, A. Chehbouni, A. Huete, Y. Kerr, and S. Sorooshian, "A modified soil adjusted vegetation index," *Remote sensing of environment,* vol. 48, pp. 119-126, 1994.
[56] L. Mateos, M. P. González-Dugo, L. Testi, and F. J. Villalobos, "Monitoring evapotranspiration of irrigated crops using crop coefficients derived from time series of satellite images. I. Method validation," *Agricultural Water Management,* vol. 125, pp. 81-91, 2013.
[57] D. J. Hunsaker, P. J. Pinter, and B. a. Kimball, "Wheat basal crop coefficients determined by normalized difference vegetation index," *Irrigation Science,* vol. 24, pp. 1-14, 2005.
[58] J. Sieber and D. Purkey, "Water Evaluation and Planning System USER GUIDE for WEAP21," *Stockholm Environment Institute, US Center,* 2007.
[59] D. A. Chin, *Water-resources Engineering*: Pearson Prentice Hall, 2006.

[60] R. H. Hawkins, A. T. Hjelmfelt Jr, and A. W. Zevenbergen, "Runoff probability, storm depth, and curve numbers," *Journal of Irrigation and Drainage Engineering,* vol. 111, pp. 330-340, 1985.
[61] U. SCS, "National engineering handbook, section 4: hydrology," *US Soil Conservation Service, USDA, Washington, DC,* 1985.
[62] D. E. Woodward, R. H. Hawkins, R. Jiang, A. T. Hjelmfelt, J. A. Van Mullem, and Q. D. Quan, "Runoff curve number method: examination of the initial abstraction ratio," in *Conference Proceeding Paper, World Water and Environmental Resources Congress*, 2003.
[63] K. R. Rushton, V. H. M. Eilers, and R. C. Carter, "Improved soil moisture balance methodology for recharge estimation," *Journal of Hydrology,* vol. 318, pp. 379-399, 2006.
[64] O. H. CIEH, "Précipitations journalières de l'origine des stations à 1965," *Républiques du Dahomey, Tchad, Côte d'Ivoire, Mali, Sénégal, Niger, Haute-Volta, Mauritanie, Togo, Gabon, Cameroun (début à 1972)—12 volumes. Orstom, Paris,* 1973.
[65] J. O. Rawlings, S. G. Pantula, and D. A. Dickey, *Applied regression analysis: a research tool*: Springer Science & Business Media, 1998.
[66] J. F. Hair, R. L. Tatham, R. E. Anderson, and W. Black, *Multivariate Data Analysis*, 5th Edition ed.: Prentice Hall, 1998.
[67] A. Pettitt, "A non-parametric approach to the change-point problem," *Applied statistics,* pp. 126-135, 1979.
[68] Y. L'hote, G. Mahé, B. Somé, and J. P. Triboulet, "Analysis of a Sahelian annual rainfall index from 1896 to 2000; the drought continues," *Hydrological Sciences Journal,* vol. 47, pp. 563-572, 2002.
[69] K. W. Hipel and A. I. McLeod, *Time series modelling of water resources and environmental systems*: Elsevier, 1994.
[70] N. E. Huang and Z. Wu, "A review on Hilbert-Huang transform: Method and its applications to geophysical studies," *Reviews of Geophysics,* vol. 46, 2008.
[71] A. Giannini, S. Salack, T. Lodoun, A. Ali, A. Gaye, and O. Ndiaye, "A unifying view of climate change in the Sahel linking intra-seasonal, interannual and longer time scales," *Environmental Research Letters,* vol. 8, p. 024010, 2013.

7. Appendix

7.1. DH-REM Calculation Procedure

7.1.1. FAO-56 Penman-Monteith Method: AET and Soil Water Balance Procedure

Recognizing the need for a uniform approach to calculating evapotranspiration (ET), due to variability among other calculation methods, the FAO developed this methodology [14]. It relies on a specialized form of the Penman-Monteith method, which is a physically based approach to calculating ET. The Penman-Monteith method is the most extensively used methodology for assessing ET from terrestrial surfaces [23], but due to the considerable data requirements, other methods are often used in its place. The regional capital of Kaolack, located near the study site, has a weather station that collects all of the required data.

The FAO-56 method modifies the Penman-Monteith method in the following way. The Penman-Monteith method allows for variation of albedo and other characteristics of the plant under study relating to surface roughness that affect moisture transfer [14]. The FAO-56 method assumes values for a grass reference crop with a set height of 12 cm, actively growing, completely covering the ground and not short of water (i.e., under no water stress). The evapotranspiration that occurs at this rate is known as the Reference ET, or ET_0. The process for calculating ET_0 was outlined in Section 2.2.2. To calculate the ET of other plants, a crop coefficient is introduced, which effectively scales the reference ET to match the actual ET of the plant in question, based on its stage of development. It also divides total ET into evaporation from bare soil, and transpiration from plants.

$$ET_{c\ adj} = (K_s K_{cb} + K_e) ET_0$$

Equation 7.1

where

$ET_{c\ adj}$ is the actual ET (mm/d)

K_s is a water stress factor (-)

K_{cb} is the crop coefficient (-)

K_e is the soil evaporation coefficient (-)

ET_0 is the reference ET (mm/d)

K_e is calculated as:

$$K_e = K_r(K_{c\ max} - K_{cb}) \leq f_{ew} K_{c\ max}$$

Equation 7.2

where

K_r is the evaporation reduction coefficient (-)

f_{ew} is the fraction of soil both exposed and wetted; here it is equal to ($1-f_c$), where f_c is fractional cover.

K_{cmax} is the maximum value of K_c (= K_{cb} + K_e), following rain or irrigation. This was set to 1.15, after González-Dugo and Mateos [15].

Fractional cover, f_c, is calculated following the method of González-Dugo and Mateos [15] (replacing SAVI with MSAVI):

$$f_c = \frac{MSAVI - MSAVI_{min}}{MSAVI_{max} - MSAVI_{min}}$$

Equation 7.3

where

$MSAVI_{min}$ is the smallest MSAVI value in the study area over the timeframe under consideration

$MSAVI_{max}$ is the largest MSAVI value in the study area

The evaporation reduction coefficient, K_r, is a measure of the effectiveness of evaporation from the soil layer. Initially, with $K_r = 1$, water is depleted at the potential rate, until a threshold, REW, is reached:

$$if\ D_{e,i-1} \leq REW, K_r = 1$$

REW, or Readily Evaporable Water, is the depth of water that can be evaporated at the potential rate. Once this threshold has been crossed, K_r begins to decline linearly, and is calculated according to the following equation (see also Figure 7.1):

$$if\ D_{e,i-1} \geq REW, K_r = \frac{TEW - D_{e,i-1}}{TEW - REW}$$

Equation 7.4

where

TEW is the maximum cumulative depth of evaporation from the soil surface layer (Total Evaporable Water, mm)

REW is the readily evaporable water (mm)

$D_{e,i-1}$ is the previous day's soil moisture depletion from the soil layer (mm).

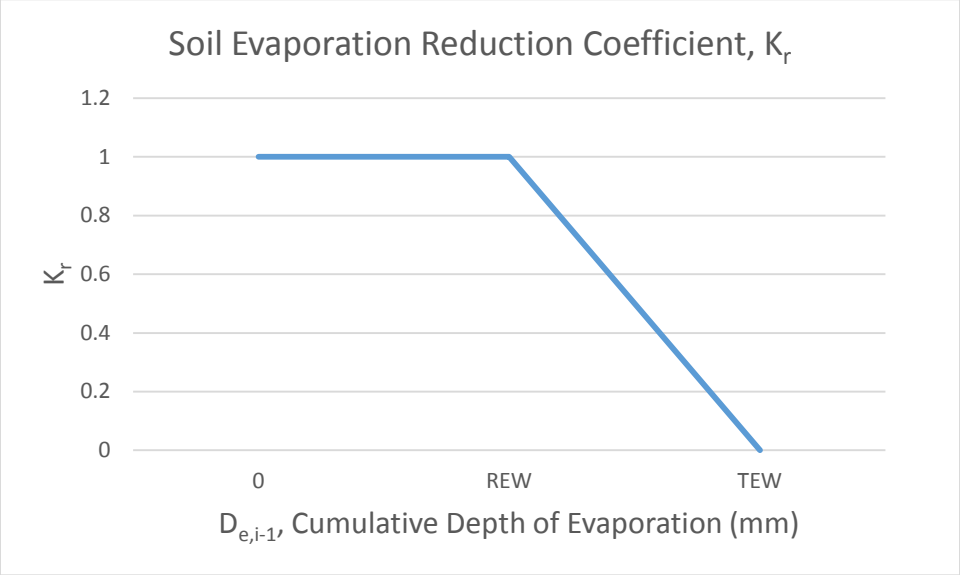

Figure 7.1 Soil Evaporation Reduction Coefficient as a Function of Evaporated Depth of Water. Graph created with data from [14]

TEW is calculated as

$$TEW = 1000(\theta_{FC} - 0.5\theta_{WP})Z_e$$

Equation 7.5

where

θ_{FC} is the soil water content at field capacity (m^3/m^3)

θ_{WP} is the soil water content at wilting point (m^3/m^3)

Z_e is the depth of the soil surface layer that is affected by evaporation (0.1 to 0.15 m, here selected as .15 m)

REW was calculated using the following equation [58]:

$$REW = (3.121TEW + 22.896)Z_e$$

Equation 7.6

González-Dugo and Mateos [15] assumed no water stress occurred in their study area, which was predominately irrigated cropland. However, in the present study area, where effectively no irrigation was applied during the rainy season to field crops, water stress was considered an essential part of the water budget calculation. As such, the full procedure outlined in the FAO-56 document was followed. K_s, the water stress coefficient, is analogous to the evaporation reduction coefficient, and is calculated as:

$$K_s = \frac{TAW - D_r}{TAW - RAW}$$

Equation 7.7

where

TAW is the total available water in the root zone (mm)

RAW is the readily available water in the root zone (mm)

D_r is the depletion of soil moisture in the root zone (mm)

As for K_r, if D_r is less than RAW, K_s is equal to one, and transpiration proceeds at the maximum rate.

TAW, analogous to TEW, is calculated as:

$$TAW = 1000(\theta_{FC} - \theta_{WP})Z_r$$

Equation 7.8

$$Z_r = Z_{r\,min} + (Z_{r\,max} - Z_{r\,min})\frac{K_{cb}}{K_{cb,max}}$$

Equation 7.9

$$RAW = pTAW$$

Equation 7.10

$$K_{cb} = K_{cb,max}f_c$$

Equation 7.11

where

Z_r is the rooting depth of the plant (m)

$Z_{r\,min}$ and $Z_{r\,max}$ are the minimum and maximum rooting depths of the plant (m). $Z_{r\,min}$ was taken to be .1 m, as recommended in [14]).

p is the fraction of TAW that can be depleted via transpiration prior to water stress (-)

The procedure to calculate K_{cb} as the product of the maximum crop factor, $K_{cb,max}$, and fractional cover, fc (Equation 0.11), follows that of González-Dugo and Mateos [15].

Values for REW, TEW, field capacity, wilting point and available water were spatially variable throughout the study area, according to Thiessen polygons as developed in ArcGIS (Figure 3.1).

The soil water depletion in the evaporative layer (that is, only bare soil) on a given day is calculated as follows:

$$D_{e,i} = D_{e,i-1} - (P_i - RO_i) + \frac{E_i}{f_{ew}} + DP_{e,i}$$

Equation 7.12

where

$D_{e,i}$ and $D_{e,i-1}$ are the soil water depletion on day i and day i-1, respectively

P_i is the rainfall on day i

RO_i is the runoff on day i

E_i is the evaporation on day i

$DP_{e,i}$ is deep percolation from the soil layer on day i

$D_{e,i}$ is constrained by:

$$0 \leq D_{e,i} \leq TEW$$

Equation 7.13

The soil water depletion in the root zone is calculated by:

$$D_{r,i} = D_{r,i-1} - (P - RO)_i + ET_{c\ adj} + DP_i$$

Equation 7.14

where

$D_{r,i}$ and $D_{r,i-1}$ are root zone depletion on day i and i-1, respectively (mm)

DP_i is the water loss from the root zone by deep percolation (mm)

$D_{r,i}$ is constrained by:

$$0 \leq D_{r,i} \leq TAW$$

Equation 7.15

To initiate the soil water balance, both D_r and D_e were set to zero at the start of each model run.

7.1.2. Runoff Estimation – The NRCS Curve Number Method

The Soil Conservation Service, now known as the National Resource Conservation Service, developed the Curve Number method as a way to estimate runoff from specific storm events in a watershed with known hydrologic properties [13]. As in the case of estimating evapotranspiration, alternate methods exist for calculating runoff. The NRCS method is one of the most well-known runoff estimation methods, owing to its widespread applicability and relative ease of use.

Total storm runoff, Q, is calculated as

$$Q = \frac{(P - I_a)^2}{(P - I_a) + S}$$

Equation 7.16

Where
P is rainfall (in)
S is potential maximum retention after runoff begins (in)
I_a is initial abstraction (in)

Initial abstraction is made up of interception (as by plant canopies), infiltration, and storage contributed by surface depressions. The original formulation of this method uses the following relationship between initial abstraction and storage:

$$I_a = .2S$$

Equation 7.17

Substituting Equation 7.16 back into Equation 7.17 results in

$$Q = \frac{(P - 0.2S)^2}{P + 0.8S}, P > I_a$$

Equation 7.18

The storage term is transformed into the curve number, CN, by the following relation (S in inches):

$$CN = \frac{1000}{10 + S}$$

Equation 7.19

In practice, the CN is selected according to a set of factors relating to soil type, land use, treatment and hydrologic condition. Soil type is generally indicative of infiltration rate, and different types of land uses include agriculture, developed land, pasture, woods and others. Treatment is a more specific description of management practices. Agricultural land can have different treatments ranging from straight row crops, to contoured planting, to incorporation of crop residue as mulch and others. Hydrologic condition refers to factors such as ground cover, frequency of burning and presence of mulch.

In addition to these factors, what is variably known as the antecedent moisture condition (AMC) or the antecedent runoff condition (ARC) also affects runoff calculation. Theoretically, if a given basin has had very little rain in the recent past (5 days for the purposes of this method), it has greater retention capacity, and will produce less runoff. Alternatively, if it has received a great deal of rain in the previous 5 days, it has correspondingly less retention capacity, and will tend to produce more runoff. This information can be used to adjust the Curve Number according to the following equations (Chin [59], referencing Hawkins, et al. [60]).

For rainfall in the growing season, if the sum of rainfall in the previous 5 days is less than 1.4 inches, or 35 mm:

$$CN_{AMC\ I} = \frac{CN_{AMC\ II}}{(2.3 - 0.013CN_{AMC\ II})}$$

Equation 7.20

If the sum of rainfall in the previous 5 days is greater than 2.1 inches, or 53 mm:

$$CN_{AMC\ III} = \frac{CN_{AMC\ II}}{(.43 + .0057CN_{AMC\ II})}$$

Equation 7.21

Potential retention, S, is then calculated according to the following equation:

$$S = \left(\frac{1000}{CN} - 10\right)$$

Equation 7.22

The thresholds for these dry and wet periods are supplied in SCS [61]. The NRCS Curve Number method, as stated above, assumes a ratio of I_a to S of 0.2. However, Woodward, et al. [62] found that this ratio is actually quite high for most cases, based on experiments in the continental US. In fact, in over 90% of cases, 0.2 was too high. According to their work, a ratio of 0.05 was more acceptable, although this ratio varies from storm to storm and between watersheds. This recommendation – using a ratio of I_a to S of 0.05 – was used in DH-REM.

Calculating storage from the curve number then requires a different expression, as follows:

$$S = 1.33\left(\frac{1000}{CN} - 10\right)^{1.15}$$

Equation 7.23

Runoff can then be calculated according to Equation 7.18.

7.2. Rainfall Analysis

7.2.1. Characterization of Rainfall Patterns

The Sahel is subject to highly variable rainfall patterns, which significantly influences recharge. Rainfall in the early part of the rainy season (May to July) will likely serve primarily to satisfy the soil moisture deficit and not contribute to recharge. Sustained wet spells may correlate with lowering the soil moisture deficit, which is an important precursor to recharge. If the majority of the rain falls in a few large events on the order of several tens of millimeters, much of the precipitation will be lost to runoff, due to the infiltration rate being exceeded, and little water will be available for recharge. On the other hand, if the majority of the rain falls in small events roughly equal to the ET demand of that particular day (typically less than 10 mm), nearly all rain that has fallen will be lost to ET and, similarly, little to no recharge will take place [30]. Because of the anticipated influence of short-term rainfall distribution on recharge, annual rainfall alone is not likely to be an adequate predictor of annual recharge. Thus, when anticipating the effects of climate change, even if the overall trend of annual precipitation is known, the resulting effect on recharge remains unknown because the relationship between rainfall and recharge is not well understood. Rushton, et al. [63] applied a soil-water balance model to semi-arid cropped land in Nigeria. In that study, they qualitatively described rainfall patterns (such as the timing of rain, annual totals and the distribution), primarily to compare these patterns and recorded crop yields with model results. However, no quantitative analysis of the relationship between rainfall and recharge was undertaken.

An important aspect of this study included the development of a set of characteristics that could appropriately describe rainfall patterns apart from the total precipitation. Further, an investigation of the relationship between these characteristics and recharge predicted by a model was also conducted.

The Office for Scientific and Technical Research Overseas (ORSTOM), a French research organization, provided daily rainfall data for numerous rain gauges in Senegal from the beginning of record-keeping to 1965 [64]. For Kaolack, record-keeping started in 1918. Daily precipitation data, also for the Kaolack weather station, was collected by the meteorological office in Dakar (the National Agency of Civil Aviation and Meteorology of Senegal (ANACIM)), covering the years 1965 to 2008. These data sets were combined to create a continuous 91-year data set.

With the rainfall data that was available for Kaolack from 1918 to 2008, the following rainfall characteristics were calculated for each rainy season (Table 7.1). These were selected because of their anticipated effect on recharge, including depth and timing of rainfall, and antecedent moisture conditions.

Table 7.1 Rainy season characteristics under consideration

Parameter	Units
Total annual rainfall	mm
Number of rainy days	Days
Average rain per rainy day	mm
Standard deviation of rainy season events	mm
Coefficient of variance for rainy season events	-
Length of season (defined as number of days from first day with more than 5 mm of rainfall to the last day with any rainfall)	Days
Skewness and kurtosis of each rainy season's rainfall events	-
Total amount of rainfall falling in the following bins:	
0-10 mm	mm
10-20 mm	mm
20-30 mm	mm
30-40 mm	mm
40-60 mm	mm
60-80 mm	mm
More than 80 mm	mm
Kurtosis and skewness of the binned rainfall depths	-
Total amount of rainfall falling in depths greater than:	
10 mm	mm
20 mm	mm
30 mm	mm
40 mm	mm
60 mm	mm
Number of days in a given antecedent moisture condition	Days
Number of dry days (days with <35 mm falling the previous 5 days)	Days
Number of average days (days with >35 mm but <53 mm falling in the previous 5 days)	Days
Number of wet days (days with >53 mm falling the previous 5 days)	Days
Number of spells, or series of days, in a given antecedent moisture condition (dry, average or wet)	Days
Average length of spells in a given antecedent moisture condition (number of dry, average or wet days divided by number of dry, average, or wet spells)	Days
Ratio of dry days to wet days	-
Total amount of rainfall falling each month (May through November)	mm
Skewness and kurtosis of the monthly rainfall distribution	-

This gave a total of 41 characteristics to analyze. Limits for dry, average and wet periods were taken from the NRCS Curve Number method [61].

7.2.2. Relationship between Rainfall and Recharge

Once DH-REM had been calibrated, it was forced with daily rainfall from 1918-2008. Note that the parameters used in the simulations explored below are not the same as those presented earlier. For these, maximum crop rooting depth was 2 meters, and the soil water depletion factor was 0.8 for both crops and forested land. ET rates and land use/land cover data from 2013 were used for each year, to isolate the effect of rainfall patterns. Annual recharge and rainfall were jointly plotted using the full data set (Figure 7.2), and subsequently for 30-year moving windows. A linear trend line was calculated to fit each data set in order to evaluate how the relationship between rainfall and recharge has changed over time. The 91-year data set was broken into 30-year windows for several reasons. First, this time frame allowed better data and trend investigation. The window was long enough to dampen random, short-term fluctuations, while still being short enough to enable evaluation of the dataset at several discrete intervals. Furthermore, the US National Weather Service uses 30 years as the length of record for determining average precipitation for a given location, and updates this every ten years [23]. Subdivision of the longer data set allowed for the evaluation of the relationship between rainfall and recharge on a more temporally localized basis, enabling consideration of a potentially variable relationship between rainfall and recharge. An additional window, covering 1968-2008, was included owing to the detection of a change point occurring in 1968 (see Section 7.2.3.1).

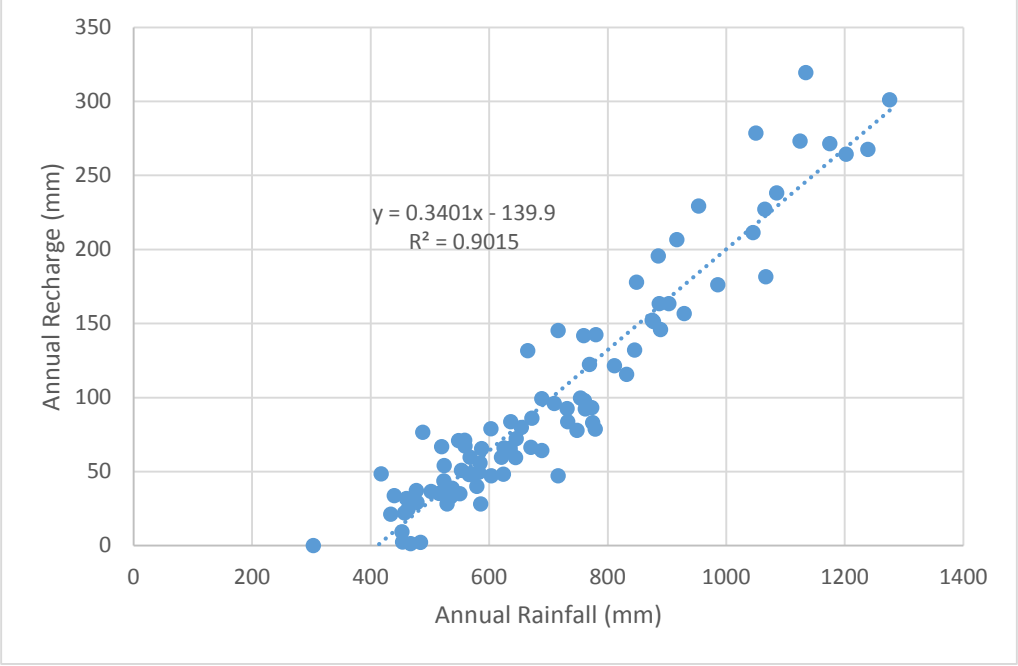

Figure 7.2 Linear Regression of Annual Recharge vs Rainfall, 1918-2008. Rainfall data collected by CIEH [64] and the National Agency of Civil Aviation and Meteorology of Senegal (ANACIM)

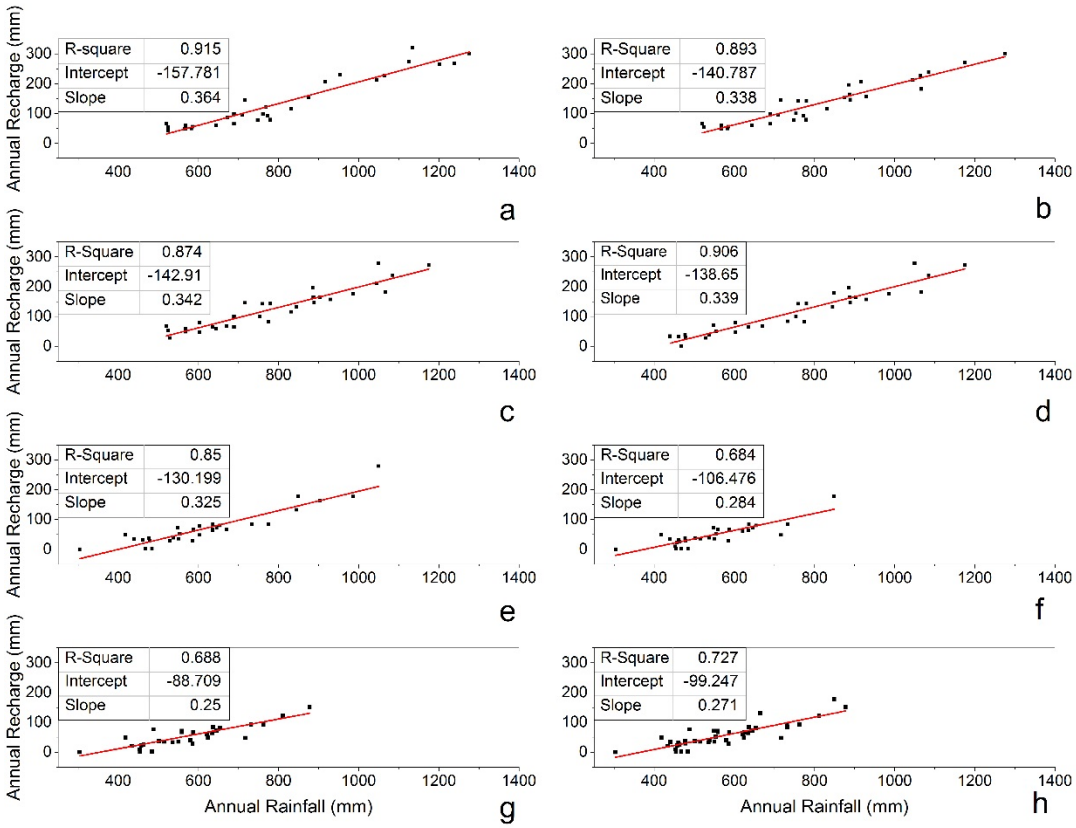

Figure 7.3 Linear Regression of Recharge vs Rainfall. a: 1918-1947, b: 1928-1957, c: 1938-1967, d: 1948-1977, e: 1958-1987, f: 1968-1997, g: 1978-2007, h: 1968-2008. Rainfall data collected by CIEH [64] and the National Agency of Civil Aviation and Meteorology of Senegal (ANACIM)

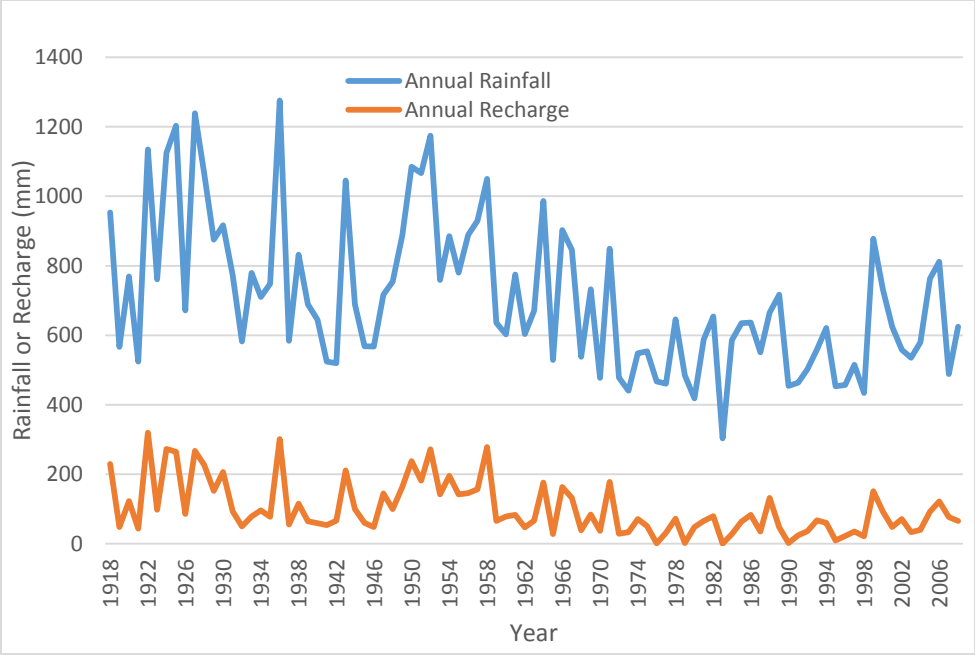

Figure 7.4 Annual Rainfall and Recharge - 1918-2008. Rainfall data collected by CIEH [64] and the National Agency of Civil Aviation and Meteorology of Senegal (ANACIM)

Rainfall has been decreasing markedly, as has recharge (Figure 7.3 and Figure 7.4). The relationship between recharge and rainfall has been shifting over the time frame under consideration. In the first three 30-year periods (Figure 7.3), recharge was about 15% of rainfall, then 13% and 10% over the next two 30-year periods, and finally dropping to about 8% of rainfall in the last three periods considered (1968-1997, 1978-2007, and 1968-2008), indicating annual rainfall has become less effective at producing recharge. The coefficient of determination, or variance explainable by annual rainfall alone, was fairly consistent (ranging from 0.85 to 0.92) through the period ending in 1987. Then in the periods after that, the coefficient of determination dropped considerably to about 0.7. Not only is the relationship between recharge and rainfall changing, but also the extent to which annual rainfall alone can be used to satisfactorily predict annual recharge is decreasing over time. In Table 7.2 is a summary of regression coefficients, the coefficient of determination (R^2) and associated t-test values for the slope coefficient for the above trials. Note that in all cases, the slope value is statistically significant (t_{obs} is greater than t_{crit}) at $p = 0.05$.

Table 7.2 Linear Regression Coefficients, Coefficient of Determination, RMSE and t-test values for each window of Recharge and Rainfall Relationships

Window	Slope	Intercept	Coefficient of Determination	RMSE	t_{crit}	t_{obs}
1918-2008	0.340	-139.898	0.902	24.267	1.987	28.548
1918-1947	0.364	-157.781	0.915	26.059	2.048	17.355
1928-1957	0.338	-140.787	0.893	23.545	2.048	15.296
1938-1967	0.342	-142.919	0.874	24.727	2.048	13.931
1948-1977	0.339	-138.655	0.906	23.662	2.048	16.410
1958-1987	0.325	-130.199	0.850	23.903	2.048	12.588
1968-1997	0.284	-106.476	0.684	21.997	2.048	7.781
1978-2007	0.250	-88.709	0.688	21.555	2.048	7.860
1968-2008	0.271	-99.247	0.727	21.036	2.023	10.183

Next, several linear regression analyses were conducted to further explore what factors affect recharge. The square root transformation was applied to recharge values in order for them to be normally distributed. All 41 variables were plotted versus the square root of recharge to determine if a linear relationship existed, based on a visual assessment. This assessment was performed twice: once for the period covering 1918-2008, and applied to all 30-year windows, and a second time for the period covering 1968-2008. Thirteen variables were determined to have a linear relationship with recharge for 1918-2008 (12 for 1968-2008) and were analyzed using a stepwise linear regression. Since some of the variables were likely collinear, two statistics regarding collinearity were reviewed after each regression was performed. These are the VIF (the Variance Inflation Factor) and the Condition Index. If a variable had a VIF higher than 10, or a condition index greater than 20 that also coincided with a high variance proportion, it was removed, and the regression redone [65, 66]. No final regression analysis resulted in a predictor variable with a condition index greater than 18.903, and the largest VIF encountered was 3.409. Both of these factors indicate minimal collinearity was present among the 13 variables studied. Finally, the condition of homoscedasticity was evaluated. The plot of residual versus predicted values was visually inspected, and all regressions appeared homoscedastic. All coefficients in the modeled relationships were significant at $p < 0.05$, and most were significant at $p < 0.01$. The parameters used in each equation, along with their coefficients and significance levels, are presented in Table 7.3.

Table 7.3 Statistical Aspects of Multilinear Regression Models

		Constant	Total	Aug Sum	Sep Sum	Stand. Devn.	10+	# Wet Days	Avg Wet Spell
1918-2008	Coefficient	-0.554	-	0.015	0.013	-	-	0.173	-
	Significance	0.1745	-	5.32E-14	4.91E-10	-	-	9.70E-12	-
1918-1947	Coefficient	1.016	-	0.014	0.011	-	-	0.144	-
	Significance	0.0797	-	9.14E-07	7.06E-05	-	-	3.32E-05	-
1928-1957	Coefficient	-0.418	0.017	-	-	-0.207	-	-	.241
	Significance	0.62945	1.65E-13	-	-	0.00561	-	-	.04736
1938-1967	Coefficient	-1.223	0.015	-	-	-	-	-	-
	Significance	0.17218	2.72E-14	-	-	-	-	-	-
1948-1977	Coefficient	-2.366	0.014	0.006	-	-	-	-	-
	Significance	0.00701	2.76E-10	0.03162	-	-	-	-	-
1958-1987	Coefficient	-2.655	0.020	-	-	-	-	-	-
	Significance	0.007821	2.64E-12	-	-	-	-	-	-
1968-1997	Coefficient	-2.813	-	.013	-	-	0.010	.142	-
	Significance	0.04023	-	.00166	-	-	0.02720	.02658	-
1978-2007	Coefficient	-2.004	-	0.013	0.015	-	-	0.257	-
	Significance	0.01209	-	9.00E-05	2.70E-04	-	-	5.64E-07	-
1968-2008	Coefficient	-1.106	-	0.015	0.013	-	-	0.194	-
	Significance	0.17601	-	3.00E-06	0.00189	-	-	1.60E-05	-

Table 7.4 Coefficient of Determination and RMSE for Simple and Multilinear Regressions and Improvement

	Coefficient of Determination		RMSE	
Window	Simple	Multi	Simple	Multi
1918-2008	0.902	0.907	24.267	21.487
1918-1947	0.915	0.945	26.059	19.953
1928-1957	0.893	0.915	23.545	19.603
1938-1967	0.874	0.878	24.727	24.369
1948-1977	0.906	0.908	23.662	21.782
1958-1987	0.850	0.830	23.903	18.561
1968-1997	0.684	0.811	21.997	14.111
1978-2007	0.688	0.888	21.555	13.244
1968-2008	0.727	0.806	21.036	13.084

Comparing the coefficient of determination and RMSE between the simple regressions (using annual rainfall as the independent variable) and the multilinear regressions, the first six windows over which multilinear regressions were applied showed little improvement, and once a slight decrease, in coefficient of determination, and slight to modest improvement in RMSE (Table 7.4). Regarding the last three time periods, all three demonstrated improvements in coefficient of determination, and the largest improvements of any periods under study. The time period with the greatest improvement in coefficient of determination was 1978-2007, indicating its analysis benefitted the most from incorporating rainy season characteristics. There is a dramatic decrease in RMSE for the last three time periods as well. The highest R^2 values, that is, the best agreement between the regression-modeled recharge and that predicted by DH-REM, occur during two windows: 1918-1947 and 1928-1957.

The inclusion of additional parameters somewhat improves the accuracy of recharge modeled using linear regression for the last three time periods. Interestingly, in all the multilinear regression equations developed, total rainfall was only selected as a predictor for the periods covering 1928-1987. This again confirms the idea that total rainfall is not as important a predictor of recharge as it has been in the past. The sum of rainfall in August was the most common predictor, followed by number of wet days, total rainfall and September rainfall. This demonstrates that rainfall later in the rainy season, as well as that occurring during a period of sustained rainfall, are the most important characteristics of rainfall that produces recharge. Rain falling in depths greater than 10 mm, the standard deviation of rainfall events (negative relationship) and the average length of wet spells were also selected. Thus, to a lesser extent, that rainfall which is relatively consistent with regard to depth and in excess of a couple days' ET demand are also important characteristics. A higher standard deviation in rainfall may point to a higher frequency of extreme events, where losses from runoff would increase, and minor events, where losses from AET would increase. While there was an important increase in accuracy for the last three time periods under study from considering multiple predictors, they also had lower coefficients of determination than most of the other subsets. This could point to the need for exploration of additional variables that could explain the variance in recharge.

7.2.3. Tests for Nonstationarity

Many approaches to quantifying water resource availability assume the condition of stationarity - that is, a time series is representative of long-term or future behavior. However,

considerable evidence from the field of climate science suggests that the climatic system which drives patterns of rainfall is changing over time [23]. Thus, an alternative set of tools is necessary for evaluating the changing nature of rainfall patterns.

There are three primary ways of assessing nonstationarity: abrupt shifts (detected herein using the Pettitt test), linear trends (either increasing or decreasing, examined in this study using the Mann-Kendall trend test), and cyclicity (assessed here using Empirical Mode Decomposition) [23].

7.2.3.1. Pettitt Test

Owing to climatic trends, anthropogenic forcing, or land use and land cover changes, environmental variables can demonstrate abrupt shifts in the mean, or in the standard deviation. Change points, as well as the time at which this shift is most likely to occur, can be identified using the Pettitt test [67].

Those rainfall characteristics identified as predictors of annual recharge in the previous section were evaluated using the Pettitt test in R. Five of the seven parameters, with the exception of standard deviation and average wet spell length, had statistically significant change points (Table 7.5).

Table 7.5 Summary of Pettitt Test Results. CoV is Coefficient of Variance, the standard deviation divided by the average

	Parameter				
	Total	10+	August	September	# Wet Days
Change Point	1968	1968	1959	1968	1969
Significance	2.77E-07	3.60E-06	8.35E-04	4.27E-04	4.497E-06
Mean before (mm/Days)	817	698	315	217	24.9
Mean after (mm/Days)	573	478	225	148	14.3
% Reduction	30%	32%	29%	32%	43%
Standard Deviation before (mm/Days)	46	30	18	24	9.2
Standard Deviation after (mm/Days)	40	33	19	5	6.6
CoV before	0.056	0.042	0.057	0.109	0.369
CoV after	0.069	0.07	0.086	0.034	0.465

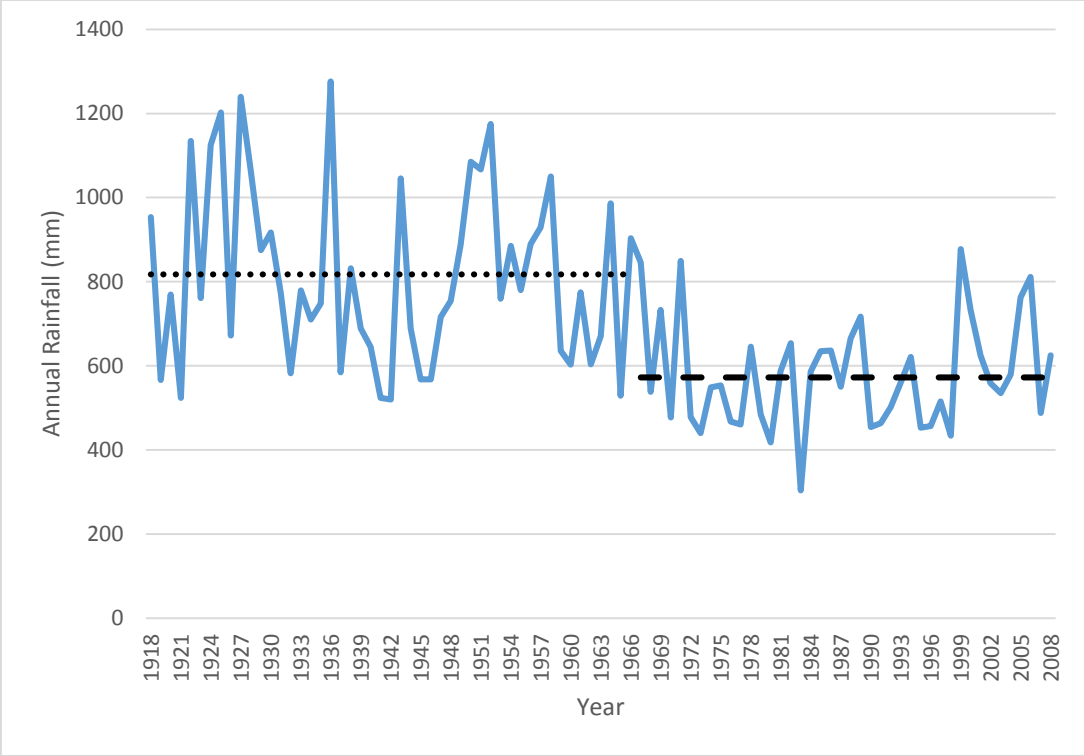

Figure 7.5 Annual rainfall, and average rainfall before and after most probable change point (dashed lines). Rainfall data collected by CIEH [64] and the National Agency of Civil Aviation and Meteorology of Senegal (ANACIM)

Nearly all change points were most likely to have occurred in 1968 or 1969 (Figure 7.5), with the exception of August rainfall (most likely to have occurred in 1959). This compares favorably with a change point in Sahelian rainfall observed between 1969 and 1970 by L'hote, et al. [68]. Each parameter also exhibited similar magnitudes in percent reduction of means from before the change point to after the change point, on the order of 30-40%. September rainfall demonstrated significant reductions in variability, as evidenced by decreases in both standard deviation and coefficient of variance, whereas the number of wet days increased in variability. The remaining parameters expressed no appreciable change in variability. Since the Pettitt test can only detect one change point in a series, additional change points may exist in the time series, but they will not be explored here.

7.2.3.2. Mann-Kendall Trend Test

Trends were evaluated for each of the rainy season characteristics using the Mann-Kendall trend test [69]. Six characteristics were found to have a trend at a significance level $p < 0.05$ (Table 7.6).

Table 7.6 Mann-Kendall Trend Test Results

	Parameter					
	Total	10+	August	September	# Wet Days	Stand. Devn.
Significance	2.92E-06	5.47E-06	2.50E-03	3.78E-04	5.85E-05	0.00578

All trends were negative over the historical record. Trends were also evaluated for each characteristic, in the series before and after the change point predicted by the Pettitt test.

However, no characteristic had a significant trend either before or after the change point detected by the Pettitt test.

7.2.3.3. Empirical Mode Decomposition

The Pettitt test can assess abrupt shifts in the mean, but is relegated to finding just one such break in a series. It also assumes series before and after the change point are homogeneous. The Mann-Kendall trend test, on the other hand, is only capable of identifying if a trend exists at a given significance level, and if such a trend is positive or negative. However, many environmental variables are not monotonic, but exhibit cyclicity, or periodic fluctuations, which cannot be evaluated appropriately using either of the aforementioned tests.

The Fast Fourier Transform (FFT), among other signal processing tools, has been applied in a variety of contexts where evaluation of recurring cycles at a fixed frequency is important. However, its use is predicated on several assumptions, one of which is that of stationarity of the system [70]. Alternatively, Empirical Mode Decomposition (EMD) is an important tool for evaluating cyclical patterns in geophysical data sets [70]. The Hilbert-Huang Transform, an improved version of EMD, has been used in the analysis of earthquakes, wind fields, rainfall patterns, and many others. In essence, EMD decomposes a given signal into component sine waves of varying frequency and wavelength, known as Intrinsic Mode Functions (IMFs). IMFs are formed by tracing upper and lower bounds of the base signal using local maxima and minima, respectively. The average of the upper and lower bounds is computed, then subtracted from the input signal. The averaged signal is then treated as the input signal, and the process repeated, until the following criteria are met: (a) the number of local extrema and crossings at zero differ by at most one, and (b) the mean of the signal at any point is zero. Once the IMFs have been extracted, a trend remains that is either monotonic or has only one extremum [70]. Each component signal can have varying frequency and wavelength properties over the time frame studied. The sum of all IMFs and the trend is equivalent to the base signal.

The parameters that were shown to be predictors for any of the multilinear regression models were analyzed using EMD. An example plot demonstrating the decomposition of a base signal (here, total annual rainfall) into IMFs and an overall trend is shown below.

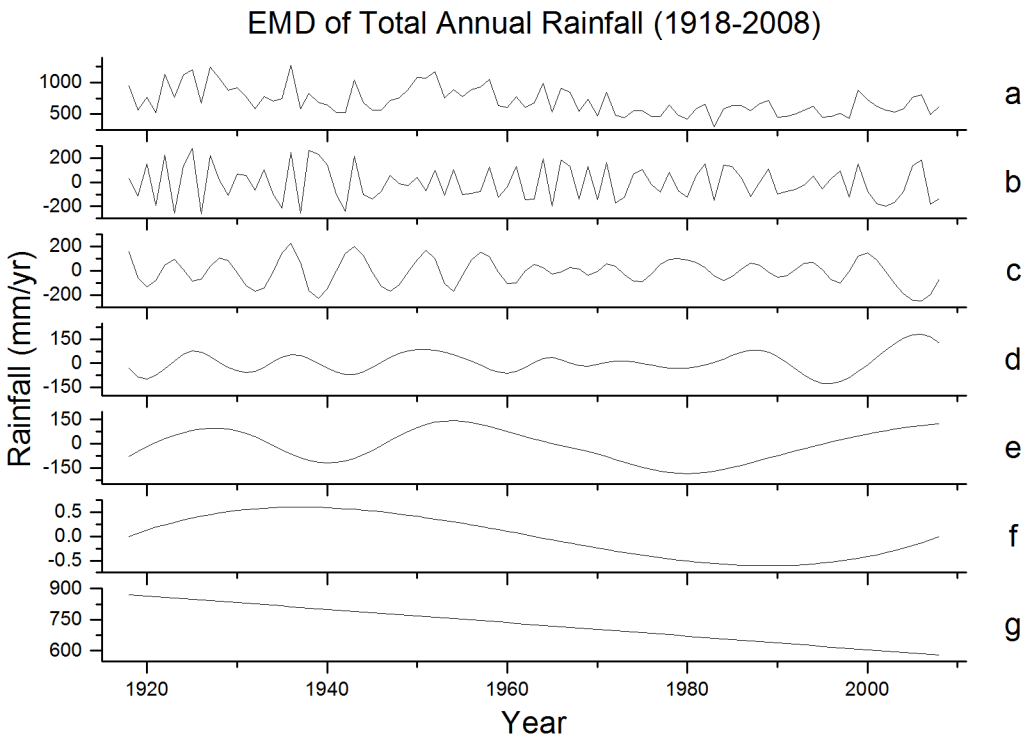

Figure 7.6 Empirical Mode Decomposition Results, as applied to total annual rainfall. a is annual rainfall. b-f are the first through fifth IMFs (Intrinsic Mode Functions). g is the trend. Rainfall data collected by CIEH [64] and the National Agency of Civil Aviation and Meteorology of Senegal (ANACIM)

From Figure 7.6, it is important to note the varying magnitude of the different IMFs. Some may have more persistent behavior, but also minor contributions to the overall signal (such as the 5th IMF). The 2nd IMF, on the other hand, has a fairly short period but also a significant magnitude and contribution to overall rainfall. The trends of regression model predictors, as extracted via EMD, were extrapolated 30 years into the future using MATLAB's interp1 function, applying a spline method. The trend predicted by EMD for number of wet days, however, showed a dramatic decrease in the near future when EMD was applied for the whole dataset, and a dramatic increase when neglecting the first 30 years of data. The trend predicted by EMD neglecting the first 15 years of data and extrapolated in MATLAB demonstrated a reasonable trend into the near future. Once the relevant trends were compiled, the regression model predicted recharge values for the time period covering 1968-2008, including the 95% lower and upper confidence limits of the model, was applied using these trends (including base and projected trend data). These produced projections, as well as 95% confidence bounds, of annual recharge into the future, taking into account only changing rainfall patterns.

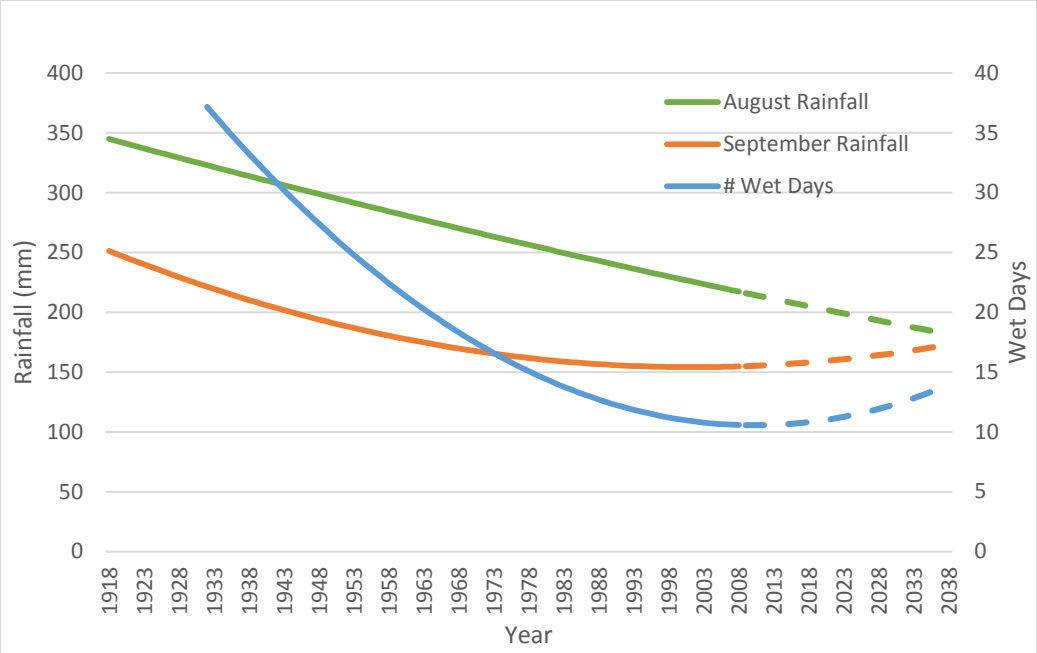

Figure 7.7 Trends of relevant regression model predictors, as estimated by EMD (1918-2008, solid lines) and projected by extrapolation (2009-2038, dashed lines)

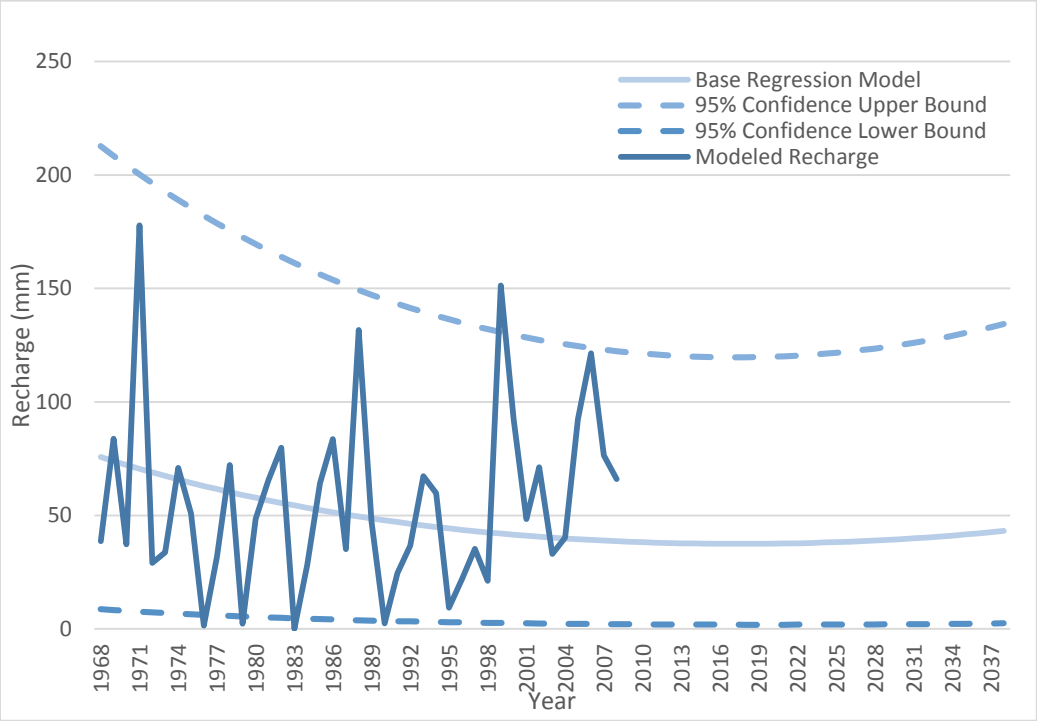

Figure 7.8 Calculated Recharge and Regression Model Projections

Of those parameters expected to predict recharge, wet days per rainy season appears most likely to change significantly in the next couple decades (Figure 7.7). While not likely to change substantially in the near future, August rainfall appears to be decreasing linearly, whereas September rainfall seems to be recovering slightly after reaching a local minimum in the late 1990s or early 2000s. When taking into account only rainfall patterns, recharge as

modeled by DH-REM has decreased significantly since the early part of the 20th century. The regression model indicates that this decline is levelling off, and the upper bound of this estimate points to a rebound in maximum likely recharge as well by 2020 (Figure 7.8). Modeled recharge exceeded the upper bound once, whereas the modeled recharge was less than the lower limit on four occasions. Thus, for 36 out of 41 years, modelled recharge was within the 95% confidence limits.

There are a number of other factors that are likely to affect recharge besides rainfall, including other climate variables and land use changes; however, these are neglected in the present study for two reasons. First, some climate variables, such as temperature, are much more likely to remain fairly steady from one year to the next. Over 1981-2008 (the years for which both temperature and rainfall data were available), average annual temperature, while generally increasing, varied from 28 to 30 °C, whereas annual precipitation ranged from roughly 300 to 900 mm (Figure 7.9). Second, it is important to quantify the impact of individual factors on recharge, in order to discern which factors have the greatest effect.

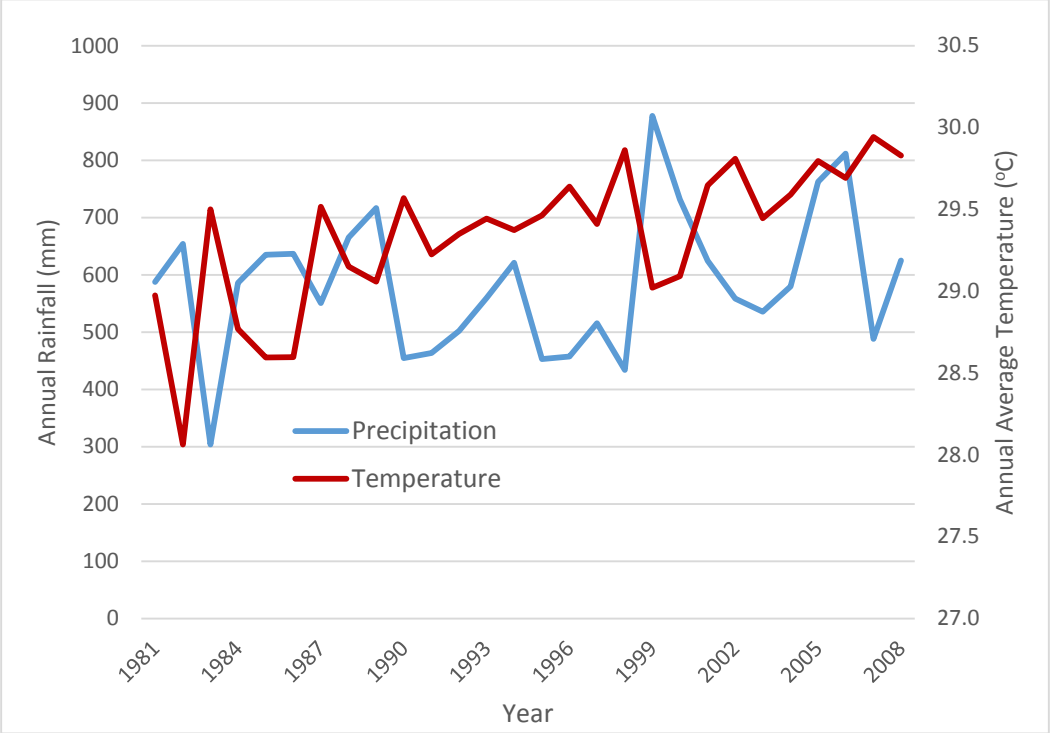

Figure 7.9 Annual Precipitation and Average Temperature, 1981-2008. Rainfall data collected by CIEH [64] and the National Agency of Civil Aviation and Meteorology of Senegal (ANACIM)

As noted above, one source of nonstationarity is a cyclical change in the climatic system, often associated with climatic indices. Since these would likely affect rainfall pattern characteristics, and recharge by extension, correlation of base signals and individual IMFs with climatic indices was also investigated. Four climatic indices were evaluated that are calculated based on sea surface temperatures (SST): the Niño 3.4 Index (N3.4, corresponding to El Niño and the Southern Oscillation, ENSO), the Pacific Decadal Oscillation (PDO), the Atlantic Multidecadal Oscillation (AMO) and a fourth index established by Giannini, et al. [71] (Table 7.7). The North Atlantic Index (NAI), as it will be referred to here, relates the difference in ocean temperature between the north Atlantic and global tropical SST. Niño 3.4 was selected because of its relatively short period, roughly three to seven years, and its widespread impact

on global weather patterns. PDO and AMO were selected on account of their longer wavelengths, on the order of decades.

Table 7.7 Climate Indices and Respective Data Sources

Index	Data Source
Niño 3.4 Index	http://www.cgd.ucar.edu/cas/catalog/climind/TNI_N34/index.html
Pacific Decadal Oscillation	http://research.jisao.washington.edu/pdo/
Atlantic Multidecadal Oscillation	http://www.esrl.noaa.gov/psd/data/timeseries/AMO/
North Atlantic Index	http://www.esrl.noaa.gov/psd/data/timeseries/

These indices were computed on annual basis from monthly data, by taking the average of index values for a water year – from November of the previous year to October of the year in question, corresponding to the end of the rainy season in the previous year to that of the year in question. The time frames used for calculation included those that were shifted three, six and nine months backwards from the end of the rainy season, allowing consideration of lag times in investigating the correlation with base signals and IMFs from EMD. The chart below summarizes these results by presenting the highest correlation coefficient calculated among the lagged climate indices, relative to the base signal or IMF in question. Correlations and their corresponding two-tailed t-test values were calculated. Those correlations with 95% or 99% significance are presented here. In general, lag times did not play a large role in determining correlation, but there were some exceptions to this. For instance, the second IMF of annual rainfall correlated with NAI at a significance level of $p = 0.05$ for a standard water year (November to the following October), but did not correlate significantly with yearly NAI signals for time periods August-July, May-April or February-January. Thus, the strength of some of these teleconnections are affected by the time of year over which they operate, whereas most are statistically significant year-round.

Table 7.8 Correlation Coefficients of Base Signals and IMFs with Four Climatic Patterns. Superscript a represents significance at the 99% level; superscript b represents significance at the 95% level.

	N3.4 (n = 90)		PDO (n = 91)		AMO (n = 91)		NAI (n = 60)	
	IMF	r	IMF	r	IMF	r	IMF	r
Total					3	0.220[b]	Base	0.637[a]
					4	0.481[a]	2	0.266[b]
					5	0.410[a]	4	0.688[a]
10+					5	0.697[a]	Base	0.538[a]
							3	0.439[a]
							4	0.653[a]
August			5	0.436[a]			3	0.301[b]
							4	0.27[b]
September					5	0.388[a]	Base	0.414[a]
							4	0.549[a]
							5	0.672[a]
# Wet Days					4	0.645[a]	Base	0.611[a]
					5	0.410[b]	3	0.262[b]
							4	0.541[a]
							5	0.736[a]
Avg Wet Spell	3	0.217[b]						

N3.4 only correlates with the third IMF from average wet spell duration (an average period of about 12 years), which is surprising given the shorter period of ENSO (roughly three to seven years, Table 7.8) [23]. The standard deviation of rainfall does not correlate with any climate index. One significant correlation was observed between the PDO and the fifth IMF of August rainfall, despite the shorter period of the PDO (46 years over the record analyzed here, whereas this IMF has a period of about 60 years). The AMO correlated significantly with the lower frequency signals (third through fifth IMFs), fitting given its long period (approximately 50 years in this dataset). Of the indices evaluated here, the NAI correlated most often with climatic parameter base signals and their corresponding IMFs, primarily low frequency signals. This supports the thesis of Giannini, et al. [71] that this index can provide insight into rainfall patterns over varying time scales. In their study, they were able to demonstrate that a temperature difference between the North Atlantic Ocean and global tropical oceans encourages the supply of moisture to the Sahel, resulting in higher rainfall, most notably in Senegal. An extremely high correlation was observed between the 5th IMF of rainfall falling in increments greater than 10 mm and the AMO, as well as between the NAI and the 4th IMF of both total rainfall, and the 5th IMF of wet days per rainy season. These correlation analyses offer an incomplete but promising look into which aspects of the climatic system affect rainfall patterns the most, and the resultant effects on recharge. While recharge is certainly affected by factors apart from rainfall patterns, the ability to quantify this interaction is essential in understanding the nature of recharge, as well as its capacity to change in the future.

7.3. DH-REM Code (MATLAB Environment):

```
% read in precip values
% read in PET values
% read in land cover map
% read in one MSAVI tiff at a time
% using land cover map and fractional cover, calculate base CN
% from amoozemeter results, all soils are class A
%     therefore:
%     crop land, straight row:
%         Less than 50% cover: 72, >50% 67
%     Woods
%         36
%     Farmsteads
%         59
% On a daily basis, cycling through rows and columns:
%    Calculate Runoff using previous model

% establish parameters

Kc_max = 1.15;
TEW = imread('TEW_final.tif');
REW = imread('REW_final.tif');
Avail_water = imread('AW_final.tif');
DP_sum = 0;
Evap_month = 0;
ET_month = 0;
Z_min = .1;

% Read in MSAVI composite images

pre_string = 'MSAVI_';
post_string = '_2013_final.tif';
rows = 277;
columns = 208;
scene = zeros(rows,columns);
scene_compiled = zeros(rows,columns);
MSAVI = zeros(rows,columns);
for N = 1:7
    scene = imread(strcat(pre_string,num2str(N+4),post_string));
    MSAVI = cat(3,MSAVI,scene);
end

% read in LU-LC map
LULC = imread('LULC_2013_final.tif');
% find smallest value of MSAVI for all scenes
MSAVI_max = max(max(max(MSAVI)));

% Calculate Runoff
% Read in rainfall from year 2013
% sheet = 2013;
% P =
xlsread('Rainfall_Transposed_III.xlsx',num2str(sheet),'A2:A185');
Days = 214;
```

```
   % Pre-allocate matrices as 3D matrix full of zeros for following
variables (speeds up processing)
   prev_5_day = zeros(rows,columns,Days);
   base_CN = zeros(rows,columns,Days);
   new_CN = zeros(rows,columns,Days);
   S = zeros(rows,columns,Days);
   Runoff_inch = zeros(rows,columns,Days);
   Runoff = zeros(rows,columns,Days);
   P_eff = zeros(rows,columns,Days);

   counter = 1;
   % Cycle through years
   for sheet = 2013
       P =
xlsread('Rainfall_Transposed_III.xlsx',num2str(sheet),'A2:A215');
       % Days = numel(P);
       % convert rainfall values to inches
       P_inch = P/25.4;
       % Cycle through days

       Z_crop = 1.05;
       Z_forest = 4;
       p_forest = .8;
       p_crop = .45;

       abs_min = .2;

       for q = 1:Days
           if q <= 31
               N =5;
           elseif q <= 61
               N =6;
           elseif q<=92
               N=7;
           elseif q <=123
               N=8;
           elseif q<=153
               N=9;
           elseif q<= 184
               N=10;
           else
               N=11;
           end
           % Cycle through rows
           for j = 1:rows
               % Cycle through columns
               for k = 1:columns
                   if q <= 5
                       prev_5_day(q) = 0;
                   else prev_5_day(q) = sum(P_inch(q-5:q));
                   end
                   % Depending on LU-LC values from LU-LC map, assign
   base
                   % Curve Number
                   if LULC(j,k) == 1
```

```
                    base_CN(j,k,q) = 36;
                elseif LULC(j,k) == 2
                    % Adjust CN based on land cover - agricultural
land
                    % only
                    if (MSAVI(j,k,N-3)-abs_min)/(MSAVI_max-abs_min)
<.5
                        base_CN(j,k,q) = 72;
                    else
                        base_CN(j,k,q) = 67;
                    end
                else
                    base_CN(j,k,q) = 59;
                end

                % Conditional statements - if sum of previous 5 days
of
                % rain is less than a certain amount (dry spell),
adjust CN
                % down (more storage). If more than a certain
amount,
                % adjust CN up (less storage). If in between, keep
base CN
                % value

                if prev_5_day(q) <= 1.4
                    new_CN(j,k,q) = (base_CN(j,k,q)*4.3)/(10-
.058*base_CN(j,k,q));
                elseif prev_5_day(q) >= 2.1
                    new_CN(j,k,q) =
(base_CN(j,k,q)*23)/(10+.13*base_CN(j,k,q));
                else
                    new_CN(j,k,q) = base_CN(j,k,q);
                end
                % Calculate storage based on CN
                S(j,k,q) = 1.33*((1000/new_CN(j,k,q))-10)^1.15;
                % If rainfall is below a certain threshold (function
of
                % storage, no runoff occurs. Else, runoff occurs.
                if P_inch(q) < .05*S(j,k,q)
                    Runoff_inch(j,k,q) = 0;
                else
                    Runoff_inch(j,k,q) = (P_inch(q) -
.05*S(j,k,q)).^2/(P_inch(q)+.95*(S(j,k,q)));
                end
                % Convert runoff back into mm
                Runoff(j,k,q) = Runoff_inch(j,k,q)*25.4;
                % Find P_eff - Rainfall minus Runoff. This is
treated as
                % rainfall for subsequent calculations
                P_eff(j,k,q) = P(q)-Runoff(j,k,q);
            end
        end
    end
```

```
        % Read in PET
        ET_0 = xlsread('ET Data for Combined
Model.xlsx','2013','A1:A214');

        % Initiate/pre-allocate ET variables
        Kcb = ones(rows,columns,Days);
        F_ew = ones(rows,columns,Days);
        Z_r = ones(rows,columns,Days);
        TAW = ones(rows,columns,Days);
        RAW = ones(rows,columns,Days);
        K_r = ones(rows,columns,Days);
        K_r_a = ones(rows,columns,Days);
        K_s = ones(rows,columns,Days);
        K_e = ones(rows,columns,Days);
        Evap = ones(rows,columns,Days);
        ETc_adj = ones(rows,columns,Days);
        Trans = ones(rows,columns,Days);
        DP_e = ones(rows,columns,Days);
        D_e = ones(rows,columns,Days);
        DP_r = ones(rows,columns,Days);
        D_r = ones(rows,columns,Days);
        frac_cover = ones(rows,columns,Days);
        Kc_adj = ones(rows,columns,Days);

        % Calculate Evaporation and Transpiration fraction
        % Cycle through days

        for q = 1:Days
            if q <= 31
                N =5;
            elseif q <= 61
                N =6;
            elseif q<=92
                N=7;
            elseif q <=123
                N=8;
            elseif q<=153
                N=9;
            elseif q <= 184
                N=10;
            else
                N=11;
            end
            % Cycle through rows
            for j = 1:rows
                % Cycle through columns
                for k = 1:columns
                    % Calculate fractional cover as proportion of local
MSAVI
                    % to MSAVI_max
                    frac_cover(j,k,q) = (MSAVI(j,k,N-3) -
abs_min)/(MSAVI_max - abs_min);
                    if frac_cover(j,k,q) > 1
                        frac_cover(j,k,q) = 1;
                    elseif frac_cover(j,k,q) < 0
```

```
                    frac_cover(j,k,q) = 0;
                end
                % Determine basal crop coefficient as max
                % crop coefficient times fractional cover
                Kcb(j,k,q) = Kc_max*frac_cover(j,k,q); % GDM Eq 11
                % Fraction of surface wetted by precipitation (100%)
                Fw = 1;
                % Fraction of soil both exposed and wetted
                F_ew(j,k,q) = min(1-frac_cover(j,k,q),Fw); % Eq 75
                % Initiate soil depletion for first day, equivalent
to
                % total available water
                D_e(j,k,1) = TEW(j,k);
                % If LULC is forest, root zone is constant at ~3m
                if LULC(j,k) == 1
                    Z_r(j,k,q) = Z_forest;
                    % For Ag land, max root zone is 1.5 m, and
scaled between
                    % Zmin and Zmax as a function of crop
coefficient
                else
                    Z_max = Z_crop;

                    if q ==1
                        Z_r(j,k,q) = Z_min + (Z_max-
Z_min)*(Kcb(j,k,q)/Kc_max); % GDM Eq 12
                    else
                        Z_r(j,k,q) = max(Z_min + (Z_max-
Z_min)*(Kcb(j,k,q)/Kc_max),Z_r(j,k,q-1));
                        % Maintains rooting depth at max once peak
development
                        % has been reached, i.e., roots do not
shrink with
                        % diminishing ground cover during senescence
                    end
                end
                % Total and readily available water calculations
                TAW(j,k,q) = 1000*Avail_water(j,k)*Z_r(j,k,q); % Eq
82
                if LULC(j,k) == 1;
                    RAW(j,k,q) = p_forest*TAW(j,k,q); % Eq 83
                else
                    RAW(j,k,q) = p_crop*TAW(j,k,q); % Eq 83
                end
                D_r(j,k,1) = TAW(j,k,1); % Initialize Root zone
depletion as TAW - Eq 87
                % Initialize K_s and K_r as 0 for day 1
                if q == 1
                    % Soil evaporation reduction coefficient
                    K_r(j,k,q) = 0;
                    % Water stress coefficient
                    K_s(j,k,q) = 0;
                else
                    if D_e(j,k,q-1) < REW(j,k)
                        K_r_a(j,k,q) = 1;
```

```
                        else
                            K_r_a(j,k,q) = (TEW(j,k) - D_e(j,k,q-
1))/(TEW(j,k) - REW(j,k)); % Eq 74
                        end
                        K_r(j,k,q) = K_r_a(j,k,q);
                        if D_r(j,k,q-1) < RAW(j,k,q)
                            K_s(j,k,q) = 1;
                        else
                            K_s(j,k,q) = (TAW(j,k,q) - D_r(j,k,q-
1))/(RAW(j,k,q)*TAW(j,k,q)); % Eq 84
                        end
                    end
                    % Calculate soil evaporation coefficient
                    K_e(j,k,q) = min((K_r(j,k,q)*(Kc_max -
Kcb(j,k,q))),F_ew(j,k,q)*Kc_max); % Eq 71
                    % Calculate actual evaporation
                    Evap(j,k,q) = K_e(j,k,q)*ET_0(q);
                    % Calculate Actual ET using dual crop coefficient
                    Kc_adj(j,k,q) = (K_s(j,k,q)*(Kcb(j,k,q))) +
K_e(j,k,q);
                    ETc_adj(j,k,q) = (Kc_adj(j,k,q) * ET_0(q)); % Eq 80
                    % Calculate transpiration
                    Trans(j,k,q) = (K_s(j,k,q)*(Kcb(j,k,q)))*ET_0(q);
                    % Calculate Deep Percolation (DP) and Soil Moisture
                    % Depletion (D) for both Evap and Transpiration

                    %%%% Below is Original code
                    if q == 1
                        % For Day 1, DP is P_eff if rain has fallen,
else 0
                        DP_e(j,k,q) = (max(0,P_eff(j,k,q) -
Evap(j,k,q))); % Eq 79
                        D_e(j,k,q) = TEW(j,k);% - P_eff(j,k,q) +
(Evap(j,k,q)/F_ew(j,k,q)) + DP_e(j,k,q); % Eq 77
                        DP_r(j,k,q) = (max(0,P_eff(j,k,q) -
ETc_adj(j,k,q) - TAW(j,k,1))); % Eq 88
                        D_r(j,k,q) = TAW(j,k,1); % Eq 85

                    else
                        DP_e(j,k,q) = (max(0,P_eff(j,k,q) - D_e(j,k,q-1)
- Evap(j,k,q))); % Eq 79
                        D_e(j,k,q) = D_e(j,k,q-1) - P_eff(j,k,q) +
(Evap(j,k,q)/F_ew(j,k,q)) + DP_e(j,k,q); % Eq 77
                        % Set limits on evaporative layer moisture
depletion (min
                        % is 0, max is TEW(j,k))
                        if D_e(j,k,q) < 0
                            D_e(j,k,q) = 0;
                        elseif D_e(j,k,q) >= TEW(j,k)
                            D_e(j,k,q) = TEW(j,k);
                        end
                        DP_r(j,k,q) = (max(0,P_eff(j,k,q) -
ETc_adj(j,k,q) - D_r(j,k,q-1))); % Eq 88
                        D_r(j,k,q) = D_r(j,k,q-1) - P_eff(j,k,q) +
ETc_adj(j,k,q) + DP_r(j,k,q); % Eq 85
```

```
                        % Set limits on root zone moisture depletion
(min
                        % is 0, max is TAW)
                        if D_r(j,k,q) < 0
                            D_r(j,k,q) = 0;
                        elseif D_r(j,k,q) >= TAW(j,k,q)
                            D_r(j,k,q) = TAW(j,k,q);
                        end
                    end
                end
            end
        end

        % Pre-allocate monthly tallies of Runoff, ET, and DP

        May_runoff = zeros(rows,columns);
        Jun_runoff = zeros(rows,columns);
        Jul_runoff = zeros(rows,columns);
        Aug_runoff = zeros(rows,columns);
        Sep_runoff = zeros(rows,columns);
        Oct_runoff = zeros(rows,columns);
        Nov_runoff = zeros(rows,columns);
        Annual_Runoff_matrix = zeros(rows,columns);

        May_ET = zeros(rows,columns);
        Jun_ET = zeros(rows,columns);
        Jul_ET = zeros(rows,columns);
        Aug_ET = zeros(rows,columns);
        Sep_ET = zeros(rows,columns);
        Oct_ET = zeros(rows,columns);
        Nov_ET = zeros(rows,columns);
        Annual_ET_matrix = zeros(rows,columns);

        May_DP = zeros(rows,columns);
        Jun_DP = zeros(rows,columns);
        Jul_DP = zeros(rows,columns);
        Aug_DP = zeros(rows,columns);
        Sep_DP = zeros(rows,columns);
        Oct_DP = zeros(rows,columns);
        Nov_DP = zeros(rows,columns);

        May_DPe = zeros(rows,columns);
        Jun_DPe = zeros(rows,columns);
        Jul_DPe = zeros(rows,columns);
        Aug_DPe = zeros(rows,columns);
        Sep_DPe = zeros(rows,columns);
        Oct_DPe = zeros(rows,columns);
        Nov_DPe = zeros(rows,columns);
        Annual_DP_matrix = zeros(rows,columns);
        %Nov_DPe = zeros(rows,columns);

        % Cycle through rows
        for j = 1:rows
            % Cycle through columns
```

```
            for k = 1:columns
                % Find monthly runoff as sum of runoff values over the
whole
                % area for a specified date range
                May_runoff(j,k) = sum(Runoff(j,k,1:31));
                Jun_runoff(j,k) = sum(Runoff(j,k,32:61));
                Jul_runoff(j,k) = sum(Runoff(j,k,62:92));
                Aug_runoff(j,k) = sum(Runoff(j,k,93:123));
                Sep_runoff(j,k) = sum(Runoff(j,k,124:153));
                Oct_runoff(j,k) = sum(Runoff(j,k,154:184));
                Nov_runoff(j,k) = sum(Runoff(j,k,185:214));
                Annual_Runoff_matrix(j,k) = sum(Runoff(j,k,1:214));
                % Find monthly ET as sum of ET values over the whole
                % area for a specified date range. nansum function
excludes
                % values NaN
                May_ET(j,k) = nansum(ETc_adj(j,k,1:31));
                Jun_ET(j,k) = nansum(ETc_adj(j,k,32:61));
                Jul_ET(j,k) = nansum(ETc_adj(j,k,62:92));
                Aug_ET(j,k) = nansum(ETc_adj(j,k,93:123));
                Sep_ET(j,k) = nansum(ETc_adj(j,k,124:153));
                Oct_ET(j,k) = nansum(ETc_adj(j,k,154:184));
                Nov_ET(j,k) = nansum(ETc_adj(j,k,185:214));
                Annual_ET_matrix(j,k) = nansum(ETc_adj(j,k,1:214));
                % Find monthly DP as sum of DP values over the whole
                % area for a specified date range
                May_DP(j,k) = sum(DP_r(j,k,1:31));%+sum(DP_e(j,k,1:31));
                Jun_DP(j,k) =
sum(DP_r(j,k,32:61));%+sum(DP_e(j,k,32:61));
                Jul_DP(j,k) =
sum(DP_r(j,k,62:92));%+sum(DP_e(j,k,62:92));
                Aug_DP(j,k) =
sum(DP_r(j,k,93:123));%+sum(DP_e(j,k,93:123));
                Sep_DP(j,k) =
sum(DP_r(j,k,124:153));%+sum(DP_e(j,k,1241:153));
                Oct_DP(j,k) =
sum(DP_r(j,k,154:184));%+sum(DP_e(j,k,154:184));
                Nov_DP(j,k) = sum(DP_r(j,k,185:214));
                Annual_DP_matrix(j,k) = sum(DP_r(j,k,1:214));

                May_DPe(j,k) = sum(DP_e(j,k,1:31));
                Jun_DPe(j,k) = sum(DP_e(j,k,32:61));
                Jul_DPe(j,k) = sum(DP_e(j,k,62:92));
                Aug_DPe(j,k) = sum(DP_e(j,k,93:123));
                Sep_DPe(j,k) = sum(DP_e(j,k,124:153));
                Oct_DPe(j,k) = sum(DP_e(j,k,154:184));
                Nov_DPe(j,k) = sum(DP_e(j,k,185:214));
            end
        end

        % Find avg, max and min of Runoff, ET and DP for all months
        May_avg_runoff = mean(mean(May_runoff));
        May_max_runoff = max(max(May_runoff));
        May_min_runoff = min(min(May_runoff));
```

```
Jun_avg_runoff = mean(mean(Jun_runoff));
Jun_max_runoff = max(max(Jun_runoff));
Jun_min_runoff = min(min(Jun_runoff));

Jul_avg_runoff = mean(mean(Jul_runoff));
Jul_max_runoff = max(max(Jul_runoff));
Jul_min_runoff = min(min(Jul_runoff));

Aug_avg_runoff = mean(mean(Aug_runoff));
Aug_max_runoff = max(max(Aug_runoff));
Aug_min_runoff = min(min(Aug_runoff));

Sep_avg_runoff = mean(mean(Sep_runoff));
Sep_max_runoff = max(max(Sep_runoff));
Sep_min_runoff = min(min(Sep_runoff));

Oct_avg_runoff = mean(mean(Oct_runoff));
Oct_max_runoff = max(max(Oct_runoff));
Oct_min_runoff = min(min(Oct_runoff));

Nov_avg_runoff = mean(mean(Nov_runoff));
Nov_max_runoff = max(max(Nov_runoff));
Nov_min_runoff = min(min(Nov_runoff));

%%%%%%%%%%%%

May_avg_ET = mean(mean(May_ET));
May_max_ET = max(max(May_ET));
May_min_ET = min(min(May_ET));

Jun_avg_ET = mean(mean(Jun_ET));
Jun_max_ET = max(max(Jun_ET));
Jun_min_ET = min(min(Jun_ET));

Jul_avg_ET = mean(mean(Jul_ET));
Jul_max_ET = max(max(Jul_ET));
Jul_min_ET = min(min(Jul_ET));

Aug_avg_ET = mean(mean(Aug_ET));
Aug_max_ET = max(max(Aug_ET));
Aug_min_ET = min(min(Aug_ET));

Sep_avg_ET = mean(mean(Sep_ET));
Sep_max_ET = max(max(Sep_ET));
Sep_min_ET = min(min(Sep_ET));

Oct_avg_ET = mean(mean(Oct_ET));
Oct_max_ET = max(max(Oct_ET));
Oct_min_ET = min(min(Oct_ET));

Nov_avg_ET = mean(mean(Nov_ET));
Nov_max_ET = max(max(Nov_ET));
Nov_min_ET = min(min(Nov_ET));
```

```
%%%%%%%%%%

May_avg_DP = mean(mean(May_DP));
May_max_DP = max(max(May_DP));
May_min_DP = min(min(May_DP));

Jun_avg_DP = mean(mean(Jun_DP));
Jun_max_DP = max(max(Jun_DP));
Jun_min_DP = min(min(Jun_DP));

Jul_avg_DP = mean(mean(Jul_DP));
Jul_max_DP = max(max(Jul_DP));
Jul_min_DP = min(min(Jul_DP));

Aug_avg_DP = mean(mean(Aug_DP));
Aug_max_DP = max(max(Aug_DP));
Aug_min_DP = min(min(Aug_DP));

Sep_avg_DP = mean(mean(Sep_DP));
Sep_max_DP = max(max(Sep_DP));
Sep_min_DP = min(min(Sep_DP));

Oct_avg_DP = mean(mean(Oct_DP));
Oct_max_DP = max(max(Oct_DP));
Oct_min_DP = min(min(Oct_DP));

Nov_avg_DP = mean(mean(Nov_DP));
Nov_max_DP = max(max(Nov_DP));
Nov_min_DP = min(min(Nov_DP));

%%%%%%%%%%

May_avg_DPe = mean(mean(May_DPe));
May_max_DPe = max(max(May_DPe));
May_min_DPe = min(min(May_DPe));

Jun_avg_DPe = mean(mean(Jun_DPe));
Jun_max_DPe = max(max(Jun_DPe));
Jun_min_DPe = min(min(Jun_DPe));

Jul_avg_DPe = mean(mean(Jul_DPe));
Jul_max_DPe = max(max(Jul_DPe));
Jul_min_DPe = min(min(Jul_DPe));

Aug_avg_DPe = mean(mean(Aug_DPe));
Aug_max_DPe = max(max(Aug_DPe));
Aug_min_DPe = min(min(Aug_DPe));

Sep_avg_DPe = mean(mean(Sep_DPe));
Sep_max_DPe = max(max(Sep_DPe));
Sep_min_DPe = min(min(Sep_DPe));
```

```
        Oct_avg_DPe = mean(mean(Oct_DPe));
        Oct_max_DPe = max(max(Oct_DPe));
        Oct_min_DPe = min(min(Oct_DPe));

        Nov_avg_DPe = mean(mean(Nov_DPe));
        Nov_max_DPe = max(max(Nov_DPe));
        Nov_min_DPe = min(min(Nov_DPe));

        % Calculate annual DP, ET and Runoff values as sum of monthly
values

        Annual_DPr = May_avg_DP + Jun_avg_DP + Jul_avg_DP + Aug_avg_DP +
Sep_avg_DP + Oct_avg_DP + Nov_avg_DP;
        Annual_DPe = May_avg_DPe + Jun_avg_DPe + Jul_avg_DPe +
Aug_avg_DPe + Sep_avg_DPe + Oct_avg_DPe + Nov_avg_DPe;
        Annual_DP = Annual_DPr + Annual_DPe;
        Annual_ET = May_avg_ET + Jun_avg_ET + Jul_avg_ET + Aug_avg_ET +
Sep_avg_ET + Oct_avg_ET + Nov_avg_ET;
        Annual_Runoff = May_avg_runoff + Jun_avg_runoff + Jul_avg_runoff
+ Aug_avg_runoff + Sep_avg_runoff + Oct_avg_runoff + Nov_avg_runoff;
        P_sum = sum(P);

        % Combine previous values into one array
        %                     Z_forest
        %                     Z_crop;
        %                     p
        Error = ((Annual_DPr - 158)/158);
        Summary_array = horzcat(May_avg_runoff, May_max_runoff,
May_min_runoff, Jun_avg_runoff, Jun_max_runoff, Jun_min_runoff,
Jul_avg_runoff, Jul_max_runoff, Jul_min_runoff,...
            Aug_avg_runoff, Aug_max_runoff, Aug_min_runoff,
Sep_avg_runoff, Sep_max_runoff, Sep_min_runoff, Oct_avg_runoff,
Oct_max_runoff, Oct_min_runoff, Nov_avg_runoff, Nov_max_runoff,
Nov_min_runoff, May_avg_ET, May_max_ET, May_min_ET, Jun_avg_ET,
Jun_max_ET, Jun_min_ET, Jul_avg_ET, Jul_max_ET, Jul_min_ET, ...
            Aug_avg_ET, Aug_max_ET, Aug_min_ET, Sep_avg_ET, Sep_max_ET,
Sep_min_ET, Oct_avg_ET, Oct_max_ET, Oct_min_ET, Nov_avg_ET, Nov_max_ET,
Nov_min_ET, May_avg_DP, May_max_DP, May_min_DP, Jun_avg_DP, Jun_max_DP,
Jun_min_DP, Jul_avg_DP, Jul_max_DP, Jul_min_DP, ...
            Aug_avg_DP, Aug_max_DP, Aug_min_DP, Sep_avg_DP, Sep_max_DP,
Sep_min_DP, Oct_avg_DP, Oct_max_DP, Oct_min_DP, Nov_avg_DP, Nov_max_DP,
Nov_min_DP, Annual_Runoff, Annual_ET, Annual_DP, Annual_DPr,
Annual_DPe, P_sum, Z_crop, Z_forest);


        write_number = num2str(counter);
        write_cell = horzcat('B',num2str(write_number));
            % Write 'Summary_array' to Excel sheet
        xlswrite('Water_Balance_Summary.xlsx',Summary_array,'2013
Results',write_cell);
        counter = counter +1;
    end
```

7.4. Permission for Figure 1.1.

File:Senegal in Africa (-mini map -rivers).svg
From Wikimedia Commons, the free media repository Jump to: navigation, search
Description
Deutsch: Lage von XY (siehe Dateiname) in Afrika. English: Location of XY (see filename) in Africa.
Date7 April 2011Own work

This file was uploaded with Commonist.

AuthorOther versions

This SVG map is part of a locator map series applying the widespread location map scheme. Please see root category to browse for more.
+more
+ Locator maps design recommendations
....corresponding imagemaps
Licensing[edit]
I, the copyright holder of this work, hereby publish it under the following licenses:

You are free:
to share – to copy, distribute and transmit the work to remix – to adapt the work
Under the following conditions:
attribution – You must attribute the work in the manner specified by the author or licensor (but not in any way that suggests that they endorse you or your use of the work).
share alike – If you alter, transform, or build upon this work, you may distribute the resulting work only under the same or similar license to this one.
Permission is granted to copy, distribute and/or modify this document under the terms of the GNU Free Documentation License, Version 1.2 or any later version published by the Free Software Foundation; with no Invariant Sections, no Front-Cover Texts, and no Back-Cover Texts. A copy of the license is included in the section entitled GNU Free Documentation License.You may select the license of your choice.

I'd greatly appreciate, that you attribute this media file to Wikimedia Commons, if used outside Wikipedia or Commons. For use in publications such as books, newspapers, blogs, websites, please insert here the following line:
{{published|author= |date= |url= |title= |org= }}and fill the applicable fields. (Example).
License terms given above still apply.

7.5. Permission for Figure 1.2.

File:Kaolack in Senegal.svg - Wikimedia Commons

Deutsch: Lage der Region XY (siehe Dateiname) in Senegal. **English:** Location of region xy (see filename) in Senegal.
Date23 November 2011Own work

This file was uploaded with **Commonist**.

AuthorOther versions

This SVG map is part of a locator map series applying the widespread location map scheme. Please see **root category** to browse for more.

+more
+ Locator maps design recommendations
....corresponding imagemaps
You are free:

to share – to copy, distribute and transmit the work **to remix** – to adapt the work

Under the following conditions:

attribution – You must attribute the work in the manner specified by the author or licensor (but not in any way that suggests that they endorse you or your use of the work).
share alike – If you alter, transform, or build upon this work, you may distribute the resulting work only under the same or similar license to this one.

I'd greatly appreciate, that you attribute this media file to *Wikimedia Commons*, if used outside Wikipedia or Commons. For use in publications such as books, newspapers, blogs, websites, please insert **here** the following line:
{{published|author= |date= |url= |title= |org= }}and fill the applicable fields. (Example).
License terms given above still apply.